Wisconsin Highway Research Program

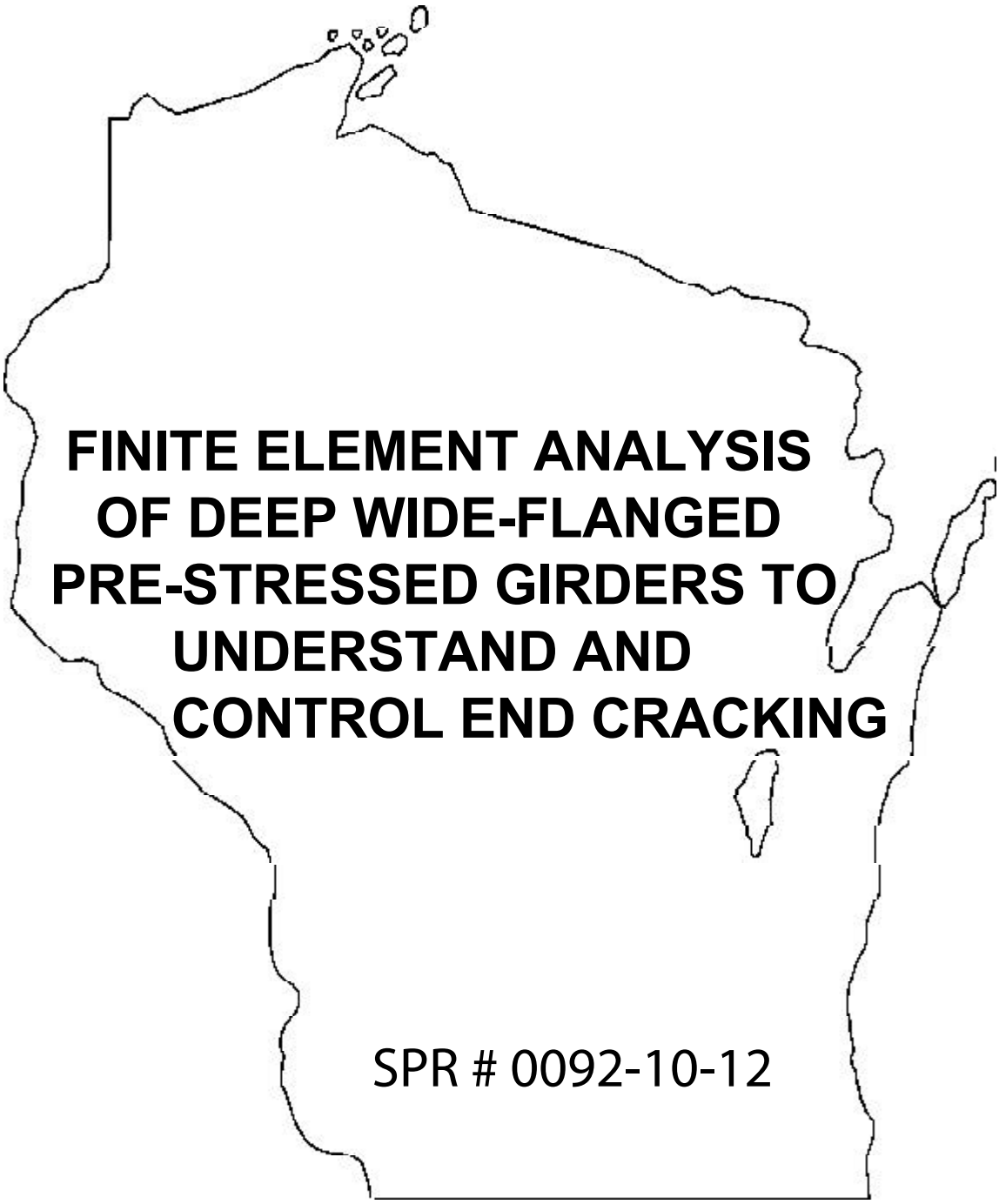

FINITE ELEMENT ANALYSIS OF DEEP WIDE-FLANGED PRE-STRESSED GIRDERS TO UNDERSTAND AND CONTROL END CRACKING

SPR # 0092-10-12

Michael G. Oliva, Ph.D
Pinar Okumus, Ph.D. Candidate

University of Wisconsin-Madison
Civil and Environmental Engineering

October 2011

WHRP 11-06

DISCLAIMER

This research was funded through the Wisconsin Highway Research Program by the Wisconsin Department of Transportation and the Federal Highway Administration under Project 0092-10-12. The contents of this report reflect the views of the authors who are responsible for the facts and accuracy of the data presented herein. The contents do not necessarily reflect the official views of the Wisconsin Department of Transportation or the Federal Highway Administration at the time of publication.

This document is disseminated under the sponsorship of the Department of Transportation in the interest of information exchange. The United States Government assumes no liability for its contents or use thereof. This report does not constitute a standard, specification or regulation.

The United States Government does not endorse products or manufacturers. Trade and manufacturers' names appear in this report only because they are considered essential to the object of the document.

Technical Report Documentation Page

1. Report No. WHRP 11-06	2. Government Accession No	3. Recipient's Catalog No
4. Title and Subtitle Finite Element Analysis of Deep Wide-Flanged Pre-stressed Girders-Draft Final Report		5. Report Date June 2011 6. Performing Organization Code Wisconsin Highway Research Program
7. Authors Michael Oliva, Ph.D. and Pinar Okumus, Ph.D. Candidate		8. Performing Organization Report No.
9. Performing Organization Name and Address University of Wisconsin-Madison Engineering Hall 1415 Engineering Drive Madison, WI 53706		10. Work Unit No. (TRAIS) 11. Contract or Grant No. WisDOT SPR# 0092-10-12
12. Sponsoring Agency Name and Address Wisconsin Department of Transportation Division of Business Services Research Coordination Section 4802 Sheboygan Ave. Rm 104 Madison, WI 53707		13. Type of Report and Period Covered Final Report, 2009-2011 14. Sponsoring Agency Code
15. Supplementary Notes		

16. Abstract Hundreds of prestressed concrete girders are used each year for building bridges in Wisconsin. The prestress transfer from the prestressing strands to concrete takes place at the girder ends. Characteristic cracks form in this end region during or immediately after detensioning. Potential solutions to control end cracking were examined via finite element models and the impact of each solution on cracking was evaluated. Modifications to reinforcement bar size, debonding ratios, strand cutting sequence and use of draped strand patterns were simulated by the models. The results from different analyses were compared to quantify the success of each method in reducing strains causing girder end cracks. The tension strains leading to cracks of all types were responsive to debonding some of the bottom flange prestressing strands. Bottom flange cracking can be prevented by methodically debonding exterior strands, keeping the draped strands bonded, and evenly distributing the remaining bonded strands over the bottom flange.

17. Key Words prestressed girders, bridge girders, girder cracking, prestress transfer, strand cutting, detensioning, debonding, draped strands, finite element models, bulb-tees	18. Distribution Statement No restriction. This document is available to the public through the National Technical Information Service 5285 Port Royal Road Springfield VA 22161

19. Security Classif.(of this report) Unclassified	19. Security Classif. (of this page) Unclassified	20. No. of Pages 128	21. Price

FINITE ELEMENT ANALYSIS of DEEP WIDE-FLANGED PRESTRESSED GIRDERS to UNDERSTAND and CONTROL END CRACKING

Wisconsin Highway Research Program

FINAL REPORT

by
Michael G. Oliva, Professor
Pinar Okumus, Ph.D. Candidate

October-2011

SUMMARY

Hundreds of prestressed concrete girders are used each year for building bridges in Wisconsin. The prestress transfer from the prestressing strands to concrete takes place at the girder ends. Characteristic cracks form in this end region during or immediately after detensioning. These cracks are more severe for the heavily prestressed deep wide flange "W" girders. Girder end cracks create durability concerns. The problem can be structurally hazardous if cracks form paths for water to reach the steel strands allowing corrosion. The cracks in the bottom flange are close to the strands and can form such paths. This research primarily focused on finite element analyses of prestressed girder end regions to understand and recommend control methods for girder end cracking.

The previous research on girder end cracks utilized empirical, simplified linear elastic analytical, or strut and tie methods. This research uses nonlinear finite element modeling to simulate the behavior of deep wide flanged prestressed girder ends. The prestress transfer mechanism, concrete nonlinear and strain softening material properties needed to represent the steel to concrete stress transfer are important and included in the analysis. Finite element models of deep wide flanged W girders that account for cracking and the nonlinear behavior of concrete were created. Principal strain directions and magnitudes in the girder end matching the typical cracking patterns were identified.

Strains monitored in two prestressed girders during the detentioning process at prestress plants in Wisconsin and strains measured by other researchers on a girder end were used to verify the accuracy of finite element models. Acceptable correlations were obtained between strains predicted by the finite element models of the beams monitored and the test strain data.

Potential solutions to control end cracking were examined via finite element models and the impact of each solution on cracking was evaluated. Modifications to reinforcement bar size, debonding ratios, strand cutting sequence and use of draped strand patterns were simulated by the models. The results from different analyses were compared to quantify the success of each method in reducing strains causing girder end cracks.

The finite element analysis results showed that the concrete tension strains in the girder web, leading to horizontal web cracking, were sensitive to an increase in the size of the vertical end zone reinforcement bars closest to the girder end. Although up to 50% strain reduction was achieved by changing bar sizes from what are currently used, it was not possible to eliminate plastic tension strains in the girder end with practically sized web reinforcement bars.

Inclined cracking can be eliminated, for some girders, by removing the draped strands. The resulting strand eccentricity will then become closer to the bottom of the girder. As a result, removing draped strands also requires removal or debonding of bottom strands as a means of decreasing the strand eccentricity and controlling tension stress at the top of the girder. This solution makes the girder

much less effective in resisting vehicle loads. Reduced inclined cracking occurs if the draped strands are spaced further apart vertically. A wider spacing also results in a lower strand eccentricity and also requires changes in the bottom strand content, reducing the effectiveness of the girder.

The tension strains leading to cracks of all types were responsive to debonding some of the bottom flange prestressing strands. Bottom flange cracking can be prevented by methodically debonding exterior strands, keeping the draped strands bonded, and evenly distributing the remaining bonded strands over the bottom flange.

Finite element models where the exterior strands were detensioned first, exhibited large bottom flange tension strain and cracks. It is recommended to detension the interior strands first where possible.

Combining the solutions involving debonding, extra reinforcing in the web, and a controlled sequence of strand detensioning should lead to elimination of end cracking.

TABLE of CONTENTS

CHAPTER 1. INTRODUCTION

1.1. Problem Definition:

Prestressed concrete members have been an economical and high performance alternative for many years in highway bridge construction. The combination of in-plant fabrication under higher quality control and prevention of concrete cracking under service loads through prestressing leads to efficient, durable, and low maintenance structures.

Deep wide flanged prestressed girders recently gained popularity over other superstructure members for their ability to efficiently span longer distances due to high load carrying capacity. Their wider top flanges allow the girders to be spaced farther apart, minimizing the number of girders. Their slender cross sectional geometry provides an efficient span to depth ratio. Wisconsin has developed a series of these special girders denoted at "W" girders.

Girder end zones, where the prestress transfer takes place, often exhibit characteristic cracking during or right after the prestress is applied to the concrete. The cracking is more severe for deeper girders with higher amounts of prestressing. The deep frequently used wide flanged W sections of Wisconsin are in this category of girders. Their deep slender cross section and large bottom flange designed to accommodate heavy prestressing makes these girders particularly prone to cracking. An 82 in deep Wisconsin wide flange girder with severe end zone cracking is shown in Figure 1.

These cracks, if not subsequently enclosed in concrete end diaphragms during bridge construction, can provide paths for water with de-icing salt to seep into the girder. The bridge supports, where the girder ends are located, are corrosion susceptive locations because of the deck expansion joints above the girders at the end of the bridge. Girder durability problems may include the corrosion of steel rebar or strands leading to adverse effects on the structural capacity. Girders manufactured with cracks may cause an increase maintenance costs over the bridge life.

The research attempting to solve this problem, since early 1960's, utilized either empirical methods, simplified linear elastic analytical concepts, or strut and tie models to explain the stress field at the girder ends in the transfer region. These cracks, to this day, remain an issue despite the girder end design provisions of the AASHTO LRFD Bridge Design Specifications (AASHTO 2010).

Due to multiple sources of nonlinearity existing in the end zone, - the material nonlinearity of concrete and the redistribution of strains after cracking, fully explaining the strain distribution after the first cracks is beyond the capabilities of linear analyses or simple free body diagrams. Previous nonlinear stress analysis of the crack prone prestressed girder ends is not apparent in the existing literature. Today, with the help of the rapidly advancing computer hardware and finite element software technology, 3-D analysis with nonlinear properties can be conducted relatively efficiently.

Creating a representative nonlinear finite element model of a prestressed concrete girder is a challenging task. The challenges rise from factors including selecting an appropriate constitutive model for concrete - especially in tension, satisfactorily simulating the stress transfer mechanism between the strands and concrete, simulating the cracks and their effect in redistributing stresses, and incorporating the interaction of reinforcement steel with concrete

Prompted by the lack of comprehensive nonlinear analysis of the girder end region in the literature, this study uses nonlinear finite element analysis to assess the stress and strain distribution at girder ends during and shortly after prestress is transferred into the concrete.

Figure 1 – Typical cracking pattern of the deep wide flanged girders.

1.2. Scope of the Project:

This project aimed to investigate the behavior of the Wisconsin W wide flanged prestressed girder ends during and right after the strand detensioning process using nonlinear finite element analysis. The main outcome desired is to identify solutions that can control cracking in the girder end zones. Cracking can be controlled by reducing the concrete tension strain or introducing sufficient reinforcing to keep the concrete tension strains low and crack width limited.

The scope of the project covered the following tasks:

- To create a nonlinear finite element model detailed enough to predict the local behavior of the prestressed girder end zones of the wide flange girders reasonably accurately.
- To verify the results of the finite element models by performing strain measurements on prestressed girders during detensioning and by using available test results in the literature.
- To obtain girder stress and strain patterns during and after the detensioning process to understand the behavior causing cracking.
- To indentify the factors playing a role in each type of cracking and to propose methods that can potentially limit the cracking at the ends.
- To model and analyze a series of girders with different characteristics with finite element analysis to evaluate the impact of the potential solutions on the girder end cracking. The level of improvement of the cracks with each modification should be classified.
- To select the most feasible solutions for controlling prestressed girder end cracks as recommendations for bridge engineers and precast manufacturers.

The finite element models were created using a commercially available finite element software package, ABAQUS/CAE 6.9 (Dassault 2009). It provides a wide range of material models in its material library, including multiple models specific for concrete. Modeling the interaction of two parts is also available using the interaction models. Abaqus can perform complicated nonlinear analyses fast using distributed memory parallel direct solver technology. Abaqus seems to be the most widely used software in the academic research of concrete due to the flexibility it provides for the users with numerous options for material models, analysis and solution techniques.

1.3. Introduction to Wide Flange Girders

The standard Wisconsin wide flange girders, 54W, 72W and 82W have identical top and bottom flanges. The letter "W" is for wide flange and the number indicates the depth of the girders in inches. The four feet wide top flange makes these girders more attractive for projects where the number of girders can be minimized with larger girder spacings. The bottom flanges are designed to accommodate up to 52 strands. The maximum number of strands is lower for shallower sections and higher for deep sections. Cross sectional views of some of these sections can be seen in Figure 2.

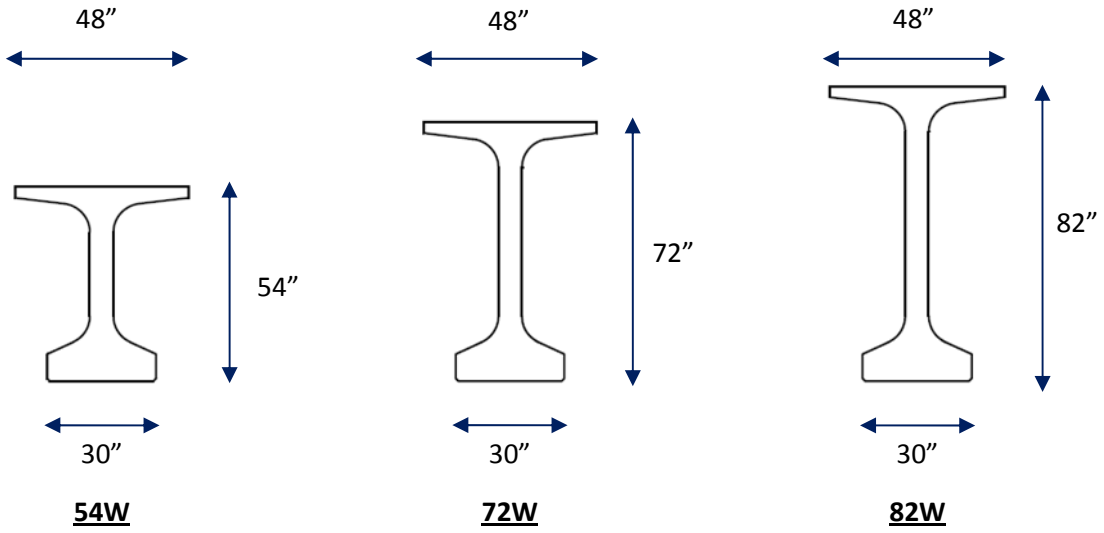

Figure 2 – Standard Wisconsin deep wide flange cross sections of 54W, 72W and 82W.

The standard end zone reinforcement details of these girders are identical and are shown in Figure 3. The standard details can be modified based on individual project needs.

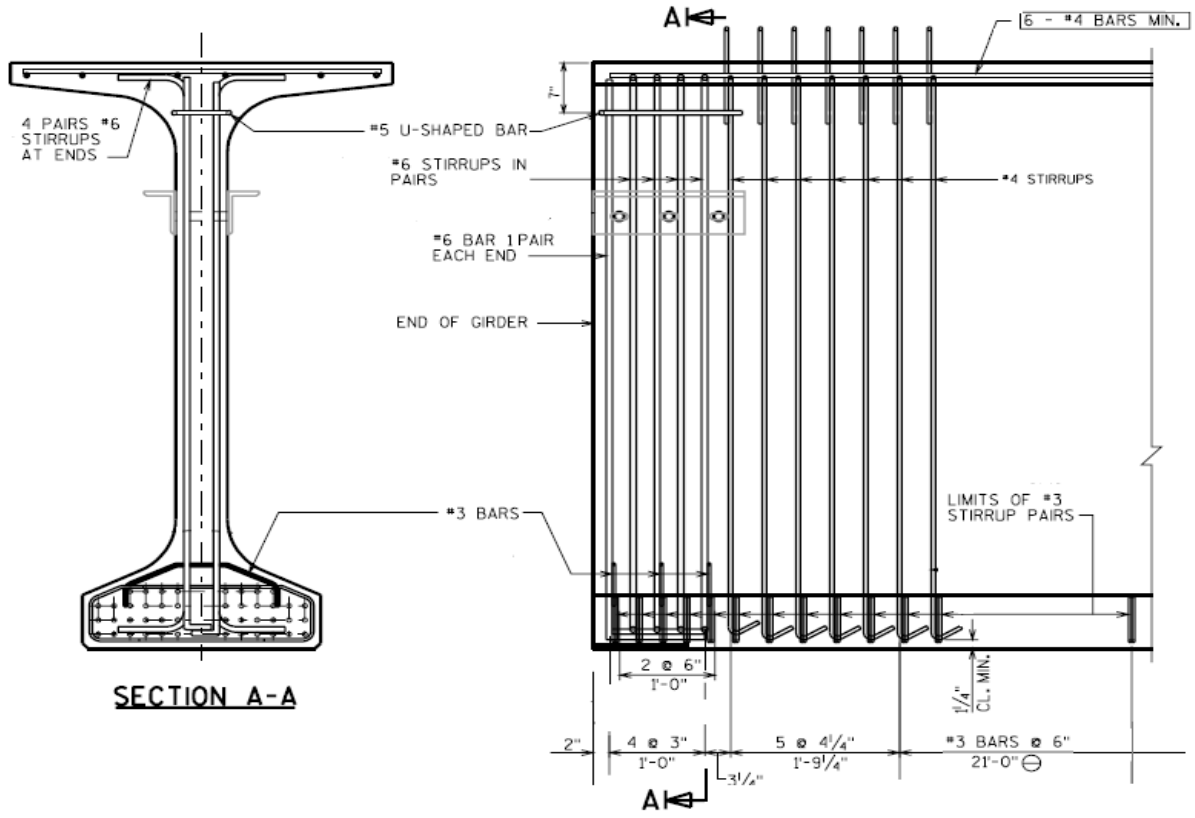

Figure 3 – Standard end zone details of 54W, 72W and 82W girders.

The two other sections in the wide flange girder family of Wisconsin are the W36 and W45. Although, these girders are categorized as wide flange girders, they have narrower top flanges. These shallower girders do not exhibit as severe cracking as the deeper sections. These girders were excluded from the finite element studies. However, in general, the research results would apply to these shallower sections as well.

1.4. Categorizing the Characteristic Cracks:

The cracks in deep wide flange girders follow characteristic patterns. Based on the typical location and the direction of the cracks, they are categorized into three groups: Inclined cracks, horizontal web cracks and Y cracks. These cracks are marked on the side and the cross section of a 72W girder end shown in Figure 4.

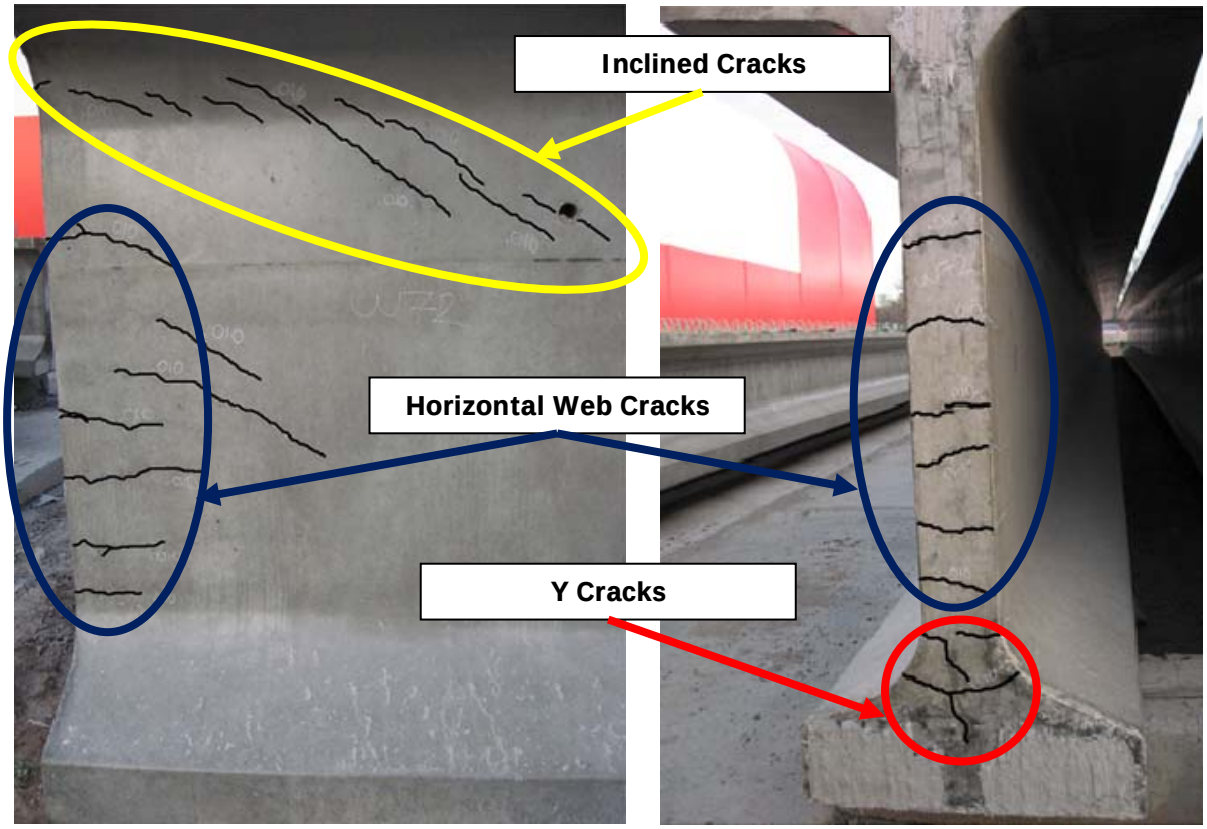

Figure 4 - Typical inclined, web and Y cracks marked on a 72W girder.

i. *Inclined Cracks:*

The inclined cracks typically form close to the draped strands. These cracks are the longest cracks detected on the ends of girders inspected during this project. Cracks as long as 54 in. are common

for deeper 82W girders. While some girders have one large inclined crack, others may have multiple smaller cracks following parallel paths. It is common to find these cracks going through weak points in the web such as the holes in the web designed to accommodate the bars for the end diaphragms. The inclined crack shown in Figure 4 crosses one of these holes.

The inclined cracks do not always extend to the girder end, indicating their formation does not likely start from the end. During lifting of the girder after prestressing, the size and length of these cracks were observed to get larger.

Since these cracks extend a long distance into the girder, they might not always be covered by cast concrete end diaphragms. These cracks will be exposed to the environment and could create durability problems.

The cracks below the main inclined cracks are transition cracks between the inclined and web cracks. Their angle with the horizontal plane gets smaller and finally becomes horizontal as they transform into horizontal web cracks.

ii. *Horizontal Web Cracks:*

These cracks lay horizontal in the web, appear to start at the very girder end and propagate into the girder. As shown in Figure 4, for most cases there are multiple horizontal web cracks lying along the entire height of the web. The length and the spacing of these cracks varies depending on the amount of prestressing and the girder depth. These cracks were observed to typically be shorter and smaller in width than the inclined cracks.

These cracks are not close to strands and it is likely that these cracks will be confined in concrete end diaphragms. Therefore, from a durability point of view, these cracks may be easier to tolerate.

iii. *Y cracks:*

When viewed from the end of a girder, these cracks resemble a Y or a T shape and are named after their shape. Figure 4 shows an example of a Y crack. These cracks separate the web, the left side of the bottom flange and the right side of the bottom flange. They appear to form at the junction of the bottom flange and the web. They are observed to start as horizontal cracks on both sides of the girder, merge in the middle of the cross section and typically move downwards to join the vertical crack in the middle plane of the bottom flange.

They are visible on the cross section at the end, and the horizontal braches propagate into the girder. They seem to start from the girder end.

These cracks are large in size, and close to the bottom flange strands. Due to their location and size, they have a high potential to form a path for corrosive salt water to reach the strands. If water reaches the strands, it can be wicked along the strand, causing extensive corrosion and threatening

structural safety. Therefore, these cracks are identified as the most hazardous of all crack types with an impact on not only the durability but also the structural capacity.

1.5. Code Compliance of the Standard Girder Ends:

The adequacy of the standard reinforcement for the end zone of the Wisconsin wide flange girders 54W, 72W and 82W was evaluated against the requirements of AASHTO LRFD Bridge Design Specifications{{60 American Association of State Highway and Transportation Officials 2008}} and CEB-FIP Model Code 1990{{85 Comité Euro-International du Béton. 1993}}.

The maximum number of strands these girders can accommodate, 52, was used for the calculations as it defines an upper bound condition. The standard reinforcement for a 54W girder was also checked with 40 strands, as this smaller section typically carries fewer stands than the maximum number.

AASHTO LRFD Bridge Design Specifications and CEB-FIP Model Code 1990 use different terminology to define the same behavior at the girder end. The bursting reinforcement defined by AASHTO LRFD Bridge Design Specification (in CEB-FIP Model Code this is called "spalling reinforcement") is a remedy for the stresses and cracking in the web. The confinement reinforcement in AASHTO LRFD Bridge Design Specifications is to confine the bottom flange strands and control the radial strains. This reinforcement is named "bursting reinforcement" in the CEB-FIP Model Code 1990.

Table 1 and Table 2 list the reinforcement area provided, compared to the reinforcement area required by both codes for bursting and confinement reinforcement respectively. They follow the AASHTO LRFD Bridge Design Specifications terminology.

Bursting Reinforcement Area (in^2)					
	Provided *in h/4 from the end*	**AASHTO 5.10.10.1** *in h/4 from the end*		**CEB-FIP Model Code** *in close vicinity*	
54W (40 strands)	3.976	3.525	√	4.485	X
W54 (52 strands)	3.976	4.570	X	6.214	X
W72 (52 strands)	4.811	4.570	√	7.663	X
W82 (52 strands)	4.811	4.570	√	8.496	X

Table 1 – Compliance of the standard wide flange girders with the code for bursting reinforcement.

Confinement Reinforcement Area/Length (in^2/in)					
	Provided *in 1.5d from the end*	**AASHTO 5.10.10.1** *in 1.5d from the end*		**CEB-FIP Model Code** *in $l_{bs}/3$ to l_{bs} from the end*	
54W (40 strands)	0.047	0.037	√	0.000	√
W54 (52 strands)	0.047	0.037	√	0.093	X
W72 (52 strands)	0.047	0.037	√	0.093	X
W82 (52 strands)	0.047	0.037	√	0.093	X

Table 2– Compliance of the standard wide flange girders with the code for confinement reinforcement.

The Tables show that all wide flange girder sections satisfy the AASHTO LRFD Bridge Design Specifications. The only exception to this is the 54W girder with 52 strands for the bursting (web) reinforcement. The longest span 54W girders are very unlikely to carry this many strands. The W52 girder with 40 strands is a better representation of the 54W girders. Overall, all it can be concluded that the girders meet the requirements of the AASHTO LRFD Bridge Design Specifications.

On the other hand, the CEB-FIP Model Code appears to be more conservative and therefore none of the standard wide flange girders satisfies this code. The basis for the CEB code is unclear.

1.6 Summary:

Prestressed precast concrete girders often present the most efficient and economical design alternative for medium span (50ft to 180ft) highway bridges. Wide flanged precast girders are more efficient than the previous AASHTO "I" type girders because they can accommodate higher prestressing. With higher prestress, the Wisconsin wide flanged girders (W sections) have exhibited increased cracking during application of the prestressing force than the previous "I" girders.

The girder end cracking can be described as three different types: 1) inclined cracks in the web generally in the vicinity of the draped strands, 2) horizontal web cracking, and 3) "Y" cracks in the bottom flanges. Of these different types, the Y cracks are thought to be the most hazardous because they have the potential to affect the durability and strength capacity of the girders.

Previous studies of girder end cracking have been empirical in nature or have utilized various forms of linear elastic analysis for stresses in the anchorage or prestress transfer region near the girder ends. Only strut and tie modeling has considered non-linear behavior, but it has only been used to predict capacity, not behavior under service loading.

Reinforcing currently used by Wisconsin near the girder ends, to restrain cracking, satisfies the AASHTO LRFD design requirements but still does not satisfactorily control the end cracking. The CEB code actually requires more end reinforcing in the 54W, 72W and 82W girders than Wisconsin uses.

This report will present a review of the current state of knowledge regarding the behavior of the end region of concrete girders where the prestress force is transferred, describe the preparation of a detailed non-linear finite element model (FEM) of girder end regions under prestress force, compare the FEM predicted internal strains with strains measured at precast plants in Wisconsin, study potential methods of controlling cracking through extensive FEM analyses, and recommend solutions that should be considered in Wisconsin.

CHAPTER 2. RESEARCH BACKGROUND

This chapter compiles selected existing research related to girder end zone cracking categorized as analytical, empirical or semi empirical and finite element analysis studies.

2.1 Analytical Studies:

Amongst the most widely known and valued analytical studies is the Gergely – Sozen model, where free body cuts are made with horizontal planes in the girder web near the end of the girder. Moments across these planes are calculated and then used to estimate the bending stresses on the plane (Gergely 1967). The maximum of these moments could be associated with the location of the first horizontal web crack and is utilized to calculate the necessary resisting vertical rebar area. This method neglects any nonlinear inelastic behavior of the concrete and therefore it would only be a valid representation of the precracked phase of concrete. The same study also used an elastic solution based on a two dimensional Airy stress function to create the contour plot of transverse stresses under a load applied at the very end, representing a post tensioned loading. Today, this type of output can easily be produced using current commercial finite element software but is unlikely to give correct results when cracking and inelasticity occurs.

Other analytical research (Castrodale 2002, Crispino 2009) investigated the strut and tie method for the design of the girder end region, or strut and tie specifically for post tensioned girders. The strut and tie method is a powerful tool to evaluate the location of tensile stresses in disturbed regions such as prestressed girder ends near the failure condition. However, it is an upper bound estimate of the failure capacity, there is more than a single truss configuration for a given case, and it is based on the assumption that cracking has already occurred.

2.2. Empirical or Semi Empirical Studies:

The majority of previous research work consists of empirical or semi empirical studies. Via strain gages, the magnitudes of strains on end zone rebars or on concrete have been measured during prestress release. AASHTO LRFD Bridge Design Specifications, Article 5.10.10.1 seems to have adopted the equation derived from the experimental study conducted by Marshall and Mattock (Marshall 1962) to calculate the stirrup area at the end of the girders.

Tuan et al. (Tuan 2004) and Dunkman et al. (Dunkman 2010) also monitored strains on the vertical end zone stirrups and made recommendations on the effectiveness of the reinforcement. The measured strain values gave rise to practical recommendations on the end zone reinforcement efficiency. Strain data collected by strain gages, however, is limited to discrete locations and may not be indicative

of the strains in the adjacent concrete due to imperfect bond between the steel and concrete and discrete locations of concrete cracks. Finite element analysis can provide the strain field for the entire continuum in any direction; can help explain what triggers cracking and can also be used for parametric studies with minimal cost.

Steinberg et al. (Stainberg 2001) measured the strains in and on the surface of rectangular girders during prestress release.

Mirza and Tawfik (Mirza 1978) investigated vertical cracks at the ends of rectangular prestressed girders through testing and a linear uniaxial spring series analogy. They noted the restraint effect, due to the uncut strands, in creating vertical cracks.

2.3. Finite Element Analysis Studies:

Kannel et al. (Kannel 1997) utilized finite element modeling to simulate the restraint that uncut strands create on concrete depending on the order in which the strands are cut in a pretensioned beam. They identified the restraint as potentially leading to vertical and horizontal crack formation. The main shortcoming of that model was the use of linear elastic material properties for the concrete. The authors emphasize that the aim of the study was to prevent cracking, and therefore for a desired crack free case the linear elastic model would be sufficient. They state that "Because of the … and the simplified assumptions used to describe the concrete behavior and stress transfer mechanisms, the finite element model was not expected to capture the complex nature of the stress field in the end region of a girder particularly accurately. However the model was judged adequate to help reveal general trends such as those related to changing the strand cutting order." They have utilized the finite element modeling software, ABAQUS. The concrete was modeled with 3D elastic elements. Truss elements were substituted for the strands. To model the concrete/strand bond behavior at the stress transfer region, two methods were implemented: assigning a varying area for the truss elements along the transfer length and using springs to connect the truss to concrete elements.

Myers et al. (Myers 2001) investigated the effect of thermal changes on girder end cracks through a two dimensional linear elastic finite element model.

Via two dimensional linear finite element models, Breen et al. (Breen 1994) simulated a post tensioned girder, where the stress transfer mechanism is concentrated at the girder end, a case much simpler compared to the gradual stress transfer in pretensioned girders.

None of the previous research directly combined inelastic material behavior (concrete cracking) and the effect of strand de-tensioning to investigate end crack under service conditions.

CHAPTER 3. FINITE ELEMENT MODEL PROPERTIES

3.1. Model Girder Description:

Detailed finite element models of Wisconsin 54W, 72W and 82W girder sections were created to identify the causes of the observed end cracking. The properties for the girders were picked considering sections that represent the higher capacity/long span range of the girder groups. Higher capacity girders have a higher tendency for cracking as they are more heavily prestressed. Selected girders for finite element modelling are shown in Table 3. The maximum spans recommended for each girder by the Wisconsin Department of Transportation Bridge Manual are also shown as a comparison. The models followed the properties of girders taken from real bridges, as also listed in Table 3.

Girder	Finite Element Model			Max Span for a Single Span
	Girder Length	Number of Strands	Resembles a girder in bridge	
54W	129 ft	32 straight + 8 draped	B-06-0159	132 ft
72W	154 ft -9 7/8 in	40 straight + 8 draped	B-28-0147 (span 1)	160 ft
82W	159 ft	38 straight + 8 draped	B-49-0141(span 11)	184 ft

Table 3 – Properties of the selected girders modeled using finite element modeling.

The finite element models use the standard geometries and the standard end zone reinforcement details of the WisDOT standards as shown previously in Figure 2 and Figure 3.

3.2. Material Properties:

3.2.1. Concrete Material Properties:

Material nonlinearity, particularly for concrete tension, was a key part of this cracking focused problem. Linear elastic material models are considerably simpler compared to nonlinear material models. They can, however, only represent the concrete behavior accurately up to the point of the first cracking. Cracking was observed to occur relatively early during the detensioning process. After cracks form, stresses are redistributed in the girder end and the reinforcement bars restrain the crack opening. Material models which do not capture the stress loss of the concrete elements during cracking are not capable of representing this redistribution. Imitating the concrete nonlinear behavior is difficult, especially in tension since tensile failures are rather brittle and tensile tests to obtain the material behavior are hard

to perform. A further difficulty can develop since misrepresenting the material model may result in convergence problems with the finite element software or lead to excessive errors in the results.

In order to decrease the computational cost, nonlinearity is only assigned for the concrete material near the girder end where cracking is expected. The rest of the girder was modeled as linear elastic. This assumption is not expected to result in measurable error, since no cracking of interest is expected away from the girder end. The length of the region at the girder end with nonlinear material properties was selected at least as long as the girder depth. At a distance equal to the depth of the girder away from the end, the girder is assumed to follow the Bernoulli beam theory with the strains linearly distributed over the beam section. Therefore, the linear material model is anticipated to be capable of capturing the behavior away from the girder ends.

Specific for concrete, three different constitutive models are available in the computer analysis software Abaqus/CAE: "the smeared cracking", "the brittle cracking" and "the concrete damaged plasticity" models. The "concrete damaged plasticity" modeling was selected for this study. It allows the users to define the nonlinear stress strain relationship of concrete both in compression and tension under arbitrary loading conditions. Degradation of elastic stiffness due to plastic straining, or stiffness recovery can be implemented.

3.2.1.1. Compression:

The "concrete damaged plasticity" model allows the users to define the stress strain relationship in two parts in the linear elastic range and the nonlinear plastic range as summarized below.

1. Abaqus software assumes that in the elastic range stresses are linearly proportional to strains. A modulus of elasticity value and an elastic stress limit are input into the material model.

For the finite element models, the elastic limit of stress was assumed to be 40% of the design strength. The modulus of elasticity for strains below this limit was calculated using AASHTO LRFD Bridge Design Specifications - Section 5.2.4.2.

2. Once the linear stress limit is exceeded, plastic deformations start to take place in compression. The relationship is no longer linear between stresses and strains. The stress function can take any shape and is input in a tabular form in Abaqus.

In the current finite element models, the mathematical model given by the FIB Model Code 2010, Volume 1, Section 5.1.8.1 was utilized to define this second portion of the stress-strain relation. This model is summarized in Figure 5 and Equation 1.

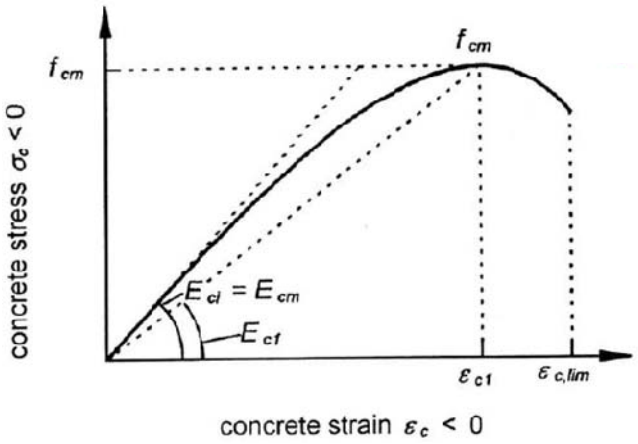

Figure 5 – Stress – strain relationship of concrete in compression by FIB 2010 Model Code to be used with Equation 1 (Fédération Internationale du Béton).

$$\frac{\sigma_c}{f_{cm}} = -\left(\frac{k \times \eta - \eta^2}{1 + (k-2) \times \eta}\right) for\ |\varepsilon_c| < |\varepsilon_{clim}| \qquad \text{Equation 1}$$

where:

$\eta = \varepsilon_c / \varepsilon_{c1}$

$k = E_{ci} / E_{c1}$

The values of the constants needed in the material model equation are provided by FIB 2010 Model Code for grade C12 (2900 psi) to C120 (18600 psi) concrete. The descending part of the compressive curve is not given in the Model Code due to the strong dependency of this part on the specimen, member geometry, size, boundary conditions and the possibilities of load redistribution in the structure. The lack of the material model for the descending portion of the stress strain diagram of concrete does not affect the current finite element models since the compression stresses studied for this research do not nearly reach or exceed the ultimate strength.

The resultant compression material model for linear elastic and nonlinear plastic parts for the 7000 psi concrete assumed for the current girders is shown as an example in Figure 6.

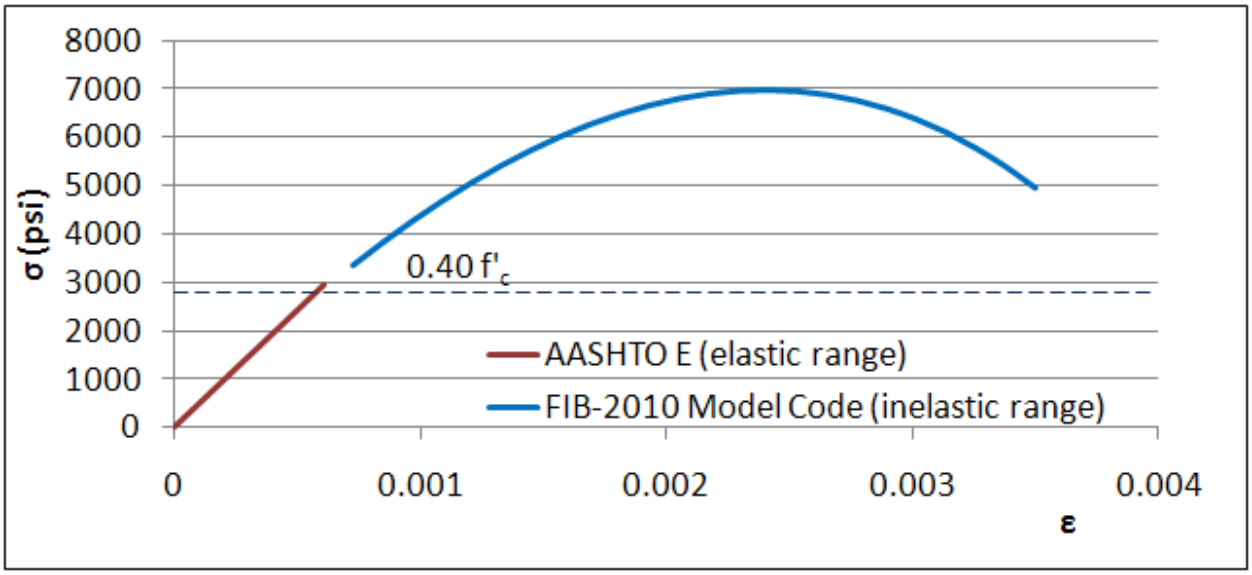

Figure 6 – Example compression model used in FEA for 7000 psi concrete.

2.2.1.2. Tension:

The tension in the "concrete damaged plasticity" model is also composed of two discrete parts: the pre cracking and post cracking stages. These stages are explained below as defined by Abaqus.

1. The Abaqus software assumes that, before concrete reaches its cracking strength, the strains are linearly proportional to stresses. A linear stress strain relationship governs this portion via defining the modulus of elasticity. A single modulus of elasticity value is defined for concrete in compression and tension. The user also defines the cracking strength of concrete in tension as a boundary for this region.

For the girder finite element models, the modulus of elasticity in the elastic strain region was calculated using AASHTO LRFD Bridge Design Specifications, Section 5.2.4.2, as for the compression behavior. The cracking strength was calculated per AASHTO LRFD Bridge Design Specifications Section C5.4.2.7.

After the stresses reach the cracking limit, cracks will start to form. The "concrete damaged plasticity" model of Abaqus then defines the material behavior in terms of strains, crack opening or the fracture energy. Abaqus allows this part of the stress function to take any form.

The Abaqus Analysis User's Manual (Dassault Systèmes Simulia Corporation 2009) discusses the potential mesh sensitivity for results due to narrower crack widths with finer meshes. Typically this problem occurs if the crack occurs at localized regions and mesh refinement does not result in additional cracks. Two methods are used to overcome this mesh sensitivity.

Using reinforcement bars connected to the concrete elements reduces the mesh sensitivity as this tends to distribute the failure strains. Tension stiffening is introduced to concrete to represent the added ductility that would be provided by the reinforcement bars after cracking. Numerical solutions are more easily achieved with larger tension stiffening.

For regions without reinforcement, using the concept of fracture energy to define a stress-displacement (crack opening) behavior rather than a stress-strain behavior is reported to generally solve the mesh sensitivity. Fracture energy (G_F) is a material property and is defined as the energy required to form a unit area of crack. Abaqus handles the conversion between the displacements and strains using "the characteristic length" of each element. This length is equal to the length of a line across an element for a first order element. Elements with aspect ratios close to one are important to avoid mesh sensitivity in the results.

The post cracking behavior of concrete was modeled using the bilinear mathematical model given by FIB 2010 Model Code, Volume 1, Section 5.1.8.2.

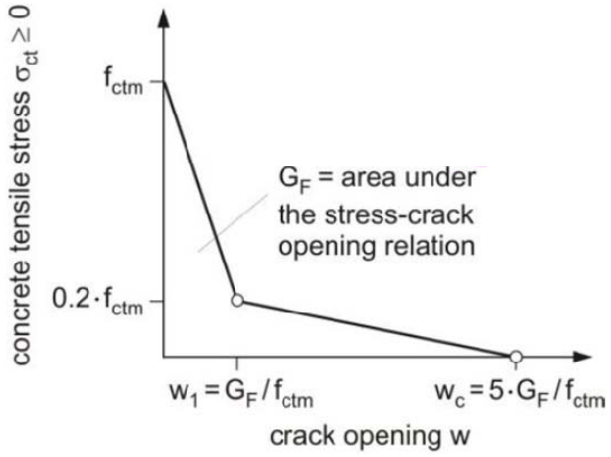

Figure 7 - Stress - crack opening relationship of post cracking behavior of concrete in tension by FIB Model Code 2010 to be used with Equation 2 and Equation 3.

$$\sigma_{ct} = f_{ctm} \times \left(1.0 - 0.8\frac{w}{w_1}\right) for\ w \leq w_1 \qquad \text{Equation 2}$$

$$\sigma_{ct} = f_{ctm} \times \left(0.25 - 0.05\frac{w}{w_1}\right) for\ w_1 < w \leq w_c \qquad \text{Equation 3}$$

In Figure 8 shows an example of tensile material input into Abaqus for 7000 psi design compressive strength concrete. The precracking behavior is expressed in terms of a stress-strain relationship, while the postcracking behavior is expressed with a stress – crack width(w) relationship.

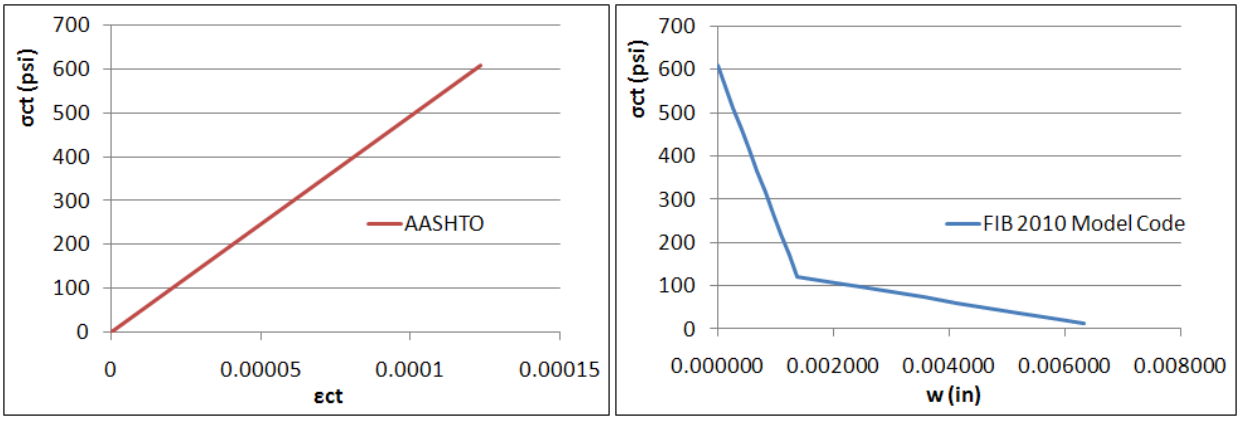

Figure 8 - Example tension model used in FEA for 7000 psi concrete for the precracking (left) and post cracking (right).

3.2.2. Reinforcement Bar Material and Bond Properties

AASHTO LRFD Bridge Design Specifications, Section 5.10.10.1 does not allow vertical girder end reinforcement bars to be designed for stresses exceeding 20 ksi. Preliminary finite element models also showed that the reinforcement bars carry stresses far below their yielding stress.

Reinforcement bars are modeled as linear elastic elements. Yielding of steel rebars is omitted from the model, since no rebars experience stresses high enough to cause yielding.

The modulus of elasticity is taken at 29000 ksi as given by the AASHTO LRFD Bridge Design Specifications, Section 6.4.1.

The interaction of reinforcement bars and concrete is modeled through tension softening (called tension stiffening in Abaqus) of concrete implicitly. The added ductility of the concrete after cracking, provided by the reinforcement bars, is included through this tension stiffening in concrete material properties. Once concrete elements reach their cracking limit, their load carrying capacity drops with increasing deformations. Larger loads are then transferred to the steel rebars. The degrees of freedom of the rebar and concrete elements are restrained to be the same and the stresses are distributed to the surrounding rebar elements once concrete elements soften.

Too little tension stiffening in the concrete material can cause local cracking failures to introduce temporary instability and eventually will lead to convergence problems. This usually indicates unreasonably low tension stiffening, as practical designs do not generally exhibit this behavior.

3.2.3. Strand Properties

The strands are not explicitly included in the finite element models. Voids are left in the concrete where the strands are located. Then the prestressing force is directly applied over the transfer length to the concrete at each strand location. The strand loads simulated were for 0.6 in diameter 270 ksi low relaxation strands. Lifting loops were ignored is the analytic model.

3.3. Boundary Conditions

The size of the model is proportional to the computational cost of the analysis. One way to decrease the size of the model is to utilize symmetry. The girder geometry is symmetric about a mid span vertical plane perpendicular to the span length and also about a vertical plane parallel to the span located at the center of the beam. The loading is also symmetric around both planes, assuming the dead and live ends of the girder do not differ from each other significantly in terms of transferring the prestress. The strands are assumed to be cut symmetrically on each side of the bottom flange which is usually the case in prestress release.

Axes used with the model are shown in Figure 9. Symmetry conditions applied at the midspan about the X-Y plane and about the Y-Z plane in the middle of the cross section are shown in Figure 9. The model size is reduced to one fourth of the full model using symmetry.

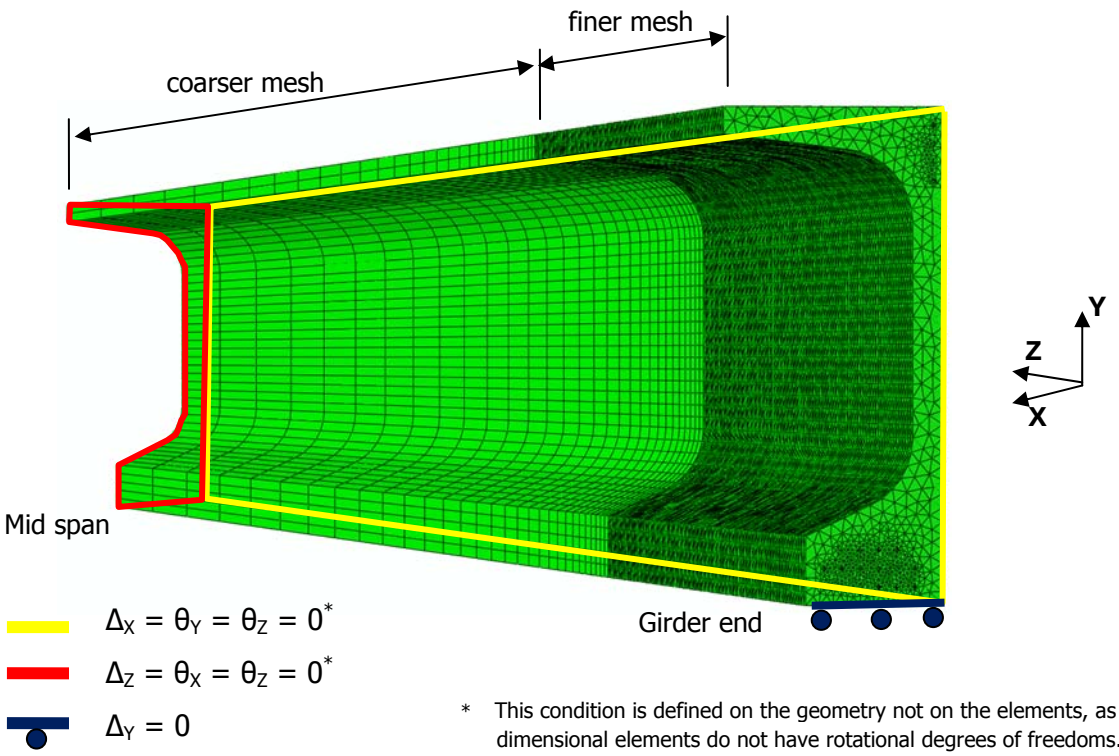

Figure 9 – The boundary conditions and the mesh of the finite element models. (yellow and red lines denote the boundaries of the sections cut by symmetry planes)

The bottom corner of the girder end is restrained against displacements in the Y direction only, the girder is free to rotate and deflect in the longitudinal or lateral direction as shown in Figure 9. This assumes that the girder will camber up at midspan and remain supported on the edge of the bottom flange at the end of the girder.

3.4. Loads

The cracking occurs immediately after the prestress release when there is no service load on the girder. Therefore the main loading considered for the finite element analyses was the prestress transfer to the girder. Time dependent effects, such as thermal contraction and creep, were irrelevant during the short interval when cracking occurred. The removal of force on the girder, at release of the draped strand hold-down, was not modeled since it occurs before the prestress release and cracking event.

The prestress load is transferred to the girder via bond and friction at the girder end over a distance called the "transfer length". The research results on measuring the transfer length in the

literature are rather scattered as stated by Buckner (Buckner 1995) and Tabatabai and Dickson (Tabatabai 1993).

The AASHTO LRFD Bridge Design Specifications, Section C.5.11.4.2, idealizes the transfer length as 60 times the strand diameter and the bond stresses as uniformly distributed over the length as shown in Figure 10. The transfer length portion is highlighted in the Figure. At the girder end, where the slip of the strands occur, the stresses in the concrete are zero. At the end of the transfer length, the concrete carries the full effective prestress from the strands.

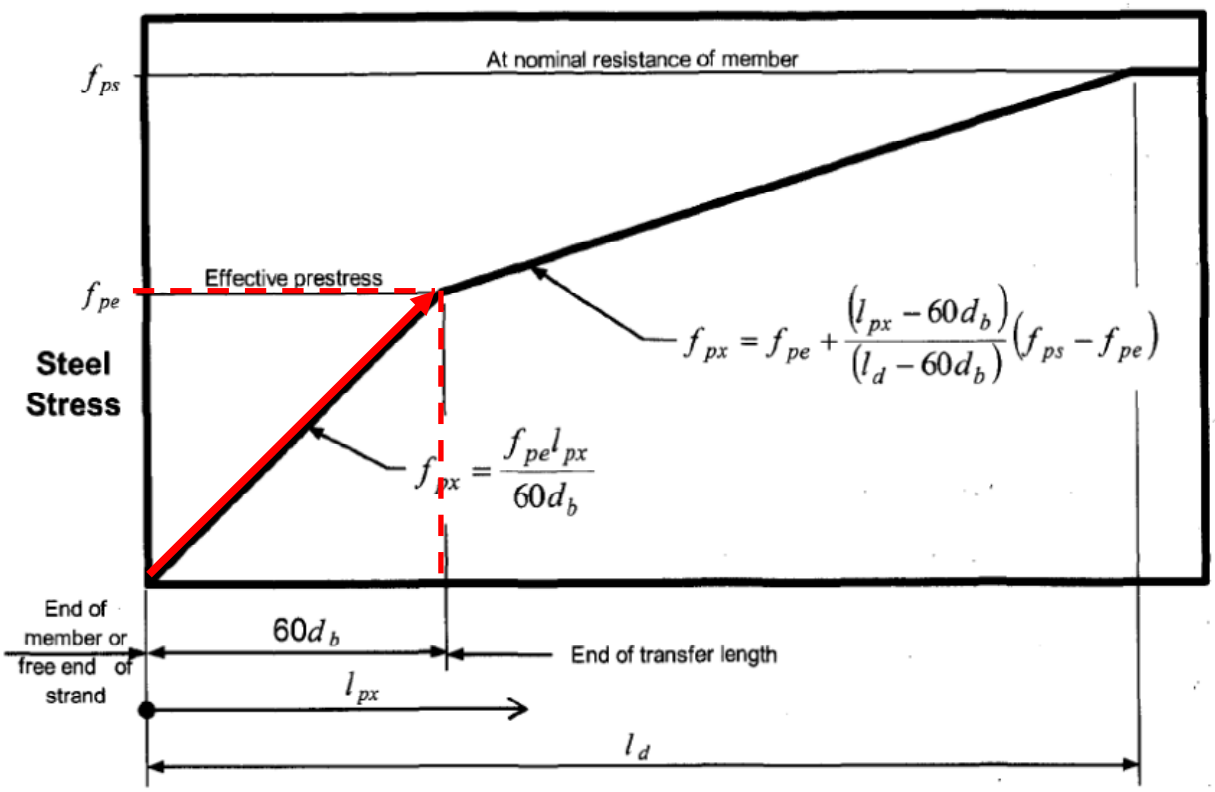

Figure 10 – Idealized relationship between the steel stress and the distance from the end (from AASHTO 2010).

The transfer length for the 0.6 in strands was calculated as 36 inches from this relationship. A 36in transfer length and a uniform bond stress distribution along the transfer length was intended to be used for all the girder models unless test data on the transfer length was available.

The strands were excluded from the models, and the bond stresses were directly applied on concrete over the transfer length at the locations of the strands. 0.6 in diameter holes were cut out from the girder, the stresses are uniformly distributed on the inner surface of these holes as shown in Figure 11. More accurate modeling would have included strands or simulated the radial expansion that occurs in the strand, due to Poisson's effect, when they are released. Preliminary calculations showed that this

radial expansion was minor compared to the strains induced by the prestress compression on the concrete and it was assumed that the Poisson effect could be ignored.

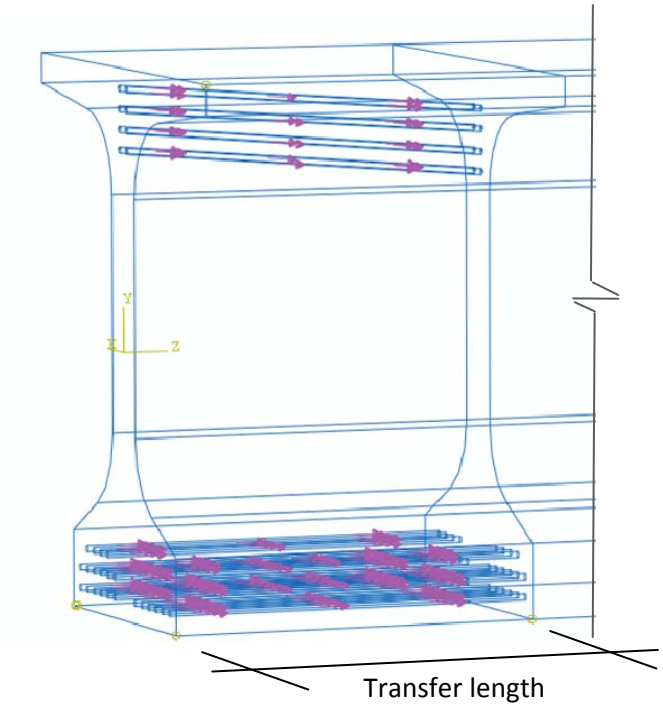

Figure 11 – Distributed bond stresses simulating the effect of the strands in applying prestress over the transfer length.

The stresses on different strand locations are applied at different steps in the analysis, simulating various sequences in which the strands are cut. This way, the instances when cracks occur or stress distribution changes can then be tracked.

Temperature induced stresses and time dependent stresses, such as shrinkage and creep, are neglected. The dynamic effects due to the sudden cut of prestressing strands are not included. The gravity loading from the weight of the member is applied in some cases where the moment created by the gravity load was important. At the end of the simply supported girders this moment is negligible. Gravity loading would be included for the parts of the girder away from the ends if those locations were to be examined as points to end debonding of strands.

3.5. Finite Element Type and Order:

3.5.1. Concrete Elements:

For the nonlinear girder end region, three dimensional tetrahedral elements (denoted as C3D4 in the Abaqus Element Library) as shown in Figure 12 were used. Tetrahedral elements are the most practical elements to fill in arbitrary shapes when automated meshing techniques are used through commercial mesh generators. The use of 0.6 in diameter holes for the strands, especially with the draped strands, leads to an irregular geometry. Although hexahedral elements are usually more cost effective in computing time, significant model preparation is avoided through the use of tetrahedral elements. The tetrahedral elements used were 4 node, first order (linear) interpolation elements, i.e. constant strain elements.

For the linear elastic region away from the girder end, three dimensional linear 6 node triangular prism elements (denoted as C3D6 in the Abaqus Element Library) were used. These elements are also shown in Figure 12.

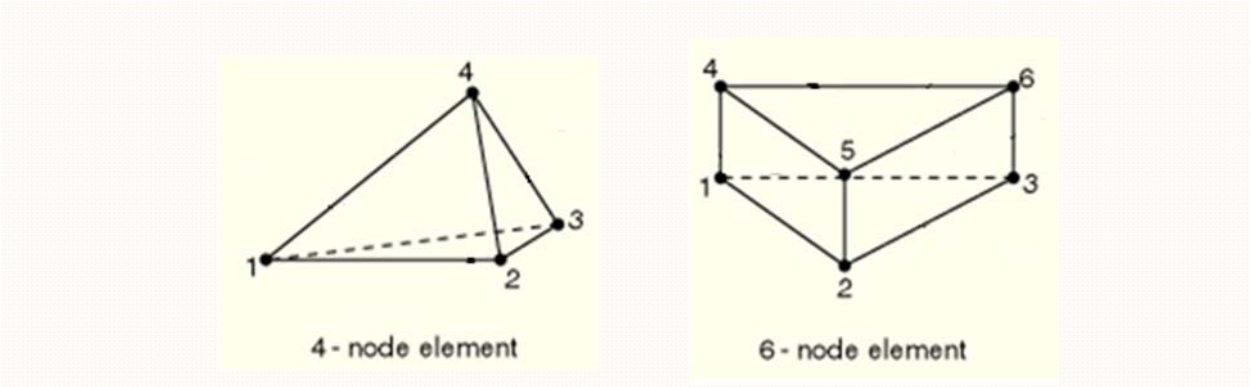

Figure 12 – 4 node linear tetrahedral (left) and 6 node linear triangular prism (right) elements (from Dassault 2009).

The Abaqus Theory Manual (Dassault 2009) notes that second order elements generally give much higher accuracy per degree of freedom for the solution of elliptic problems such as elasticity problems. The level of mesh refinement needed for second order elements is smaller than the first order elements. However, for plasticity applications of hyperbolic behavior, the Abaqus Theory Manual reports that the first order elements are in general preferred.

3.5.2. Steel Reinforcement Bar Elements:

Steel reinforcement bars were created as 2 node linear three dimensional trusses (denoted as T3D2 in the Abaqus Element Library).

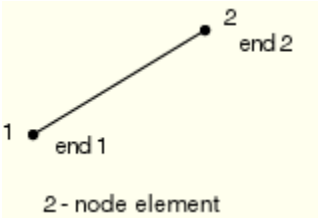

Figure 13 – 2 node linear truss element (from Dassault 2009).

The rebar elements were "embedded" in concrete. In Abaqus, this means that the response of the concrete elements is used to constrain the translational degrees of freedom of the rebar nodes. Translational degrees of freedom of the rebar elements are constrained to the interpolated values of the corresponding degrees of freedom of the concrete elements.

3.6. The Mesh:

Due to material nonlinearity, the models need considerable computation time and space. Finer meshes lead to more accurate results but the computational cost was also a factor in selecting the mesh size.

At the girder end, the main region of interest, a finer mesh was used. A finer mesh is expected to provide a much more accurate solution for this inelastic material. Since errors away from the girder end can be more easily tolerated, the element size was gradually increased along the girder length away from the end. An example of a meshed model was shown in Figure 9.

Error indicators provided by Abaqus were used to judge the relative accuracy of the models and the corresponding computational cost with a varying mesh size at the girder end. Element energy density records the solution of each step and is suitable for nonlinear problems with multiple steps. These error indicators should not be interpreted as the percentage error in the resultant strain or stresses. Figure 14 presents the normalized error in the models and the CPU times with increasing number of elements for a 54W girder.

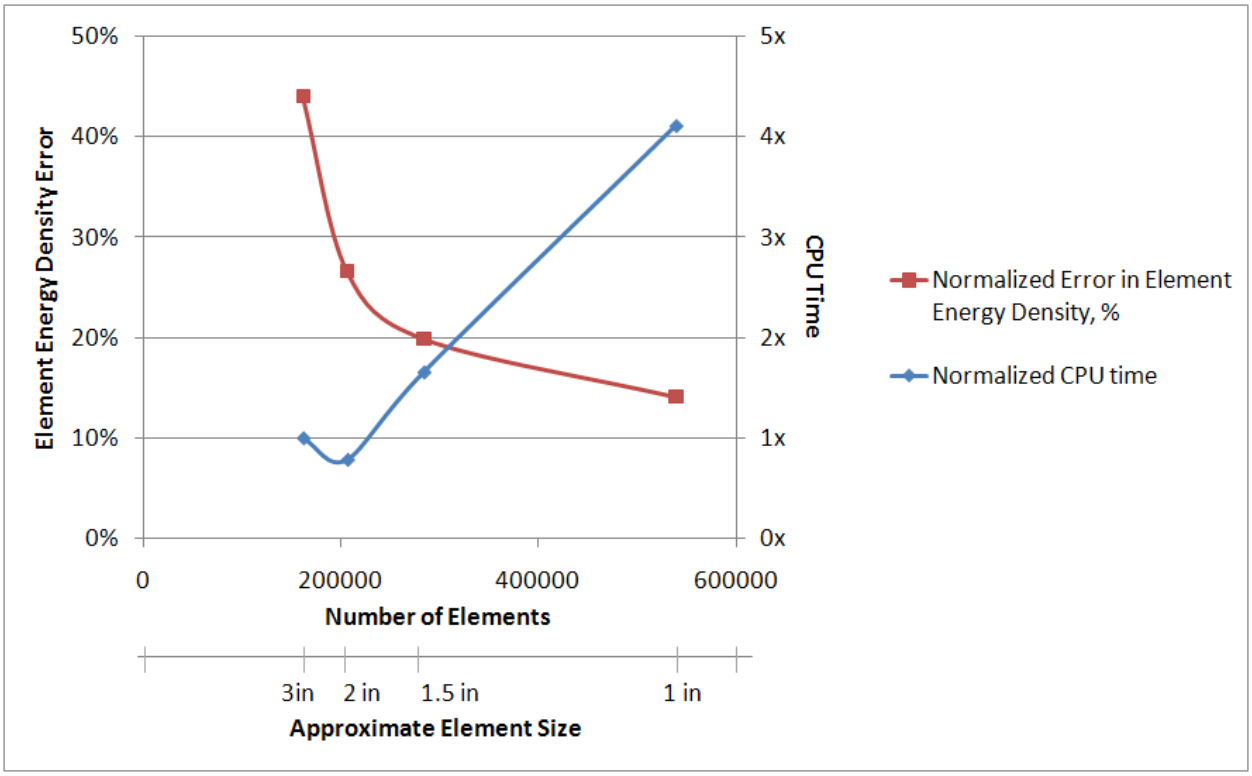

Figure 14 – Normalized Element Energy Density Error and CPU time versus mesh size for a 54W girder.

1.5 in element size seems to lower the element energy density error reasonably well. Therefore for this study, none of the models had element side lengths exceeding 1.5in in the inelastic region. Convergence could not be achieved with element sizes of 3in and larger.

Element sizes compatible with the concrete elements were used for the rebar elements as this was observed to improve the convergence.

3.7. Solution Method:

All analyses performed were nonlinear static analyses.

The equation solver used was "direct" as opposed to "iterative". In nonlinear analysis, Abaqus solves a set of linear equations at each iteration. The "direct" equation solver uses a sparse, direct, Gauss elimination method. This part is the most time consuming part of the analysis especially for large models and storage of the equations also takes the largest disk space. On the other hand, the "iterative" solver finds approximate solutions to the linear system of equations. It is likely to be faster than the direct solver for large structures. However, this method was not preferred since the convergence of the nonlinear problem is affected by the convergence of the iterative solver. If the analysis fails to converge, it is difficult to determine the origin of the failure as it could be the solver or the solution failing to converge. Any ill conditioning with the model, or large discontinuities in the material model would also

lead to slower convergence and would irrationalize the use of this method (Dassault 2009). The nonlinear analysis used the "Full Newton" method as the solution technique.

During each load step, Abaqus adjusts the load increments by judging if convergence is likely or not. The user has control over the initial load increment size of each load application step. For this analysis the initial load increment size was decreased for steps where cracks or nonlinear behavior was expected to avoid unnecessary iterations and to accelerate the analysis.

3.8. Simplifications, Limitations or Assumptions

Some characteristics of the girder end zone behavior were neglected to simplify the analysis. These factors, some of which were discussed in more detail earlier, are listed as:

- The transfer length of each strand was assumed to be the same regardless of their location. AASHTO LRFD Bridge Design Specifications were followed in determining the transfer length and the bond stress distribution.
- The load from the strands to concrete is transferred rapidly during the pretension release process. The dynamic loading effect when each strand is cut was neglected. The dependence of the concrete material property response on rapid loading was also neglected.
- The creep and shrinkage induced strains are neglected. These strains are anticipated to be considerably lower than those created by the prestress load.
- The compression strength values used in the models were specified strengths at release or strengths determined by cylinder tests at release - if available. The material constitutive models in compression and tension were created with these early strength values. The stress strain relationship given by AASHTO LRFD Bridge Design Specifications or FIB Model Code 2010, on the other hand, represented 28 day concrete behavior.
- The restraint provided by the uncut strands during prestress release was neglected. This effect was mentioned as the cause of vertical cracks in the literature (Mirza 1976, Kannel 1997). Since Wisconsin does not experience these vertical cracks, the impact of strand restraint on the present cracks was excluded from this study.
- The mechanical interlock of the strands into the concrete was neglected. The strands, when cut will expand radially and exert a radial pressure on concrete. This pressure may be small compared to other radial pressures such as the bursting pressure.
- The reinforcement bar slip was not modeled explicitly but is rather accounted for by introducing the tension stiffening in the material properties of concrete as discussed in more detail in Chapter 3.2.2.

- The bond loss between the strand and concrete due to crack formation was neglected. Excluding this effect from the models was assumed conservative in predicting girder end strains.

CHAPTER 4. VERIFICATION of THE FINITE ELEMENT MODEL

Finite element analysis is an idealization of the geometry, material properties, boundary conditions and loadings of a structure to create a mathematical representation of the problem. Including every detail of the physical system in the model, especially for problems of a complex nature, will compromise the computational efficiency. For the current modeling of concrete precast girders, details that were not needed to significantly improve the accuracy were omitted from the models. Assumptions which simplify the analysis were implemented as discussed in the previous section. This chapter checks the level of accuracy of the FEM models as compared to test data taken from multiple cases.

Strains in two 54W girders, each manufactured by two different precasters in Wisconsin, were monitored during prestress release and shortly after the release. The two girders, from *Spancrete, Inc* and *County Materials Corporation*, had different designs and a different number of strands. Strain gages were placed in different locations in the two girders. The strains could serve as a basis for comparing with predicted strains from a FEM model. The results of this comparison is not meant to examine the manufacturing process of the two manufacturers, it is rather to gather data to be able to verify the finite element models.

Additional verification of the finite element models was obtained through reported test data identified through the literature review. Research by O' Callaghan (O'Callaghan 2008) included comprehensive testing of 70in deep Texas girders and reported strain values for reinforcement that could be used as additional means of verifying FEM analysis predictions.

A theoretical cracking strain for the test specimens was calculated assuming a linearly proportional strain stress relationship for concrete in tension until cracking. **Equation 4** and **Equation 5** were used as given by AASHTO LRFD Bridge Specifications Section C5.4.2.7 and Section 5.2.4.2, respectively.

$$f_r = 0.23 \times \sqrt{f'_c} \qquad \text{Equation 4}$$

$$E_c = 33000 \times K_1 \times {w_c}^{1.5} \times \sqrt{f'_c} \qquad \text{Equation 5}$$

where

$f'_c = specified\ compressive\ strength\ of\ concrete\ (ksi)$

$E_c = modulus\ of\ elasticity\ of\ concrete$ (ksi)

$K_1 = correction\ factor\ for\ source\ of\ aggregate\ (taken\ as\ 1)$

$w_c = unit\ weight\ of\ concrete\ (kcf)$

4.1. 54W Girder Manufactured by Spancrete, Inc:

4.1.1. Girder properties:

An initial pilot program of data measuring with a prestressed wide flange girder was undertaken at a Spancrete precast plant, and was one of nine girders manufactured in December 2009 for a single span Wisconsin bridge numbered as B-06-159. The girders were standard 54W (54in deep, wide flange) girders with the cross section and end reinforcement details shown in Figure 15. The prestressing strands are excluded in the Figure. This standard shape used in Wisconsin is a cross section that was expected to develop the characteristic cracking based on previous experience.

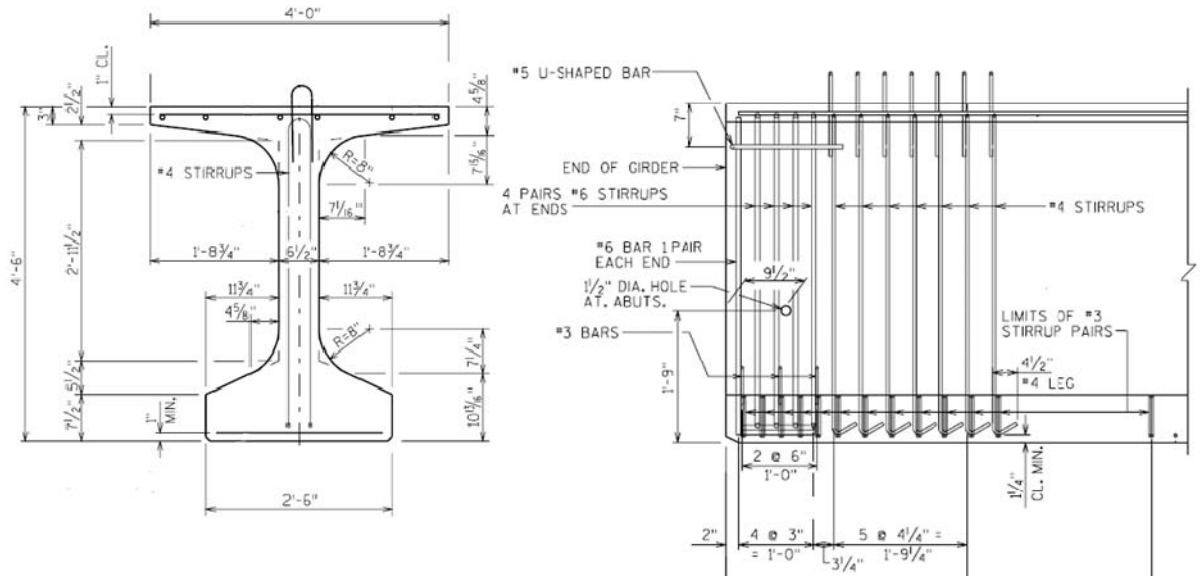

Figure 15 – Cross section details and end reinforcement of the Spancrete 54W girder (from Wisconsin Bridge Manual).

The girder was 129 ft long. It had 8 draped and 32 straight 270 ksi low relaxation strands. The center of gravity of the draped strands was 5 inches from the top of the girder. The strand pattern at the end of the girder is shown in Figure 16. Cylinder strengths at prestress release were made available via cylinder tests performed by Spancrete Inc. prior to the de-tensioning of the strands. The prestress transfer occurred approximately 19 hours after the girders were cast.

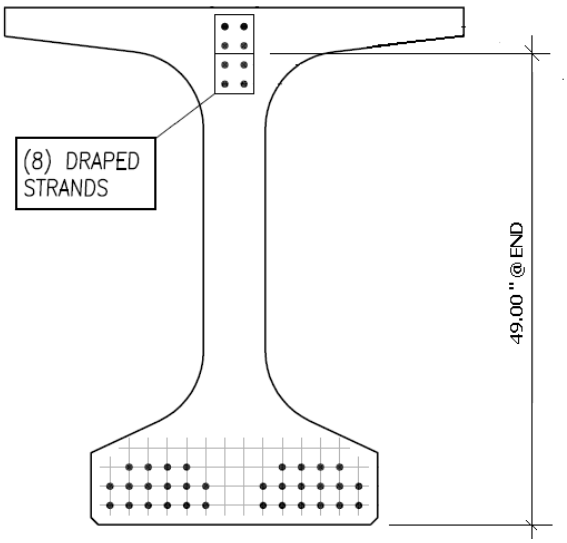

Figure 16 – Cross section showing the strand pattern at the end of the girder.

4.1.2. Instrumentation:

The girder end was instrumented with 4 two inch long Geokon Model 4202 vibrating wire strain gages (Figure 17). Each gage also includes a thermistor for temperature measurement. The gages are designed to be embedded in concrete and therefore can provide strain and temperature data during concrete hardening and prestress release. The temperature readings are used to correct for the differential elongation between the steel wire in the gages and the concrete, each with different coefficients of expansion. The reported accuracy of the gages is ± 15 με out of the 3000 με strain range.

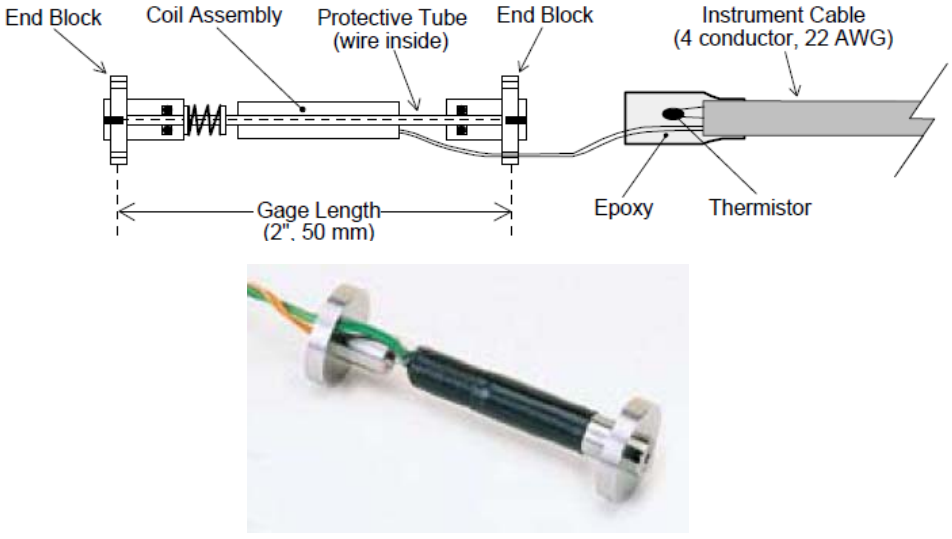

Figure 17 – Vibrating wire strain gages (Geokon 2010).

The locations and orientations of the gages on the girder end are marked on Figure 18. The mountings were set near the middle of the girder's web. The gages were mostly mounted at regions where compressive strains were expected so that the gages would not cross potential cracks and the data read after cracking occurs could still be meaningful.

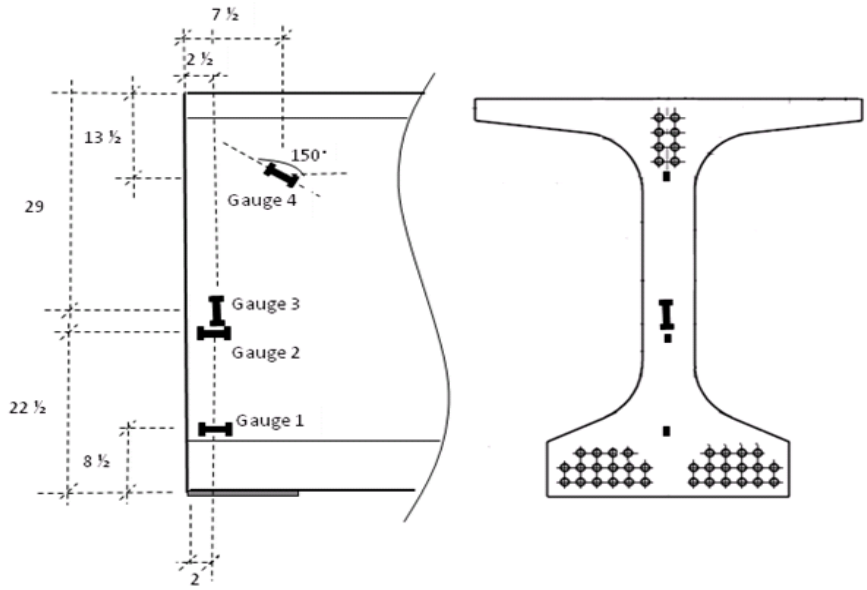

Figure 18 –Locations and orientations of the 4 gages installed on the pilot girder marked on the side view (left) and the cross section view (right).

4.1.3. Strain Readings

Spancrete uses two large hydraulic jacks to tension and detension the prestressing strands. One jack gang pulls the draped strands, the second gang pulls the straight strands. During the detensioning process the force in the jacks is stepwise reduced by the amount of prestress force provided by two strands. Then two strands are flame cut at the opposite end of the beams. This process re-occurs until the full prestress force has been released from the jacks and all strands have been cut.

The strains in the pilot girder were recorded right after the concrete was cast, after concrete was hardened, at each step of the detensioning process when the strand tension was reduced, after the detensioning process was over, and right after the girder was lifted and carried to the storage yard while sitting on simple supports. In order to observe the stability of the crack amount and width, more readings were taken when the girder was two weeks, three and a half months, and five and a half months old in the storage yard. A final reading was collected when the girder was six months old, right after the girder was placed on the abutment at the bridge site. These readings are shown in Figure 19.

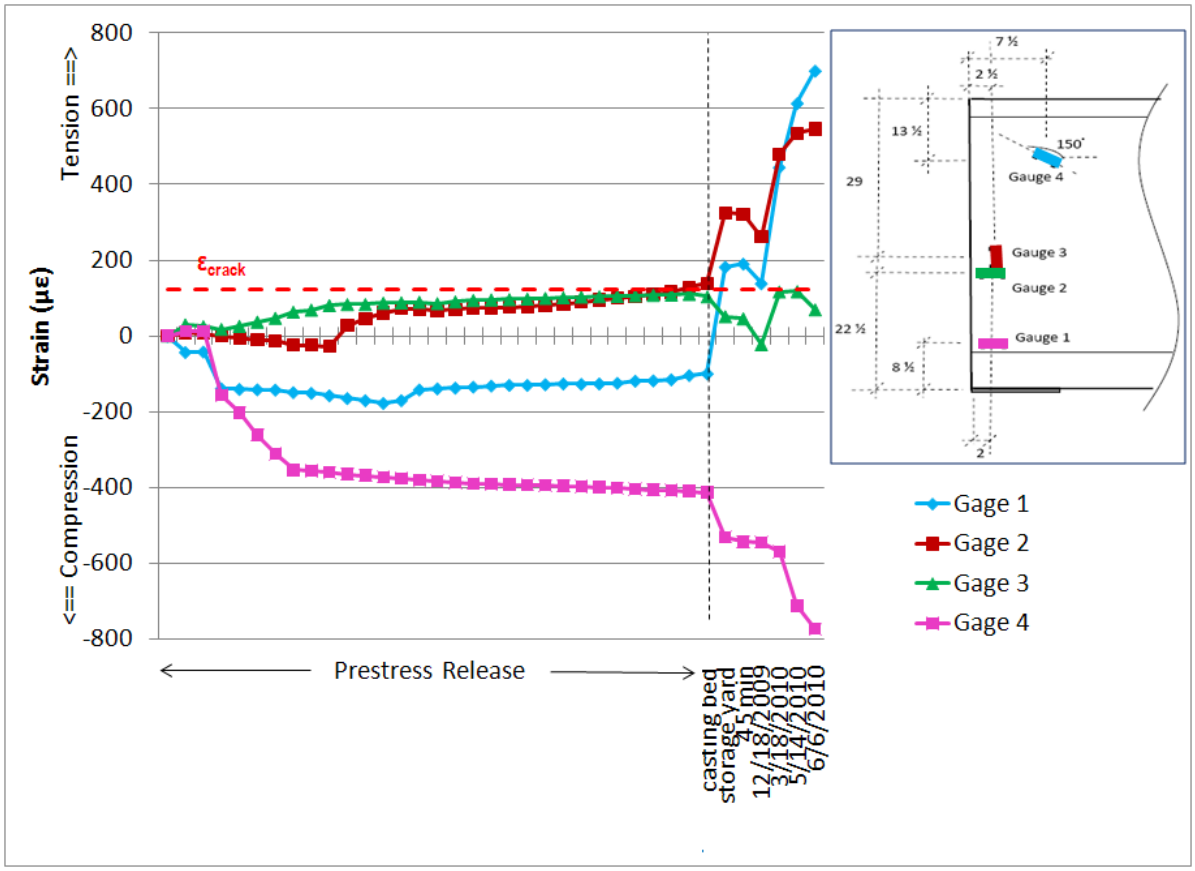

Figure 19 – Strains in four locations in concrete during and after detensioning.

The girder end where the strain gages were located exhibited the crack pattern shown in Figure 20. The gage locations are also marked with respect to the cracks on the same figure.

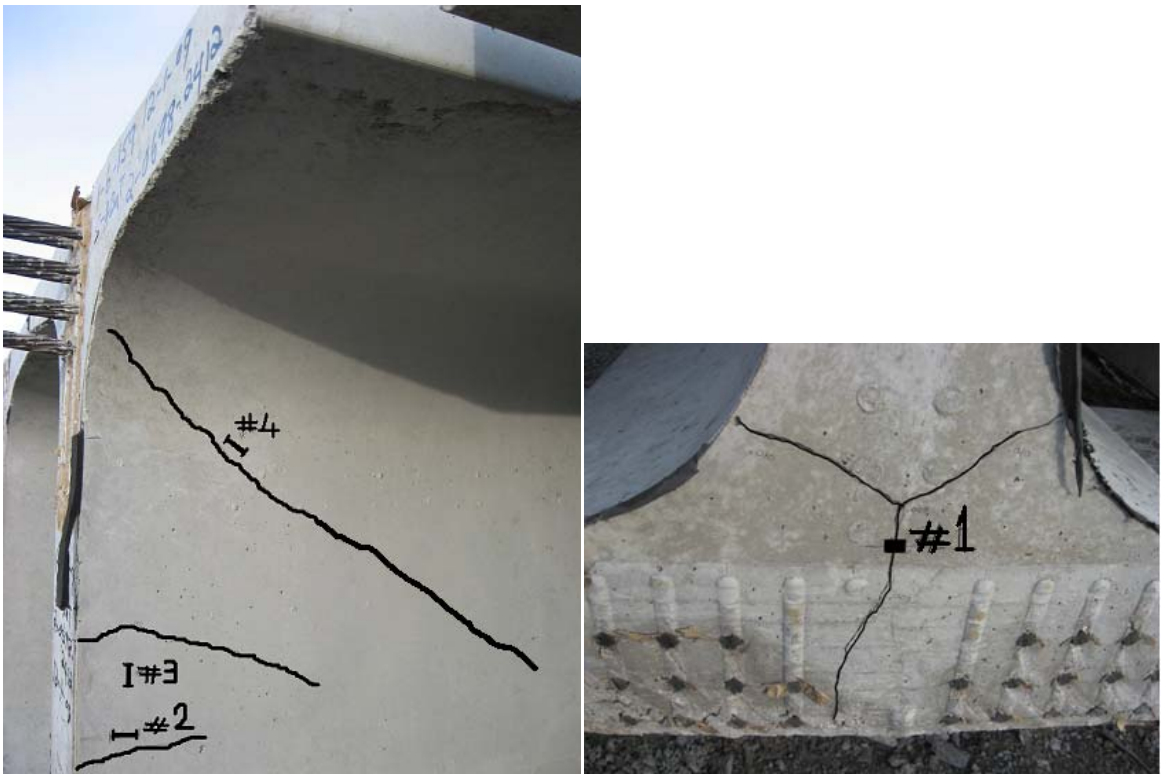

Figure 20 – Major crack locations with respect to the gage locations.

4.1.4. Comparison with the Finite Element Model Results

The strains measured are plotted with the prestressing forces transferred to the concrete for each vibrating wire strain gage. The strains obtained through nonlinear finite element modeling are plotted on the same graphs for a comparison in Figure 21 through Figure 24. The last step where the force remains constant occurred when the girder was lifted from the form and transferred to the yard for storage.

The finite element model for this purpose used a concrete strength of 7000psi since the actual breaks at the precast plant before transfer were at 6974psi. In the absence of actual strain measurements along the strands, the transfer length of the strand was taken as 36in., the AASHTO suggested length. The bond stress along that transfer length was assumed to be uniform.

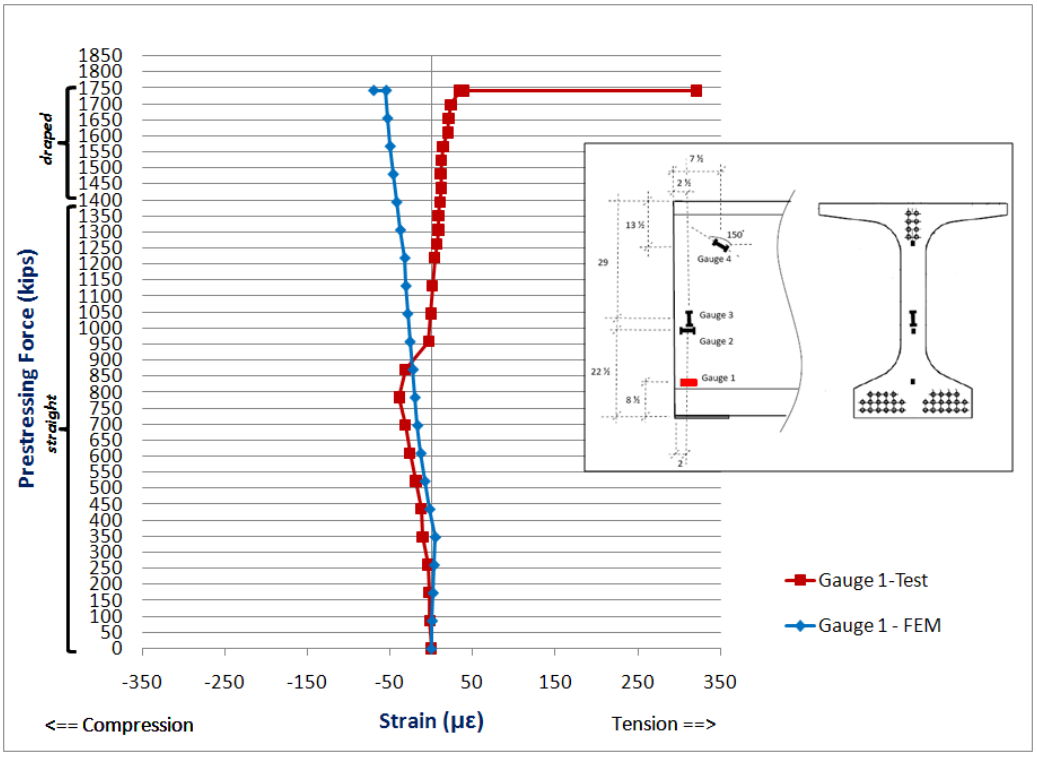

Figure 21 – Strains obtained via gage 1 and finite element model during prestress release.

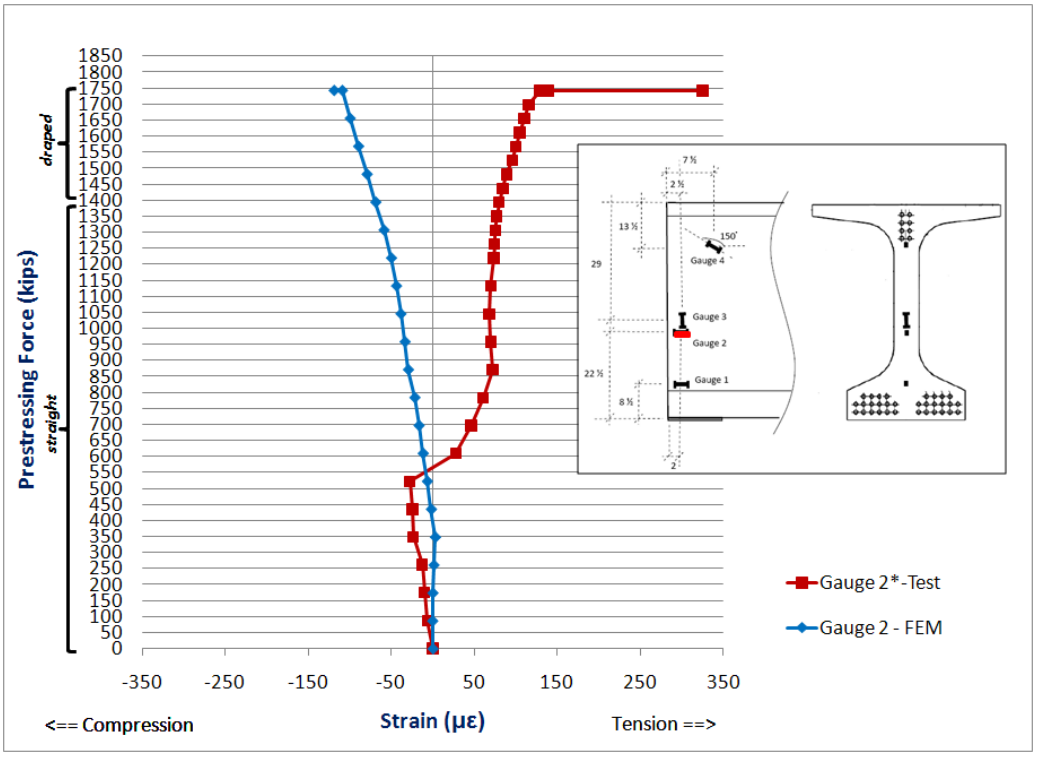

Figure 22 - Strains obtained via gage 2 and finite element model during prestress release.

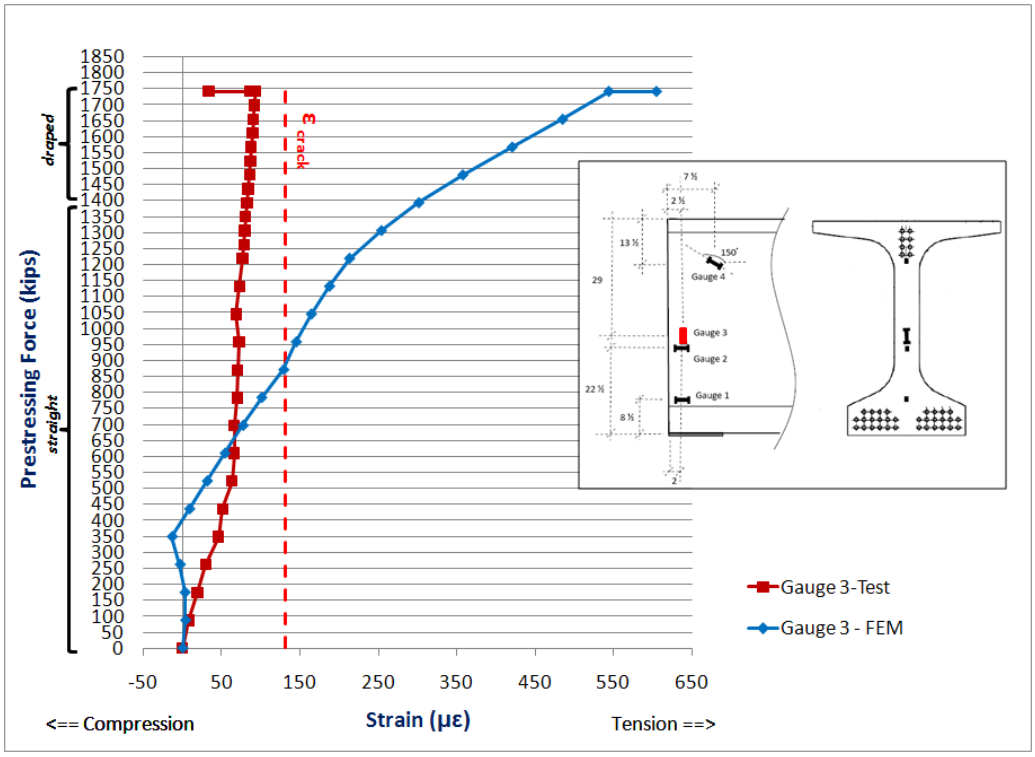

Figure 23 - Strains obtained via gage 3 and finite element model during prestress release.

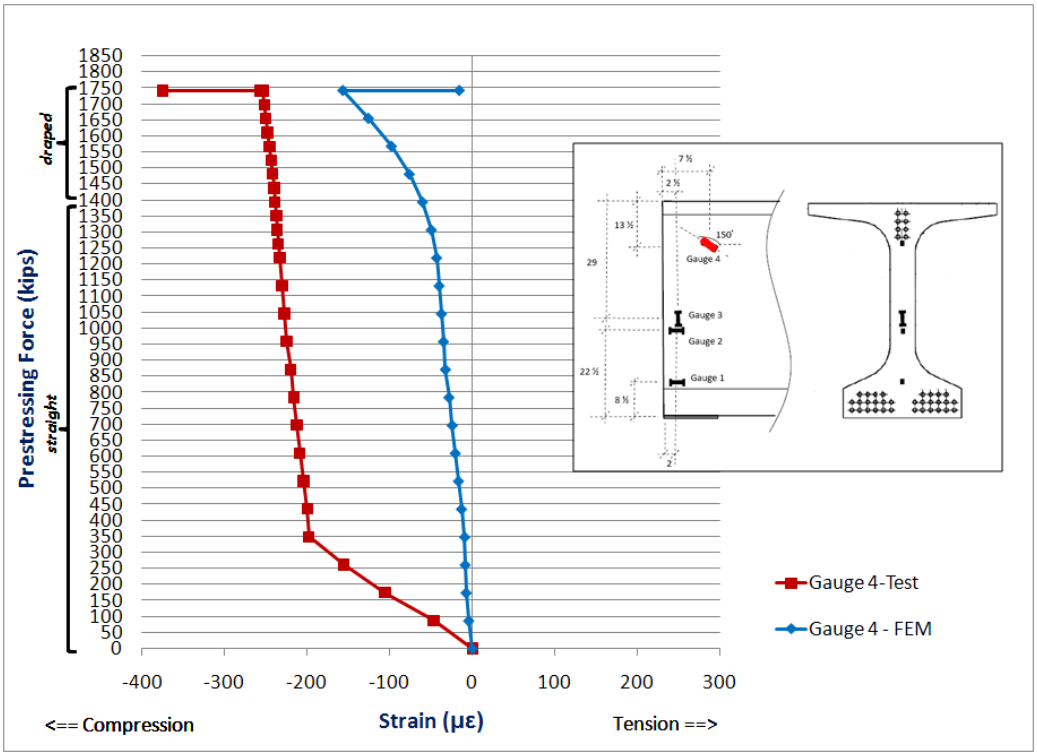

Figure 24 - Strains obtained via gage 4 and finite element model during prestress release.

Gages 1, 2 and 4 were expected to be compression measuring gages as they are close to and in the direction of the strands (gage 1 and 4) or they are perpendicular to the height in the web where horizontal cracking occurs (gage 2). Figure 21 and Figure 22 indicate that gages 1 and 2 were measuring compression and in agreement with the FEM predicted strains until 500-800k of prestress was transferred. They then abruptly changed to measuring tensile strains through to the end of the process. The reversal is believed to be caused by concrete cracking in the vicinity of the gages – causing a redistribution of strains and behavior. The finite element model predicts compression strains at both locations and diverges from the test results. For gage 4, the finite element model predicts much higher strains than measured through the test. Gage 4 does not seem to capture the higher strains expected when the draped strands are cut although it is located close to the draped strands.

Gage 3 was placed as a tensile strain measuring gage near where a horizontal crack was expected. The measured values of strains from gage 3 are in general quite low, less than 50$\mu\varepsilon$ before the initial cracking is believed to have started. They are lower than the values predicted via finite element modeling. This might be due to the reduction in strain at location 3 due to the horizontal cracking above and/or below the gage and a redistribution of strains. The finite element model assumes smeared cracks and would not exhibit the identical behavior once cracking started.

In all cases, the strains increased considerably during lifting (horizontal lines at top of plot). Any dynamic effect during lifting or moving of the girder is not considered in the finite element models.

The isolation of gages 2&3 between horizontal cracks as shown in Figure 20, and isolation of gage 4 above the inclined crack is believed to have contributed to discrepancies between the FEM results and the data after cracking had occurred. The proximity of gages to cracks and simplifications in the finite element model discussed earlier might have contributed to the discrepancies between the finite element model and the test results.

The crack pattern of an identical Spancrete girder end and the finite element model are presented side by side in Figure 25 for a qualitative comparison. Contours of the principal concrete tension strains are shown in the FEM model. Dark blue areas have tension strains near zero. Light blue regions have strains above the expected cracking strain. Red and grey colored areas have tension strains > 2000$\mu\varepsilon$ and would definitely be cracked regions. The FEM predicted crack regions generally agree with the visually detected cracks.

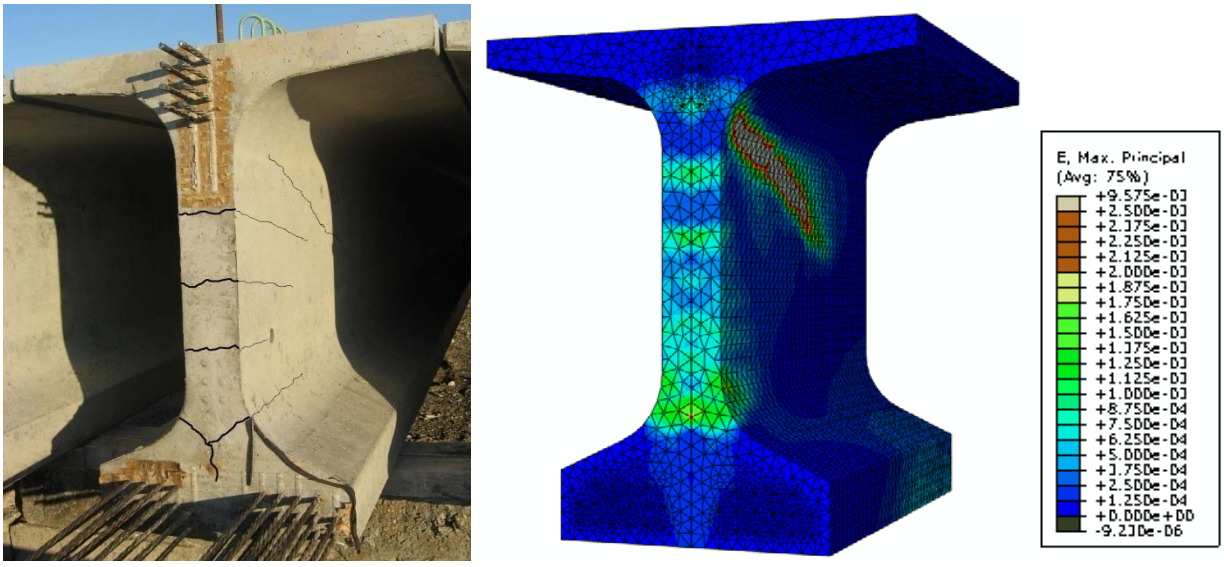

Figure 25 - Cracks on the girder instrumented (left), and high principal maximum tension strains predicted by the finite element model (right).

4.2. 54W Girder Manufactured by County Materials Corporation:

4.2.1. Girder Properties

A second more comprehensive instrumentation program was undertaken at the County Materials Corporation production facility with another 54W that was destined for the tunnel on the Racine I-94 project. The girders were 71'2" long and were manufactured for the bridge project numbered B-40-821. The end reinforcement pattern is shown in elevation view in Figure 26.

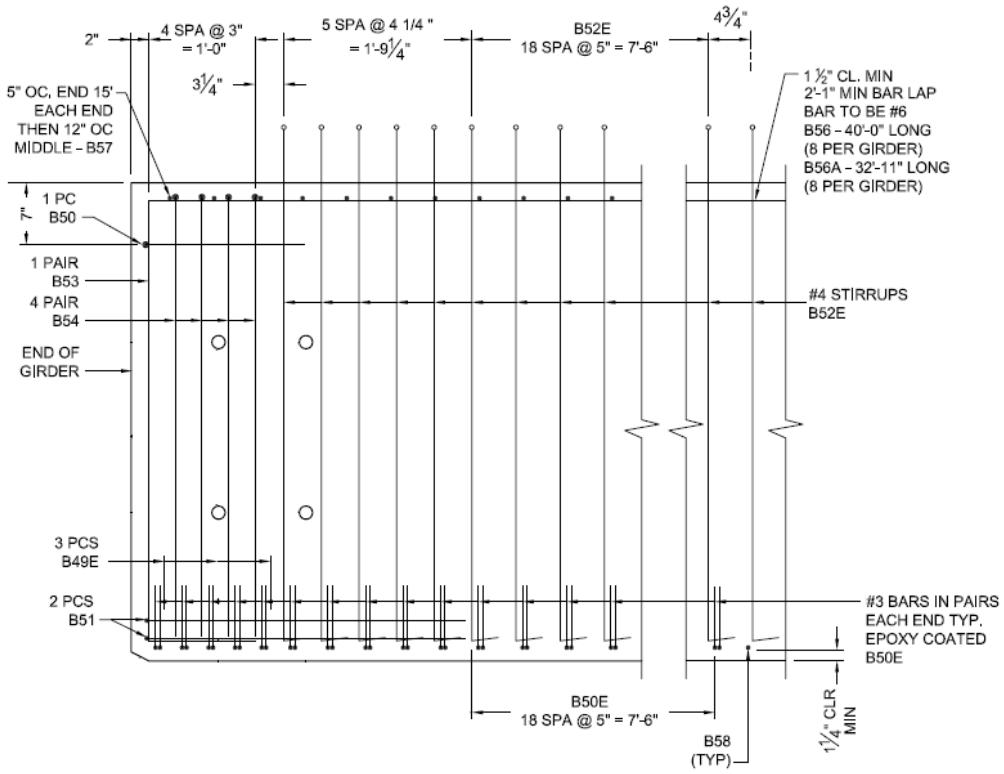

Figure 26 – County Materials 54W girder end reinforcement.

The girder had 8 draped and 28 straight 270 ksi low relaxation strands. The center of gravity of the draped strands at the girder end was 31 inches from the bottom of the girder. The strand pattern is shown on the cross sectional view taken from the girder end in Figure 27.

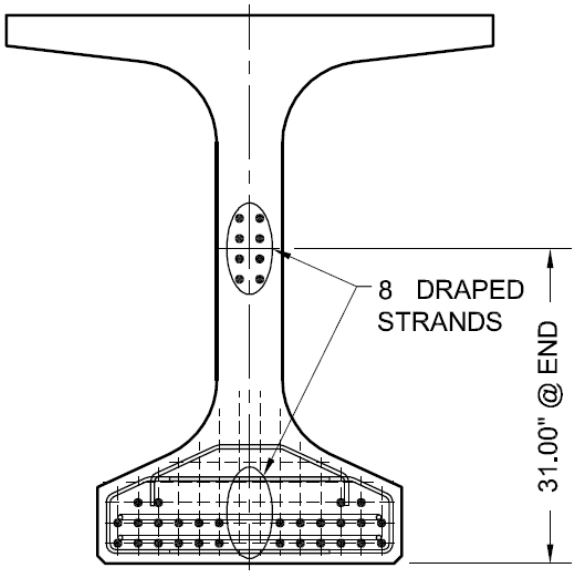

Figure 27 – Strand pattern of the County 54W girder at the end.

4.2.2. Instrumentation

Gages were placed in the girder end to collect strain data 1) directly in the concrete, 2) in the strands and 3) in the vertical reinforcement bars near the end. While vibrating wire embedment gages were used to measure concrete strains, surface gages were mounted on selected strand and reinforcement bars.

To be able to determine the stress transfer rate from strands to concrete, eight surface gages were mounted on the strands. Surface gages manufactured by Tokyo Sokki Kenkyujo Co. with 2mm (0.08in) gage length (type FLA-2-23-3LT) were glued on a single wire along the direction of the wire in the seven wire strands as shown in Figure 28. The gages were then waterproofed with nitrile rubber coating, covered with soft putty as a means of additional protection, and wrapped with aluminum tape. The strain gage wires were also secured against pullout during concrete pouring.

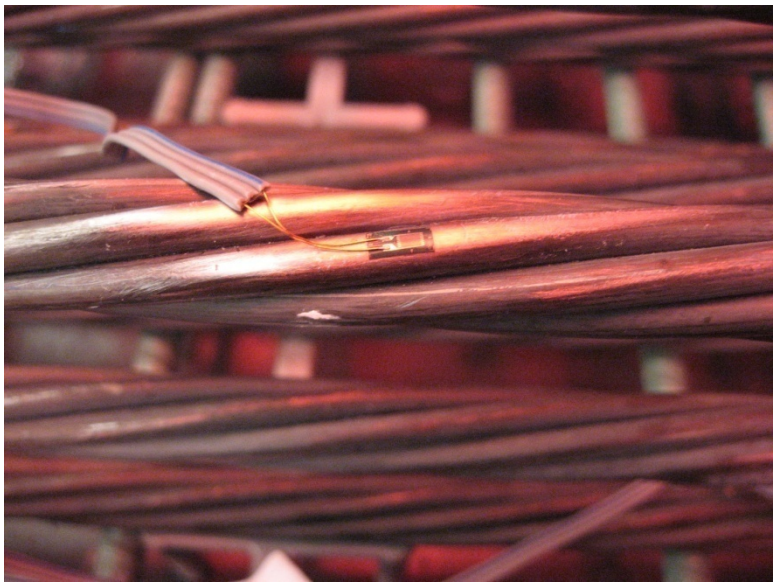

Figure 28 – Surface gage mounted on a strand.

These gages were located along two strands within the first 45 in from the girder end to identify the transfer length from the strain change in the strands. An exterior strand 6 inches up from the bottom of the girder, and an interior strand 4 inches up from the bottom of the girder had 5 and 3 gages respectively at locations shown in Figure 29.

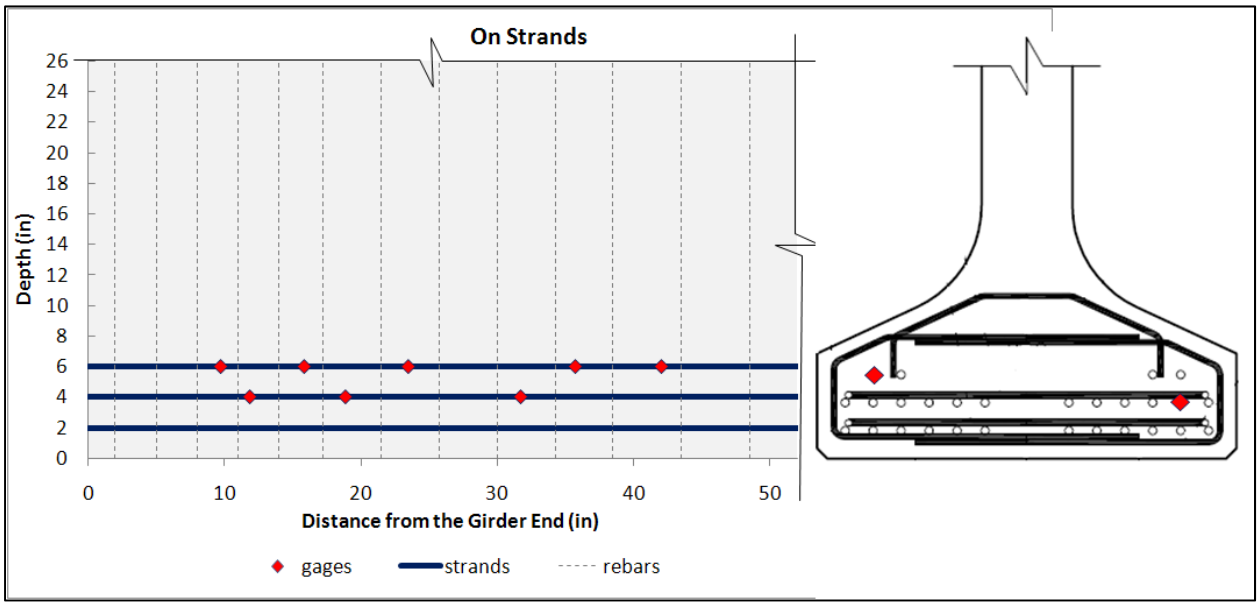

Figure 29 – Locations of strain gages on strands shown on elevation view (left) and cross section view (right).

Eight surface gages manufactured by Tokyo Sokki Kenkyujo Co. with 1mm (0.04in) gage length (Type FLA-1-11-3L) were mounted between the ribs of the vertical reinforcement bars along the direction of the bars. Five of these gages were placed and silicone coated for waterproofing and protection as shown in Figure 30. The three remaining gages were placed on the bottom flange stirrups and silicone coated as shown in Figure 31. For enhanced bond, epoxy was scraped off of the epoxy coated bars. All gages were wrapped with aluminum tape for additional protection.

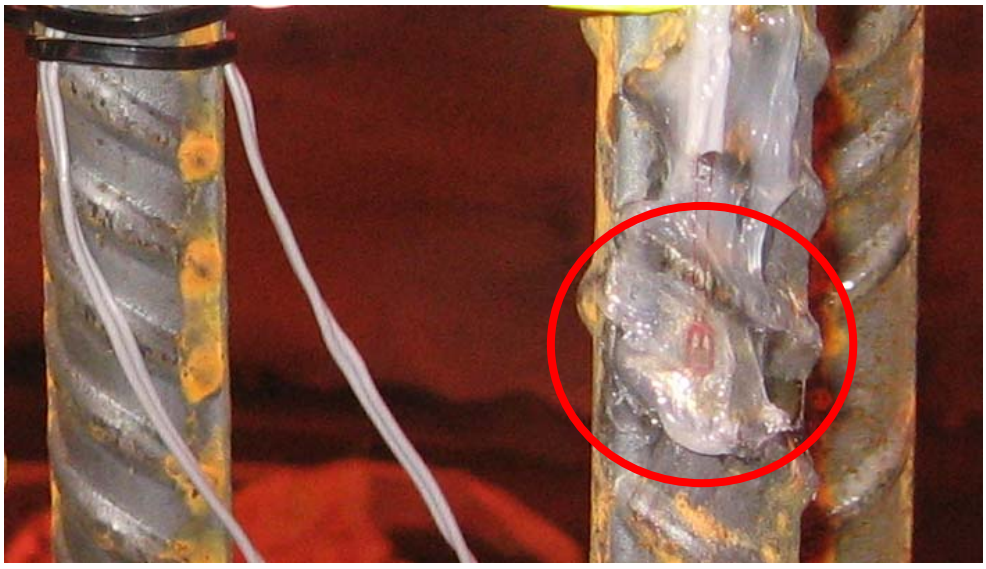

Figure 30 – Surface gage mounted on a vertical rebar and silicone coating.

Figure 31 – Surface gage mounted on an epoxy coated bottom flange stirrup and silicone coating.

The reinforcement bar gages were placed on rebars at three different heights from the bottom, at points where the expected strain pattern would have maximum or minimum values. Since the bottom flange bursting stresses were expected to grow further into the girder, these gages were placed away from the girder end. The locations of the reinforcement bar gages are marked on Figure 32.

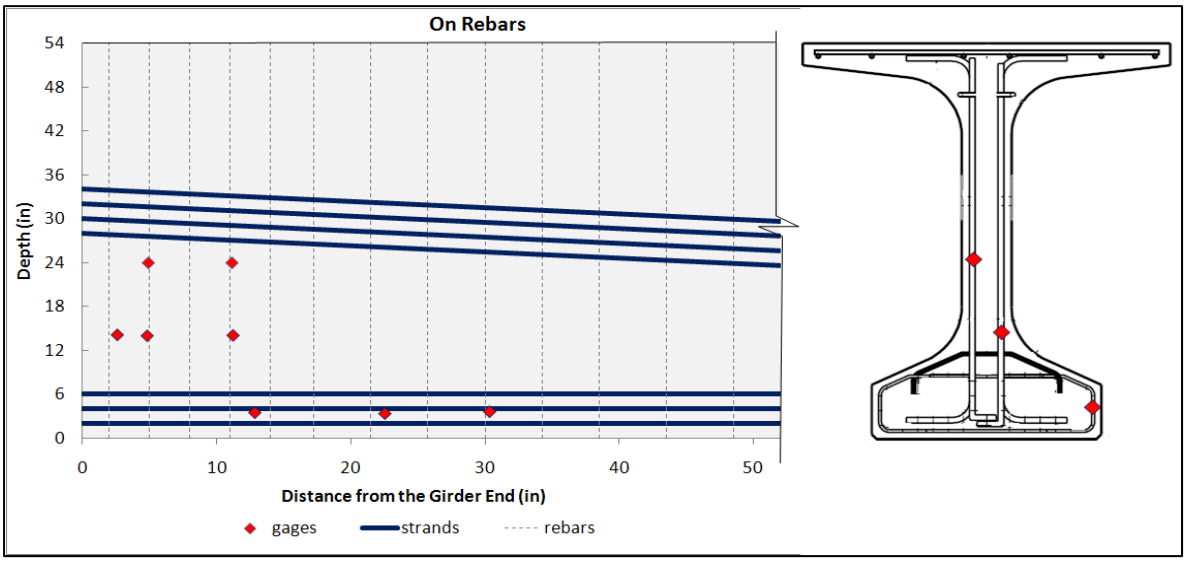

Figure 32 – Locations of strain gages on the rebars shown on elevation view (left) and cross section view (right).

Five vibrating wire gages (four Rocktest 2in long model EM-2 and one Geokon 6in long model 4200 gage) were embedded in the concrete to measure concrete strains directly. The gages were positioned using soft plastic assemblies attached to rebars as shown in Figure 33.

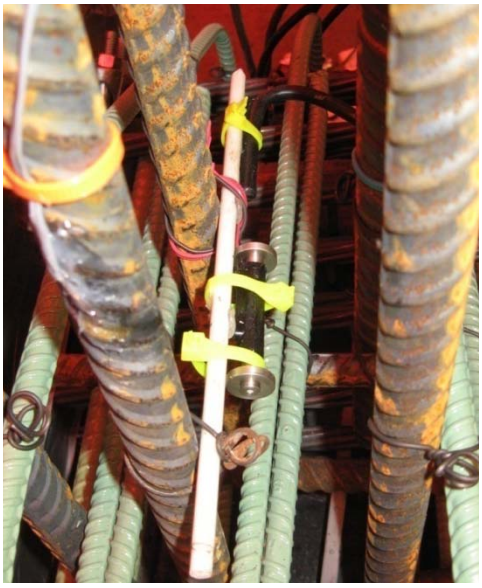

Figure 33 – 2in vibrating wire gage positioned in concrete through nonstructural attachments to rebar.

The locations of the embedded concrete gages are marked in Figure 34. Gages 1 and 2 are located along the length of the girder in the expected concrete compression strut created by the bottom strands. Gages number 3 and 4 are placed horizontal and transverse in the cross sections to understand the "Y" cracking that occurs in the bottom flange-web junction. Concrete gage number 5 was placed parallel to the vertical end reinforcement in the web cracking region as a comparison to the strain gages placed on the rebars at the same height.

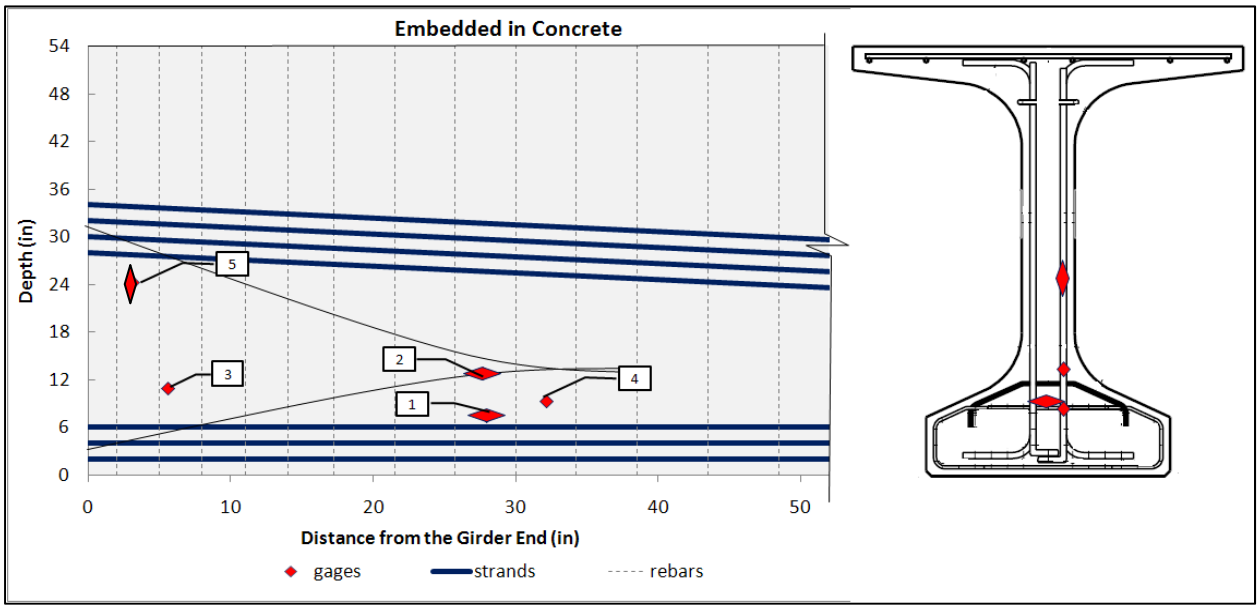

Figure 34 – Locations of embedded strain gages in concrete shown on elevation view (left) and cross section view (right).

Two compression cylinder tests and one split tension test were performed 10 hours after the strand were cut and the prestress was transferred. The compression cylinder strengths measured right before the detensioning by County Materials were also obtained and showed an average strength of 7784psi. Tests run at the University 6 hours later had a strength of 8873psi.

4.2.3. Strain Readings

The readings from the gages on the vertical reinforcement bars are thought to be unreliable. Two of the strain gages on the rebars were dysfunctional after the concrete pour. Two others failed during the detensioning, possibly due to a sudden strain increase and physically breaking the gage or the gage wires. Contrary to what was expected, 3 of the remaining gages read compression or excessive tension indicating gage failures. In this case, the remaining one gage was not considered to provide reliable readings.

The change in strains measured along the transfer length of the strands exhibited a slight concave down curve as shown in Figure 35. The bond stresses and the transfer length calculated using this data were used to update the simulated stress transfer in the finite element models. The difference between the strains from the two strands is relatively minor. Variations in strain can be attributed to the difference in the location of the strands in the concrete and the radial stiffness of the concrete around the strands providing interlock, the sequence of detensioning and measurement accuracy.

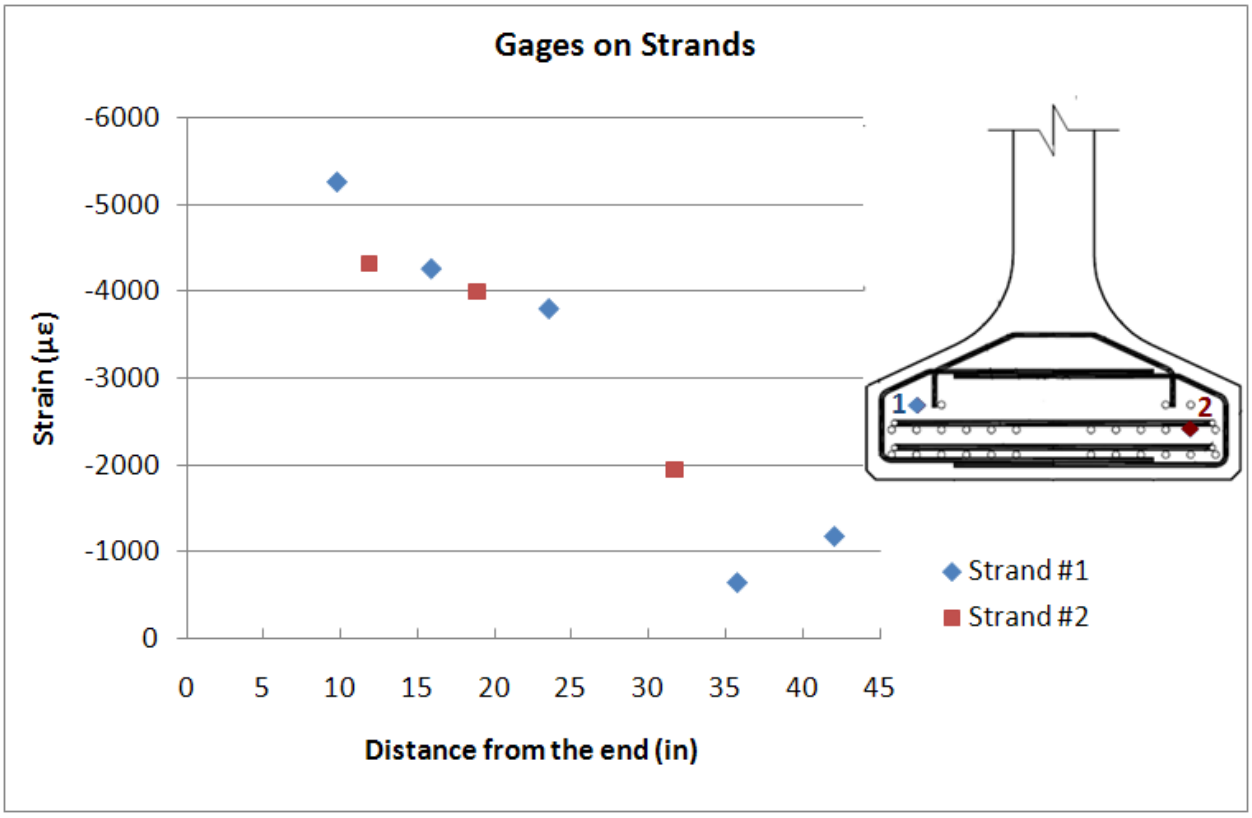

Figure 35 – Strain readings from the gages on strands.

The strain change monitored by the vibrating wire gages in the concrete at five different locations during prestress release is plotted in Figure 36. It should be noted that the strain readings from gage 5 were unsteady, results were beyond the expected strain range and therefore may not be reliable. The results from concrete gage 2 were adjusted (see Figure 41) as the initial reading appeared to be hand recorded inaccurately. In order to inspect the crack growth and stress change in the girder after the prestress release, four sets of additional concrete strain readings were taken when the girder was 3, 7, 14 and 28 days old.

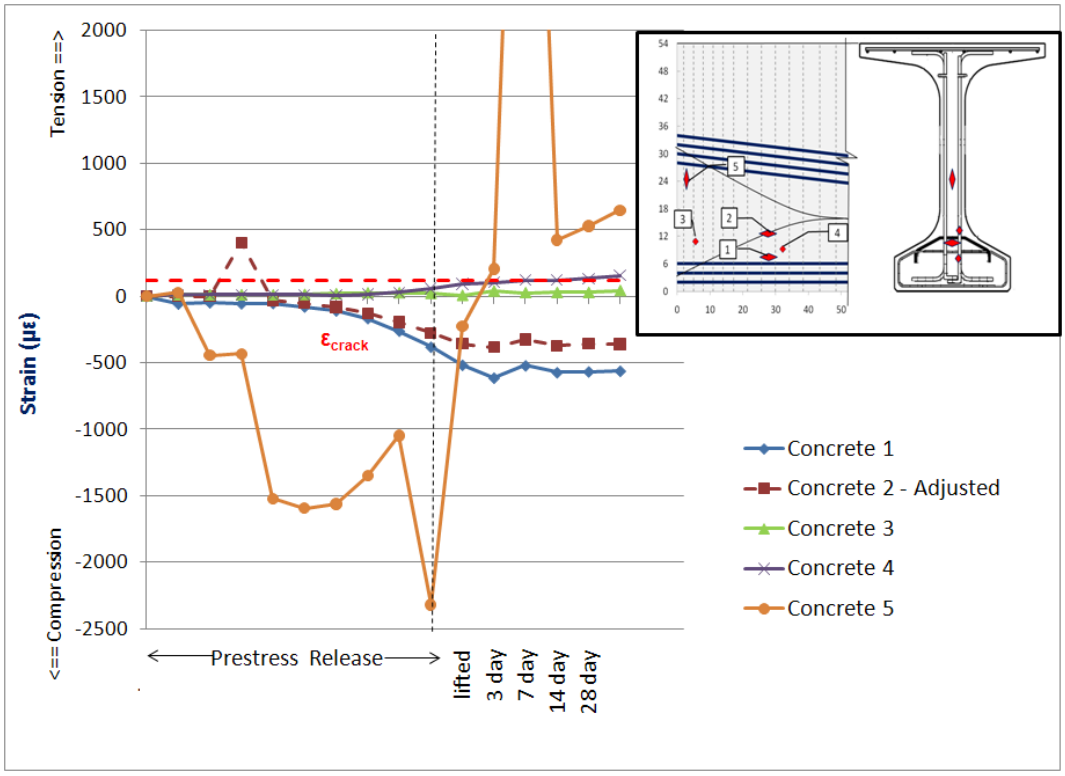

Figure 36– Strain readings from the gages embedded in concrete during and after the prestress release.

This girder did not experience as much cracking as the Spancrete girder, probably due to the small eccentricity in the draped strands. The cracks observed on the girder end are presented in Figure 37.

Figure 37 – Initial crack locations and widths in the monitored girder.

4.2.4. Comparison with the Finite Element Model Results

The strains obtained from the gages on reinforcement bars after prestress transfer was completed are shown in Figure 38 together with the expected strains from the finite element model. The disagreement between the results was not expected, is difficult to explain, but may be due to cracking near the gages.

The finite element model used an assumed concrete strength of 9000psi while the actual cylinder breaks before transfer were 6974psi at the plant and 8873psi when tested at the University 6 hours later. A transfer length for the strands of 44in., different then the length suggested by AASHTO, was used since strand strain measurements of Figure 35 appeared to indicate that this was the actual transfer length. The bond stresses along the transfer length were assumed to be uniform, as apparent by the linear variation of strand strain in Figure 35.

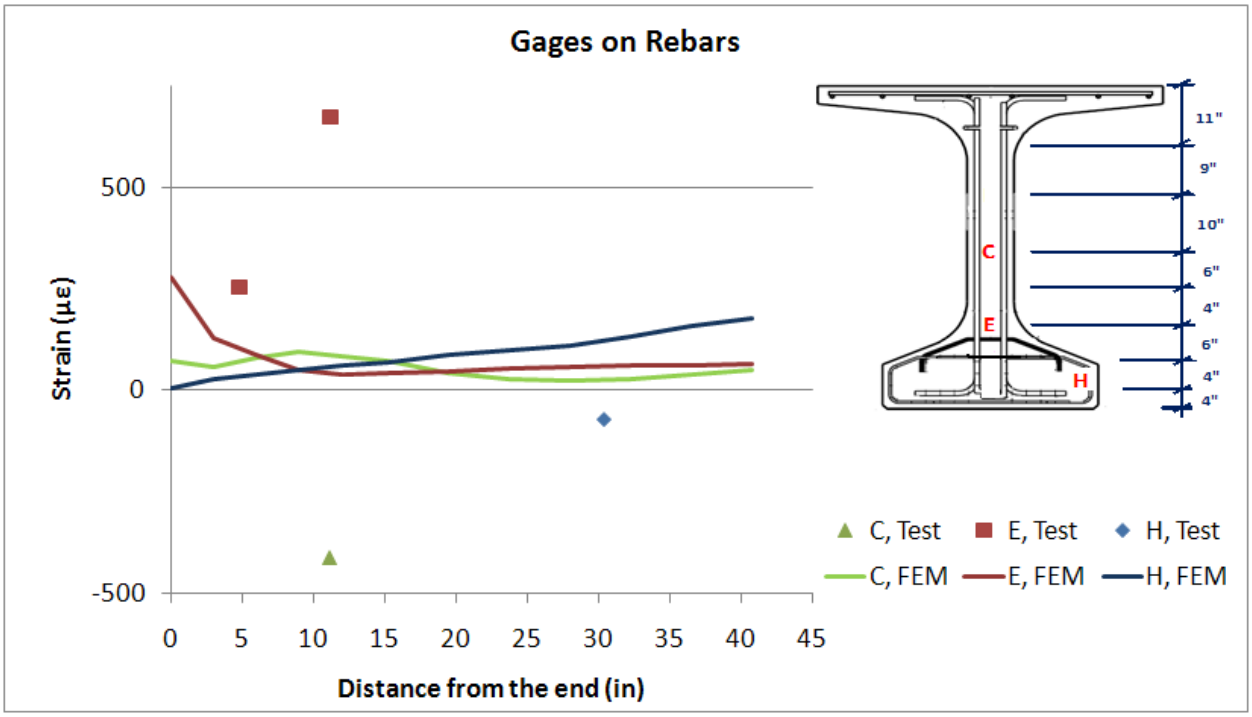

Figure 38 – Strain readings from the gages on the vertical rebars and stirrups.

The strains measured along the strands were used to determine the transfer length and the bond stress distribution between the strands and concrete. Figure 39 shows the force change in the strands during detensioning along the length of the strands. Linear trend lines, their equations and the coefficient of determination (R^2) values are also shown for each strand data set excluding the outliers. A linear approximation of the force change in the strands would coincide with a uniform bond stress. The average of the data for the two strands suggested a transfer length of 44 inches, 22% longer than the 36 inches suggested by the AASHTO LRFD Bridge Design Specifications.

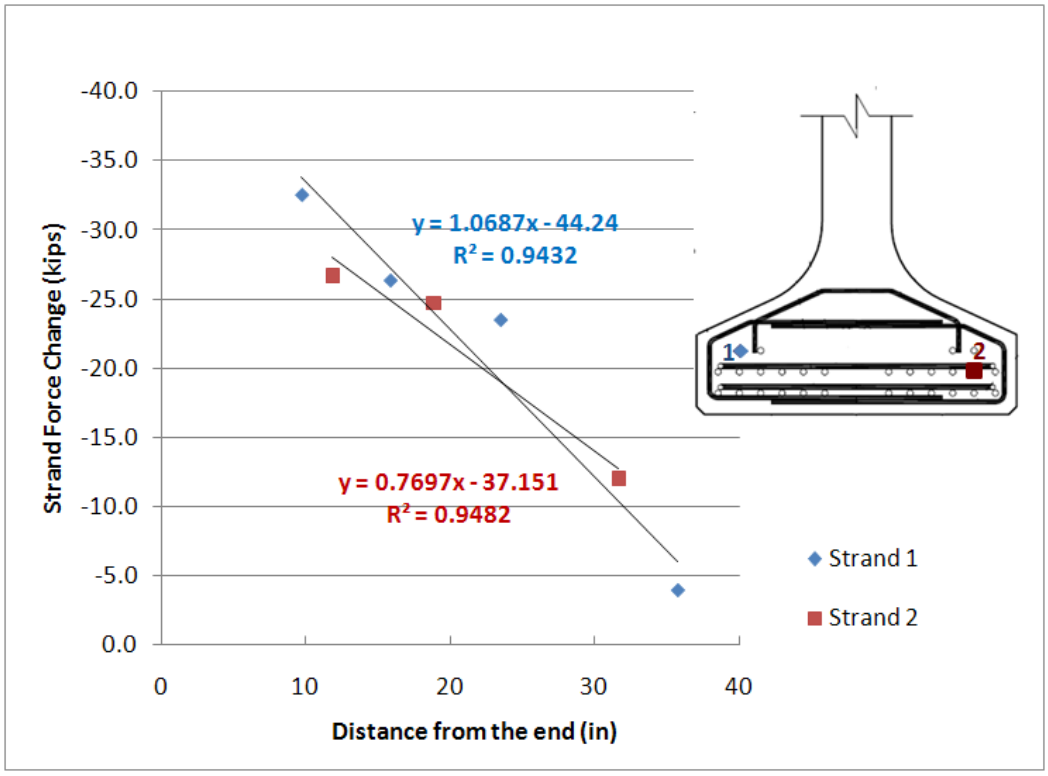

Figure 39 – Trendlines fitted to strand force data to estimate a transfer length and bond stresses.

The comparison between the embedded concrete strain gage results and finite element modeling results is presented in Figure 40 through Figure 44. The strains are plotted against the prestressing load transferred to the concrete.

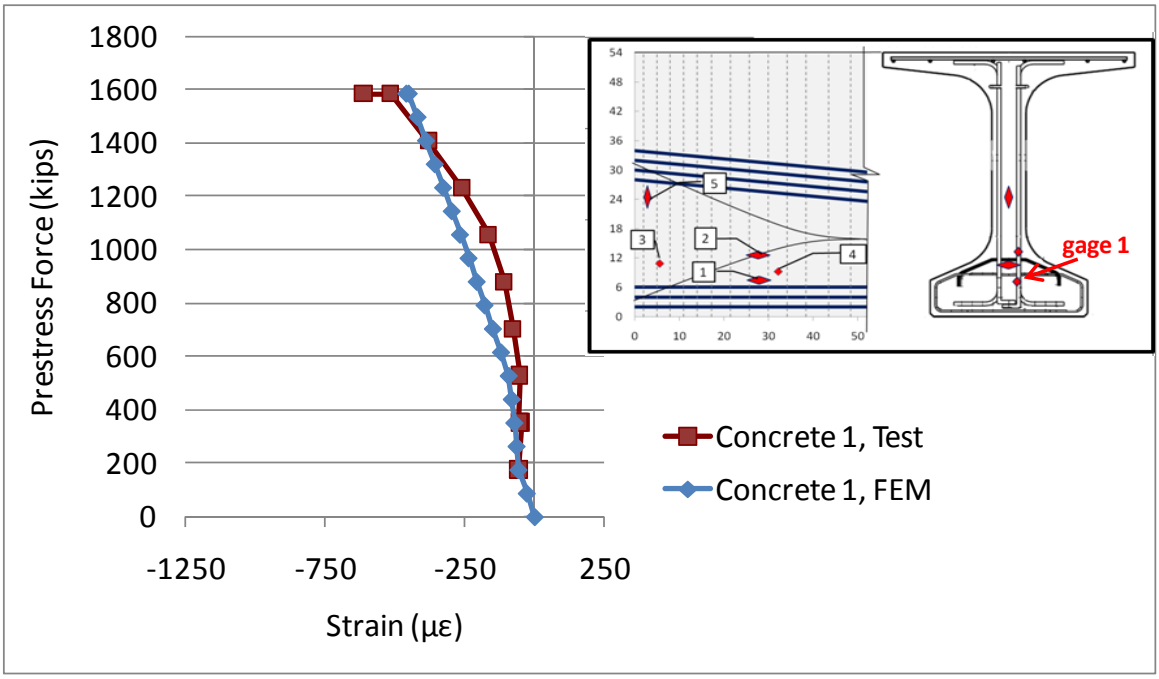

Figure 40 – Strains determined via gage 1 and finite element model during prestress release.

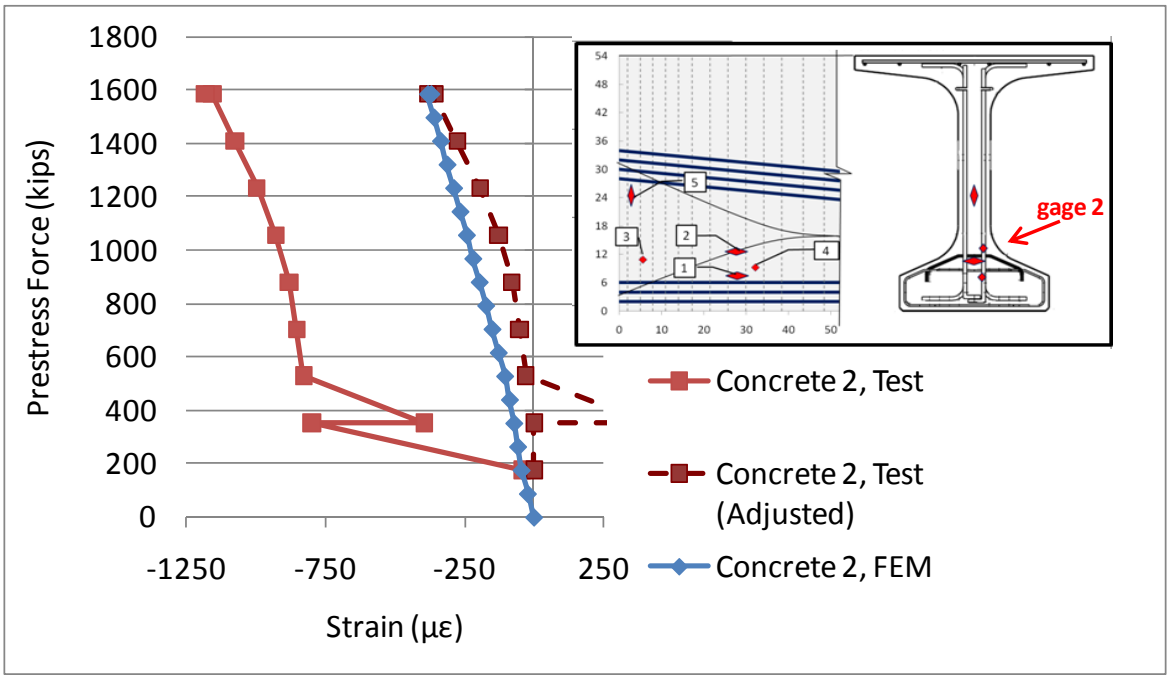

Figure 41– Strains determined via gage 2 and finite element model during prestress release.

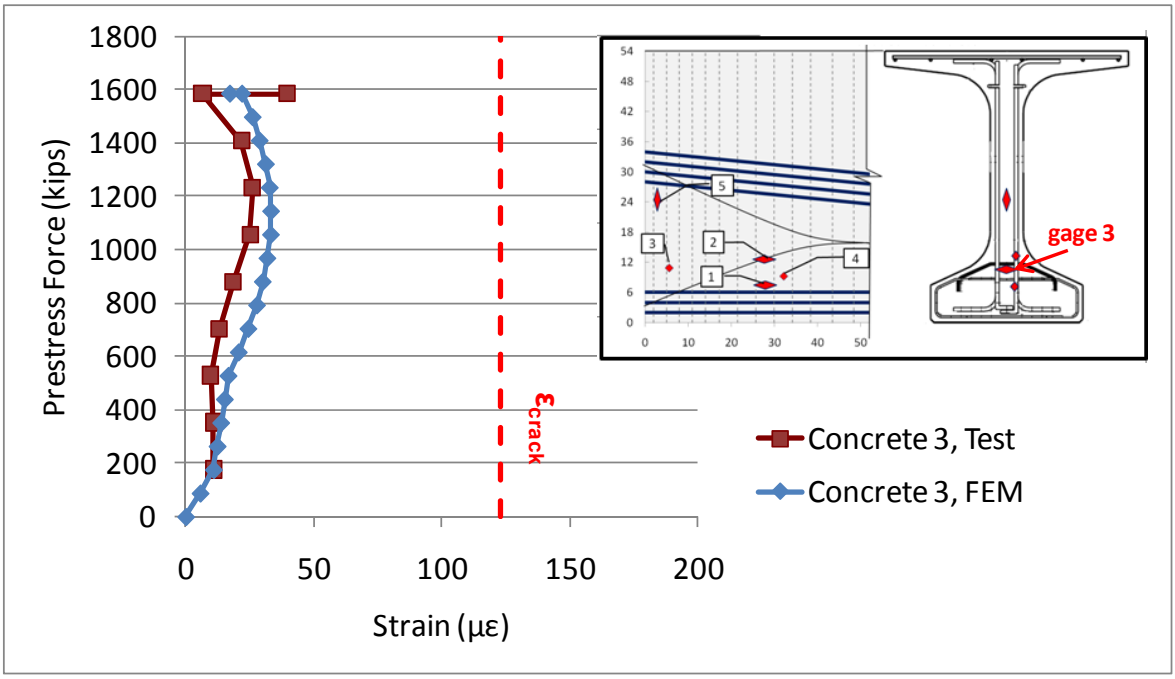

Figure 42– Strains determined via gage 3 and finite element model during prestress release.

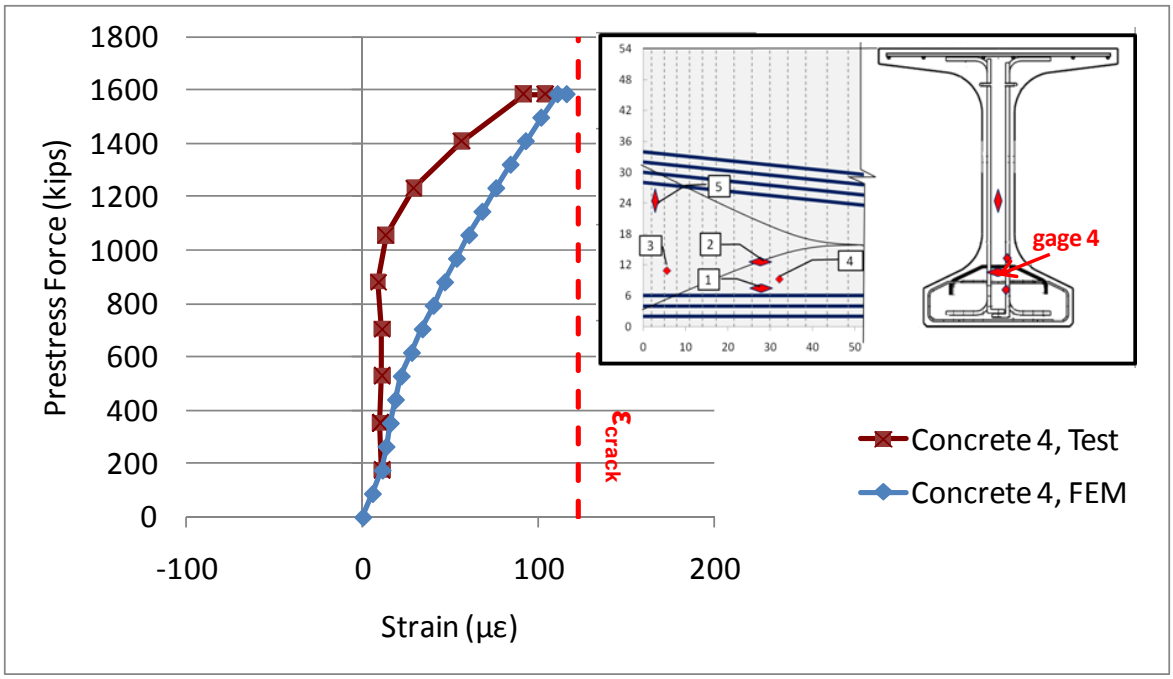

Figure 43– Strains determined via gage 4 and finite element model during prestress release.

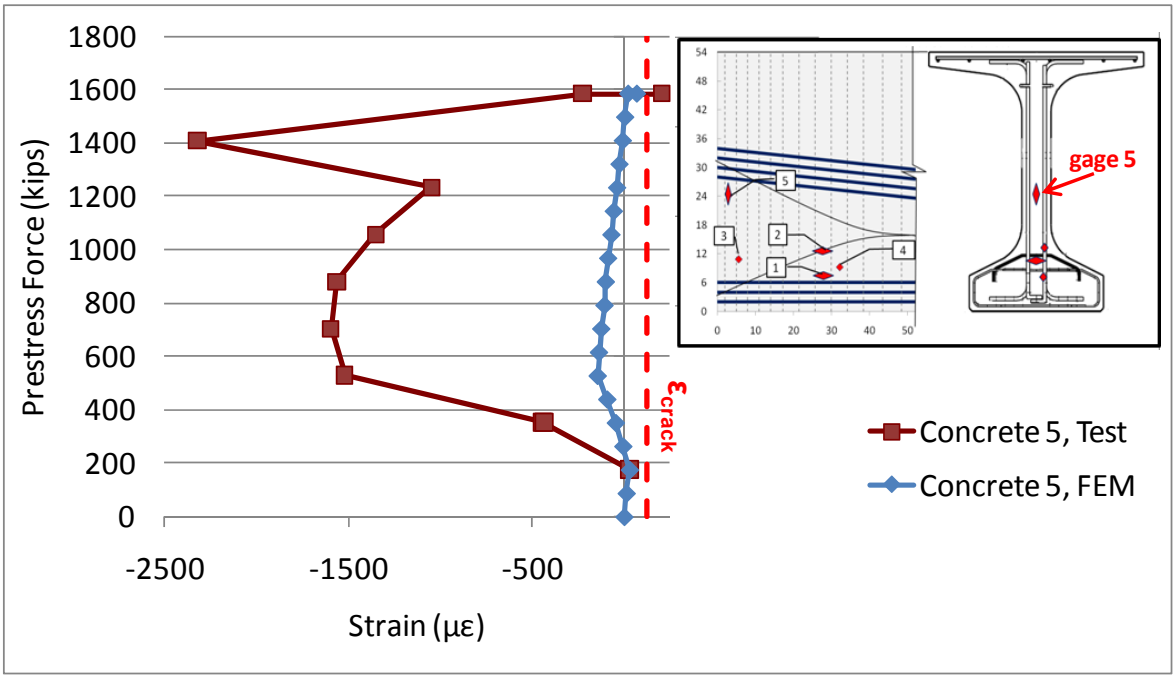

Figure 44– Strains determined via gage 5 and finite element model during prestress release.

Strains measured by gages 1 thru 4 correlate reasonably with the strains determined at the same locations in the girder by finite element modeling. The trend of strain increase during stress release is similar between the test and finite element analysis results. Readings in gage 5 were unsteady during detensioning and the mismatch with the finite element analysis results was expected as this gage was not expected to be reliable.

A qualitative evaluation of the finite element model can be made using Figure 45. The locations where high tension strains (light blue or green) were predicted using the finite element model coincides with the locations of the cracks on the girder.

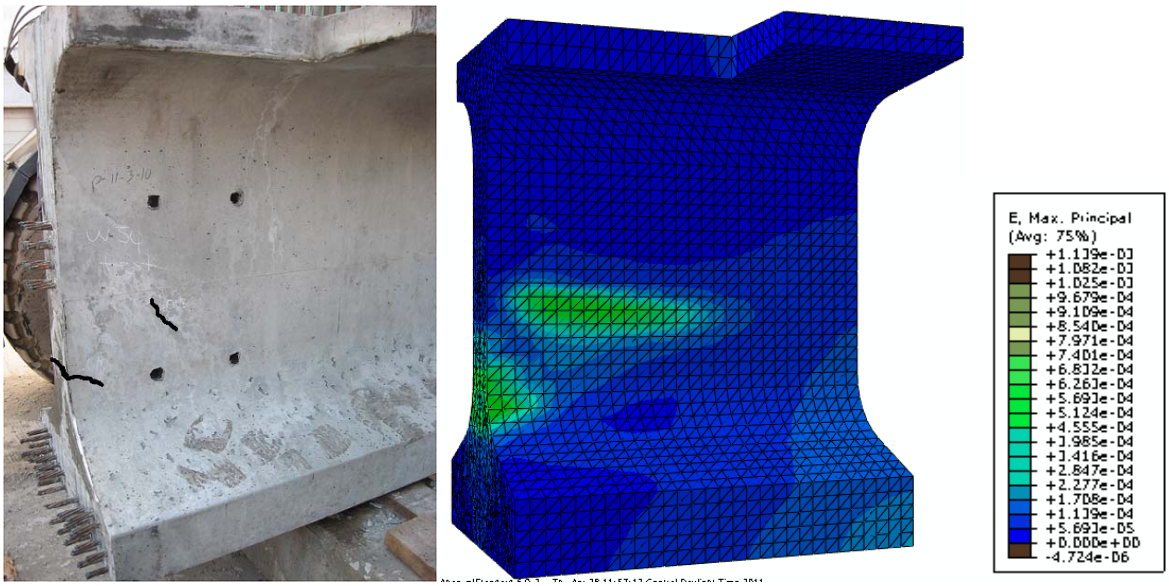

Figure 45 – Cracks on the girder monitored (on the left), high principal maximum strain locations on the finite element model (right).

4.3. Texas 70in deep girder

Research conducted at the University of Texas, Austin involved testing two 28”, one 46” and one 70” deep Texas girders to investigate end cracking after prestress release. (O'Callaghan 2008, Dunkman et al. 2010) Effects of both live and the dead ends were measured with strain gages. Each test was performed under laboratory conditions.

The research presents the important and relatively complete information required to model a prestressed girder analytically. The results of the reported research were, therefore, also selected to be used in the verification of the finite element modeling technique in this research.

Their research reports the transfer length and the strand stress variation along selected strands for each girder using surface strain gages attached to strands in the end region. The measured transfer length and the bond stress distribution were used to correctly model the stress transfer during release in the finite element models.

The vertical reinforcement bar stresses from numerous locations were also made available by O’Callaghan as measured with surface strain gages along the girder length where the cracks were expected. Figure 46 presents the numerous strain gage locations near the Tx70 girder end.

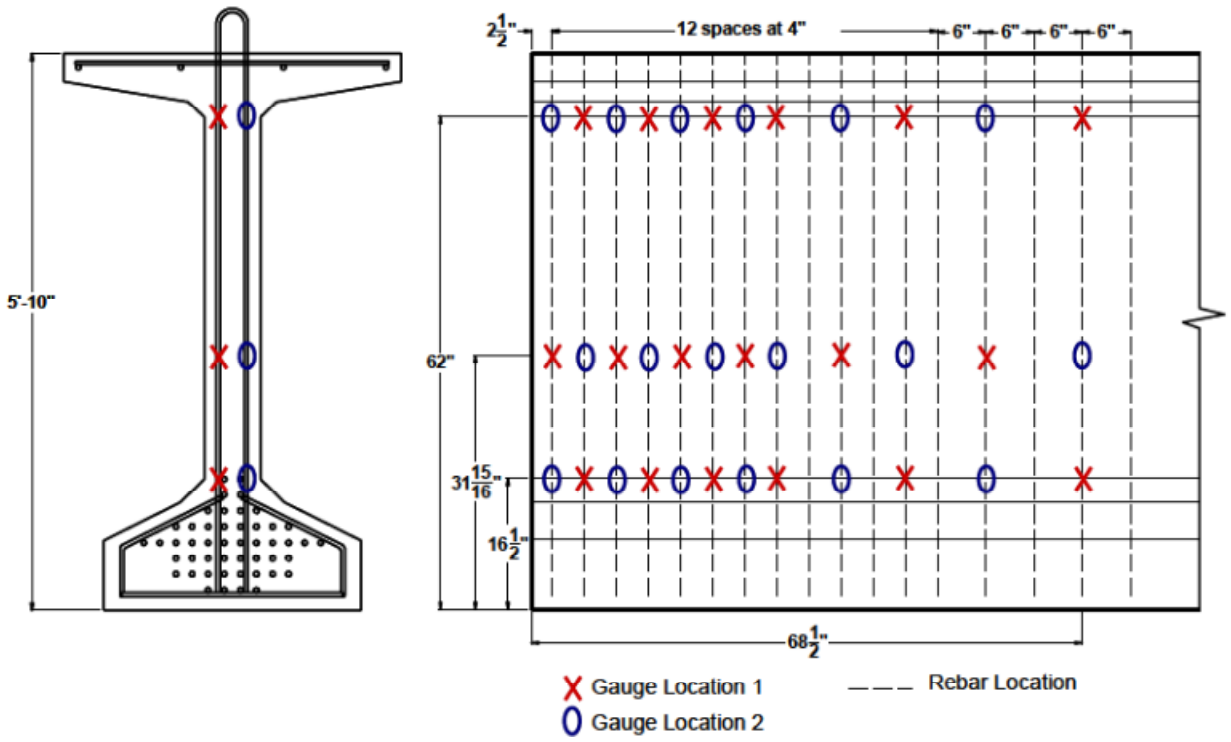

Figure 46 – Strain gage locations on vertical rebars at the live end given by O'Callaghan(from O'Callaghan 2008).

Using finite element modeling, the live end of a Tx70 girder was replicated. The transfer length and the bond stress distribution over the transfer length were modeled in accordance with the reported test results. The test results showed that the bond stress has a nearly linear variation along the transfer length. The compression cylinder test results reported, 6675psi, were rounded to 7000psi for input into the concrete material model. Material model, boundary conditions, loading, discretization and the solution techniques were kept the same as previously described in Chapter 3.

The stresses on the rebars obtained through finite element modeling were compared to the stresses measured via testing. The results are presented in Figure 47, Figure 48 and Figure 49.

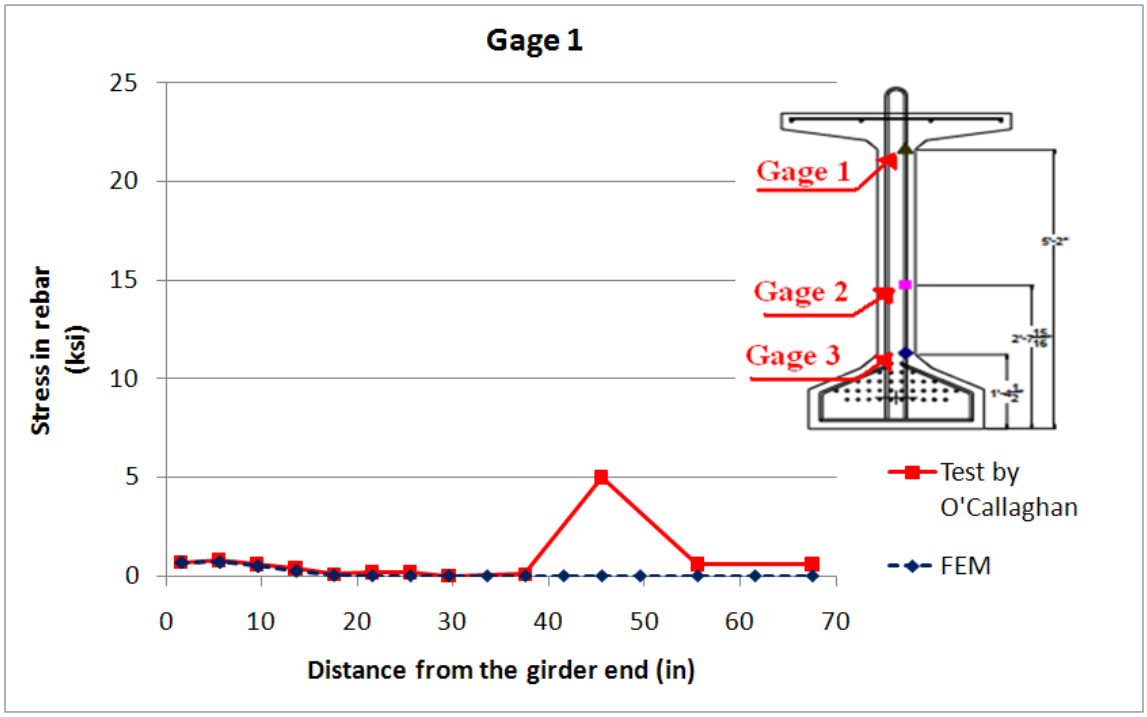

Figure 47 – Test results reported by O'Callaghan (O'Callaghan 2008) compared to the results of the FEA for gage set 1.

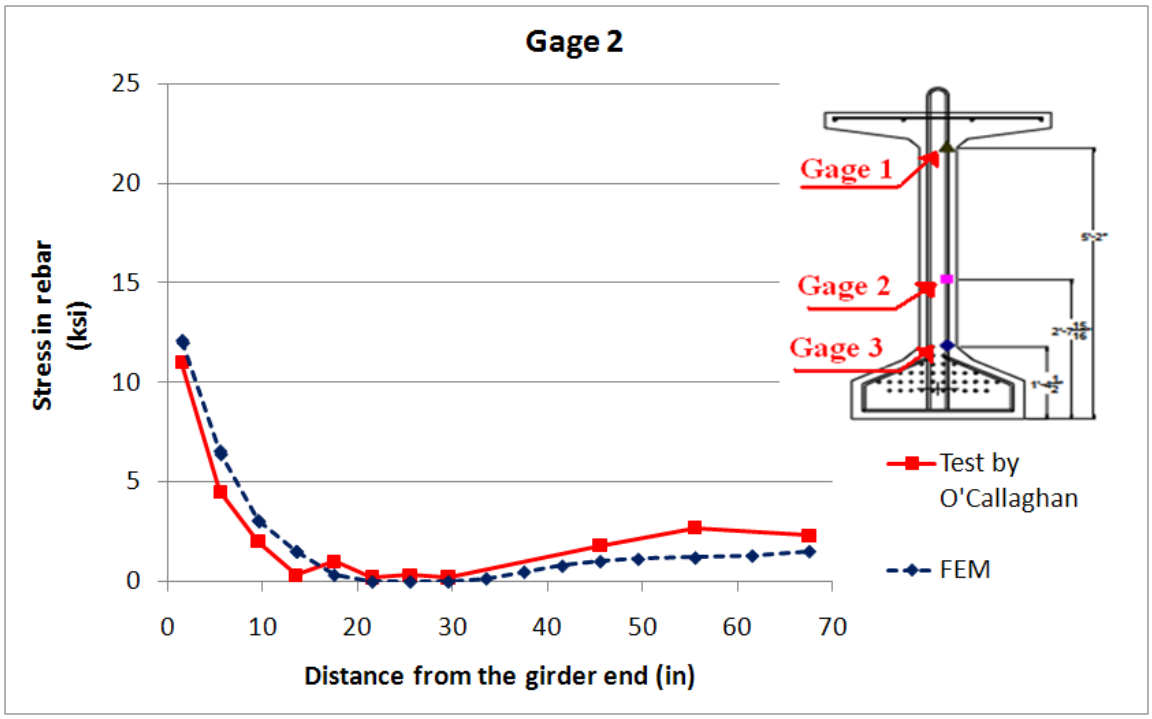

Figure 48– Test results reported by O'Callaghan (O'Callaghan 2008) compared to the results of the FEA for gage set 2.

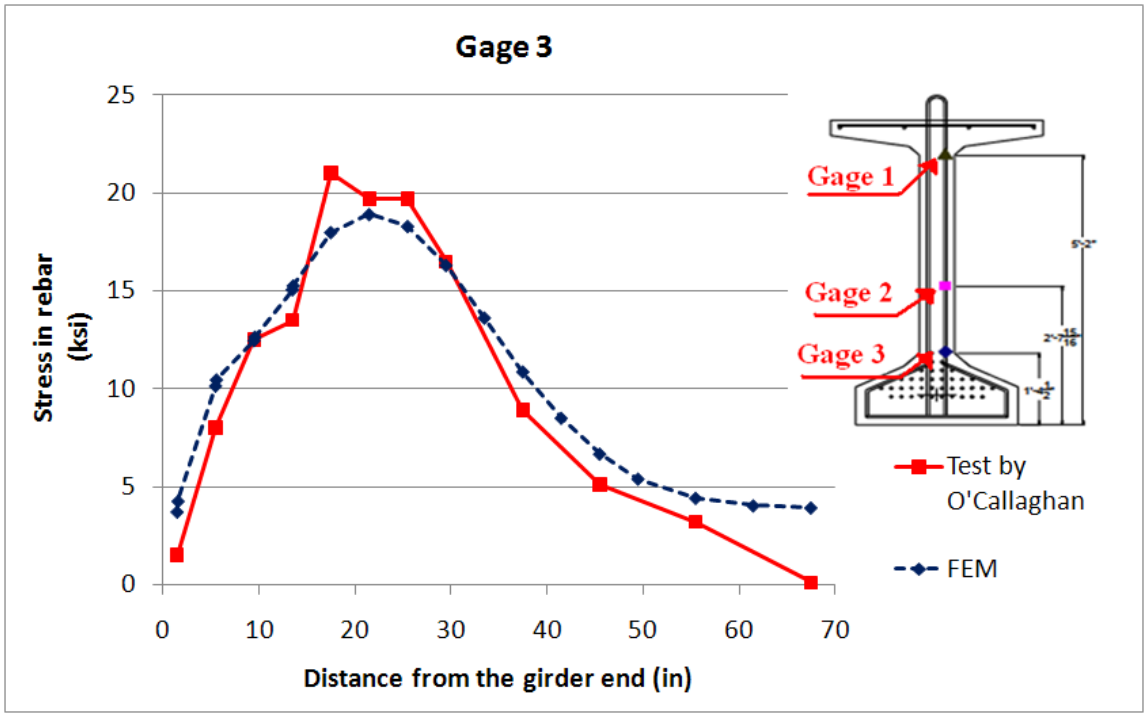

Figure 49– Test results reported by O'Callaghan (O'Callaghan 2008) compared to the results of the FEA for gage set 3.

A good correlation was achieved between the stresses in rebar predicted by the finite element analysis and the stresses measured and reported by O'Callaghan for each set of gages. Performing the actual test under controlled conditions in a laboratory, and obtaining data through numerous strain gages provided high quality data for comparison with the FEM model predictions.

The ability of the FEM analysis was further corroborated through the qualitative surface strain results from the girder concrete as shown in Figure 50 and compared with the crack locations described by O'Callaghan. Regions shown in light blue to red by the FEM model would be expected to be cracked. Those regions agree with O'Callaghan's crack locations.

In conclusion, numerical and qualitative evaluation of the finite element models with respect to test results give enough confidence to use these models to further explain the behavior of the girder end zone and to study the impact of potential improvements.

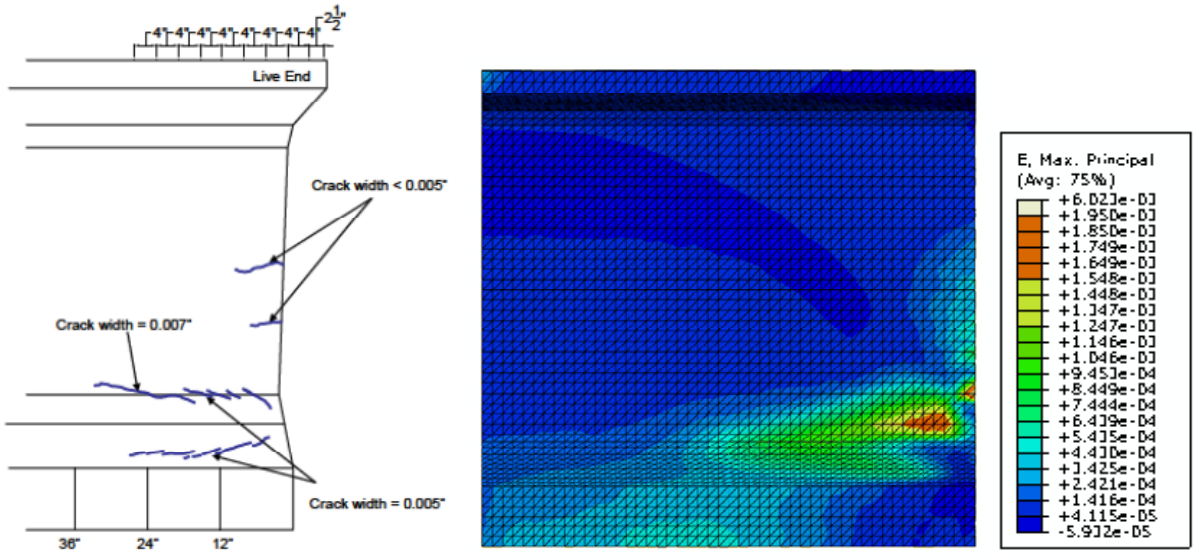

Figure 50 - Cracks on the girder tested as given by O'Callaghan (O'Callaghan 2008) (on the left), high principal maximum strain locations on the finite element model (right).

CHAPTER 5. RESULTS of the FINITE ELEMENT ANALYSIS

One of the major advantages of finite element analysis is the ability to obtain information on the entire domain modeled as opposed to experimental testing where the information comes from measuring locations and data collected at different times. The finite element analysis gives the analyst a wider vision in understanding the problem.

Abaqus/CAE can provide the reactions of the structure under arbitrary loading in terms of strains and stresses in any direction. Of particular importance to this research were the principal components of strains. The principal tensile strains and their directions determine where and in which direction cracking could occur. Plastic principal tensile strains and strain paths are another way of interpreting the cracks and explaining the behavior near the girder ends.

This chapter presents the resultant behavior in the concrete and reinforcement steel at the end of concrete wide flanged girders during and after prestressing and lifting. A discussion is carried on regarding the relationship of each characteristic crack with the stresses or strains causing them. Factors contributing to strain increase and hence cracking are also discussed.

The material property of the concrete was defined so that after concrete elements reach their tension cracking strain, they undergo increasing plastic deformations and lose their ability to carry further loads. The cracking limit was as discussed in Chapter 3 and based on an assumed concrete strength at transfer of 7000psi. For locations (cracks) where plastic strains develop, the magnitude of stress drops while the strain increases. For this reason, using strains for investigation of the behavior was preferred over using stresses. On the other hand, steel reinforcement bars were modeled as linear elastic since no yielding was anticipated. The effects in the rebars can be presented as stresses or strains.

The strands were assumed to have a transfer length equal to the AASHTO suggested distance of 36in. for the 0.6in. diameter strands. The bond stress along the strands was assumed as uniform. Modelling methods were described in Chapter 3.

The results in this chapter are given for a 54W girder with 32 straight and 8 draped strands. The girder is similar to the girder monitored at the Spancrete, Inc. plant described in Chapter 4. The girder is representative of the noted cracking problem as it exhibits all characteristics cracks. The trends the results follow are applicable for all similar wide flange girders.

5.1. Resultant Effects in Concrete

After all the prestressing force was transferred to the concrete, the magnitudes of the principal tensile strains in the concrete of the 54W girder are as shown in the side and end views of Figure 51.

Tension strain amplitudes are shown by means of contour plots to indicate where cracking is likely to occur. The principal tension strains at the surface of the girder are shown by various colors and range up to 1900με.

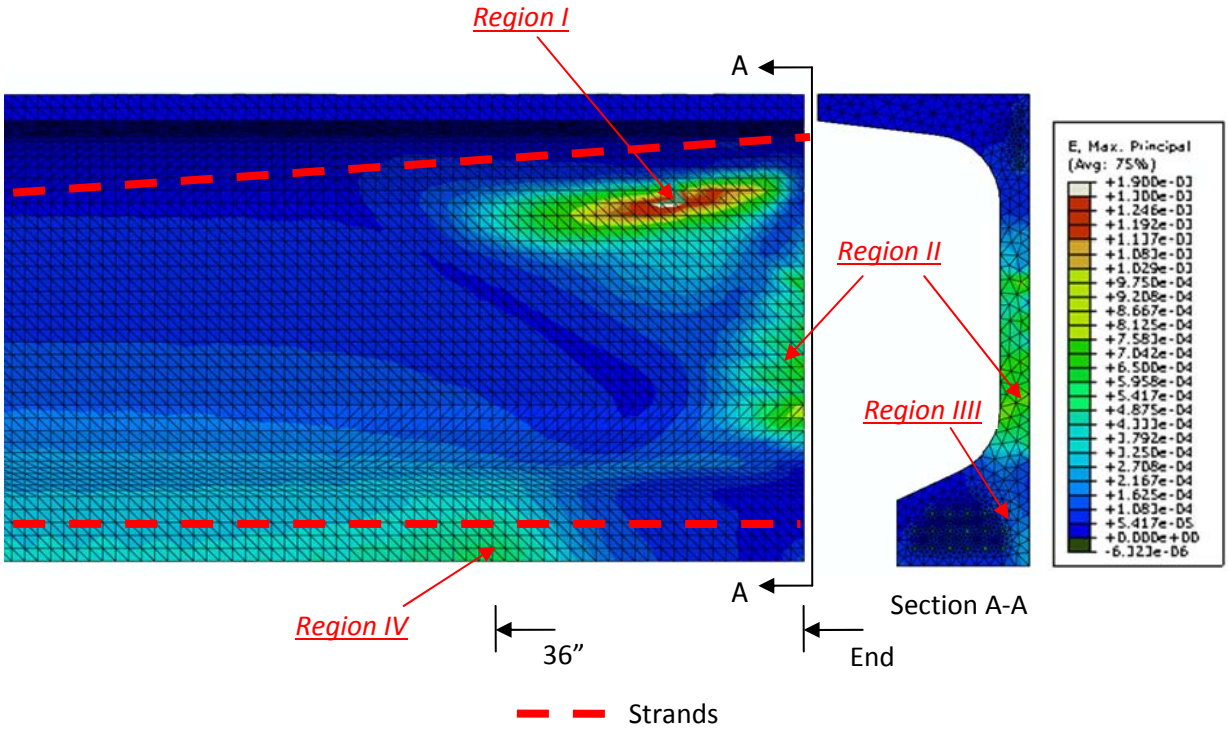

Figure 51 – Principal tensile strain contours of concrete in elevation view (left) and in cross section at the end (right).

Four regions of the girder where the principal tensile strains were significantly higher than average strains are marked on the same figure. As expected, most of these locations coincide with the cracking locations observed in the field. The largest magnitude strains occur in region I. This area is close to the draped strands, where the inclined cracks are found in typical girders. The strains on the vertical plane undergo a sudden increase around this region.

The second largest strain location is in region II. The strains are high all through the web, and the highest are at the lower portion of the web close to the bottom flange web junction. The locations of these high strains match the observed locations of horizontal web cracking.

The region III is located in the bottom flange close the middle of the width of the flange. It marks a region of high strains starting from the bottom of the girder, moving upwards to meet the horizontal cracking region (region II). The formation of the Y cracks as observed on girders is attributed to the high strains on the cross section in the bottom flange.

Region IV marks high strains in the bottom flange area peaking at the transfer length away from the girder end. These strains represent the radial pressure, sometimes referred as the bursting stresses, perpendicular to the compression introduced by the bottom flange strands. Although the finite element analysis indicated that these strains exceed the elastic limit, no cracking in this region was visible on any girders investigated at Wisconsin prestressed concrete production plants.

The contour plots of Figure 51 provide a clue to where cracking is likely to occur, but are insufficient alone. The principal strain direction plots as given in Figure 52 for compression and tension can be used to supplement the previous contour plots to explain cracking.

The direction of the principal tensile strains determines the direction of crack opening. Principal strains are indicated by lines with arrows. The direction of the line shows the direction of the strain and the length of the line is indicative of the size of the strain. The locations where arrows/lines are long in length and coincide in direction through the region, as in Regions I, II, and IV, indicate possible cracking locations. The principal compressive strain direction arrows are larger around the centerlines of strands in Region I and IV. The compression strut, created by the bond stresses with transfer, spreads out into the girder as prestressing is transferred along the length.

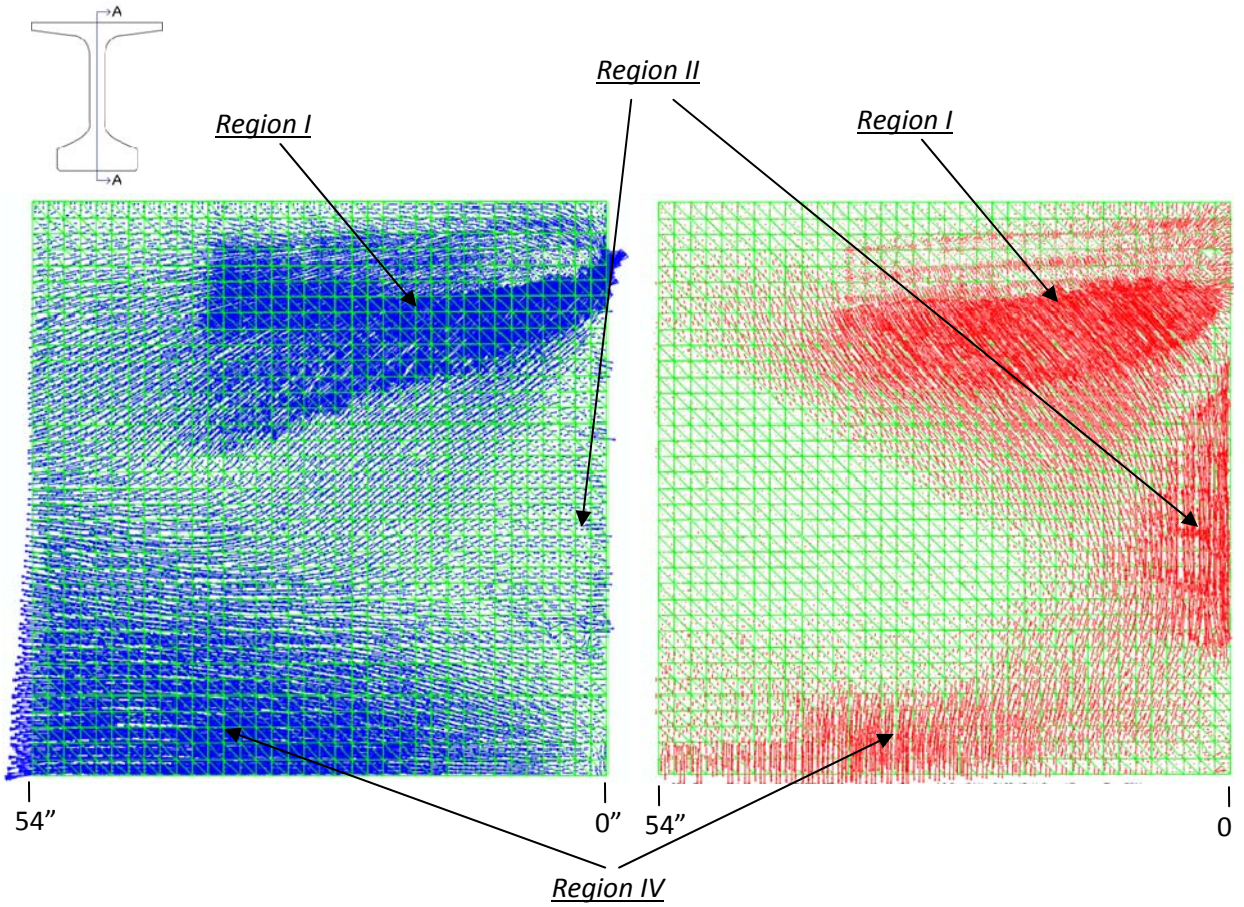

Figure 52 – Principal strain directions in elevation view in compression (left) and tension (right) for a girder with draped strands.

As the principal compression strains spread out into the girder, principal tensile strains form in a direction perpendicular to the compression strains in Regions I and IV.

On the other hand due to the opposite direction moments created by the eccentricity of the straight and the draped strands along the girder height, principal tensile strains form in the area bordered by straight and the draped strands in Region II. This tension tie lies in the direction of the girder height.

In order to evaluate role of the draped strands in this strain pattern, a girder without any draped strands was analyzed. This girder has 32 straight strands. It does not meet the top fiber tensile stress limit requirement and was only studied as a comparison to the girder with 32 straight and 8 draped strands.

The resultant principal tensile strain directions for a girder with no draped strands are shown in Figure 53. The strain field is very similar for a girder with and without draped strands. The draped strands, however, create larger inclined strains in the upper web/flange area. The direction of these strains, however, would not be significantly difference without the draped strands.

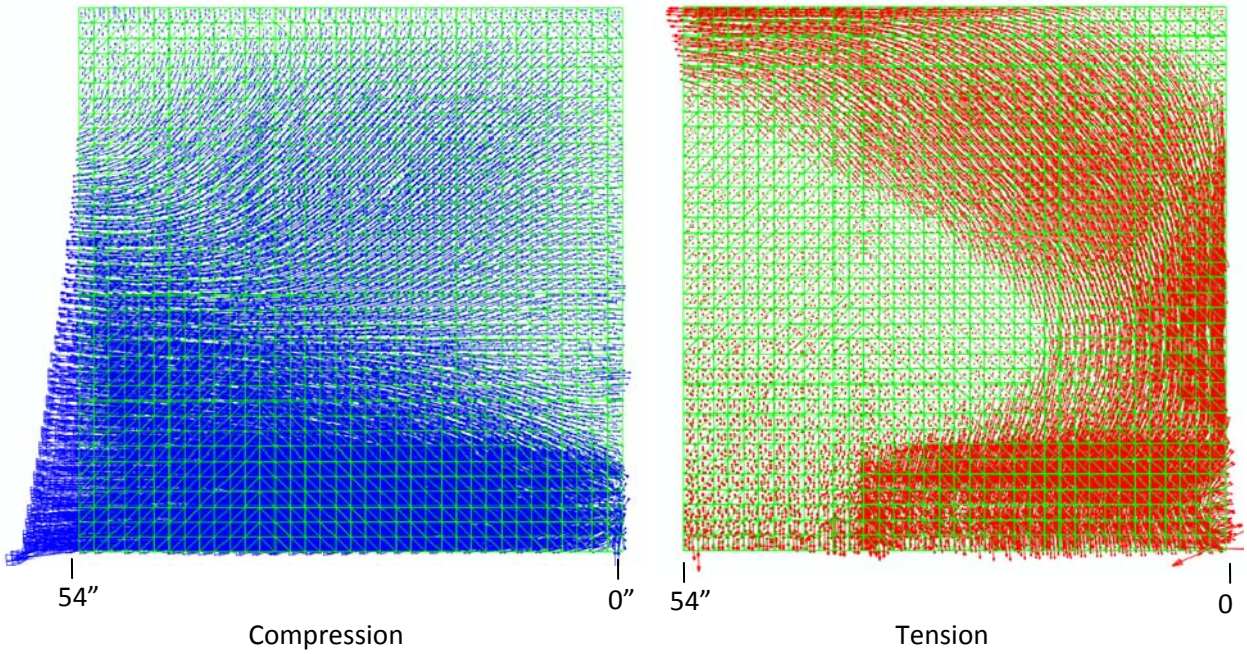

Figure 53 - Principal strain directions in elevation view in compression (left) and tension (right) for a girder with no draped strands.

The principal strain directions in the cross section of the bottom flange at 0, 6, 12, 18, 24, 36, 42, and 48 inches in from the girder end are shown in Figure 54 to investigate the strains causing Y cracking. These plots also are helpful in explaining the excessive bottom flange strains in Region IV.

To predict where cracks will occur, it is important to examine the tension strain trajectories in the section. If the strains in the material along any line on the cross section are all in the same or similar orientation, and their size becomes large enough, a crack is likely. If the orientation of the strains changes, then either a crack is unlikely to occur or the crack will change direction as it crosses the section.

Considering the sequence of plots in Figure 54, it is apparent that at the very end of the girder the principal tensile strain directions near the middle of the flange are all horizontal in direction. This represents a pattern which could lead to a vertical crack (the start of a “Y” crack) at the middle of the flange. Toward the top of this region the principal tension strains are no longer horizontal, but instead become tangent to the radius of the web-to-flange joint. The vertical crack that might have started in the

flange would turn toward one or both sides of the girder in the region of the radius – forming the "Y" crack. Between 6 and 18 inches in from the end the strains at the middle of the flange are no longer horizontal. A region of horizontal tensile strains has shifted slightly from center towards the exterior sides of the girder. From 18 in to 36 in, the strain directions follow a circular pattern around the strands suggesting outwards radial pressure (bursting strains) without any clear line where a crack through the section would likely develop (since cracks would be perpendicular to the strains). After 36 inches, no distinct trend in tension strain direction can be identified.

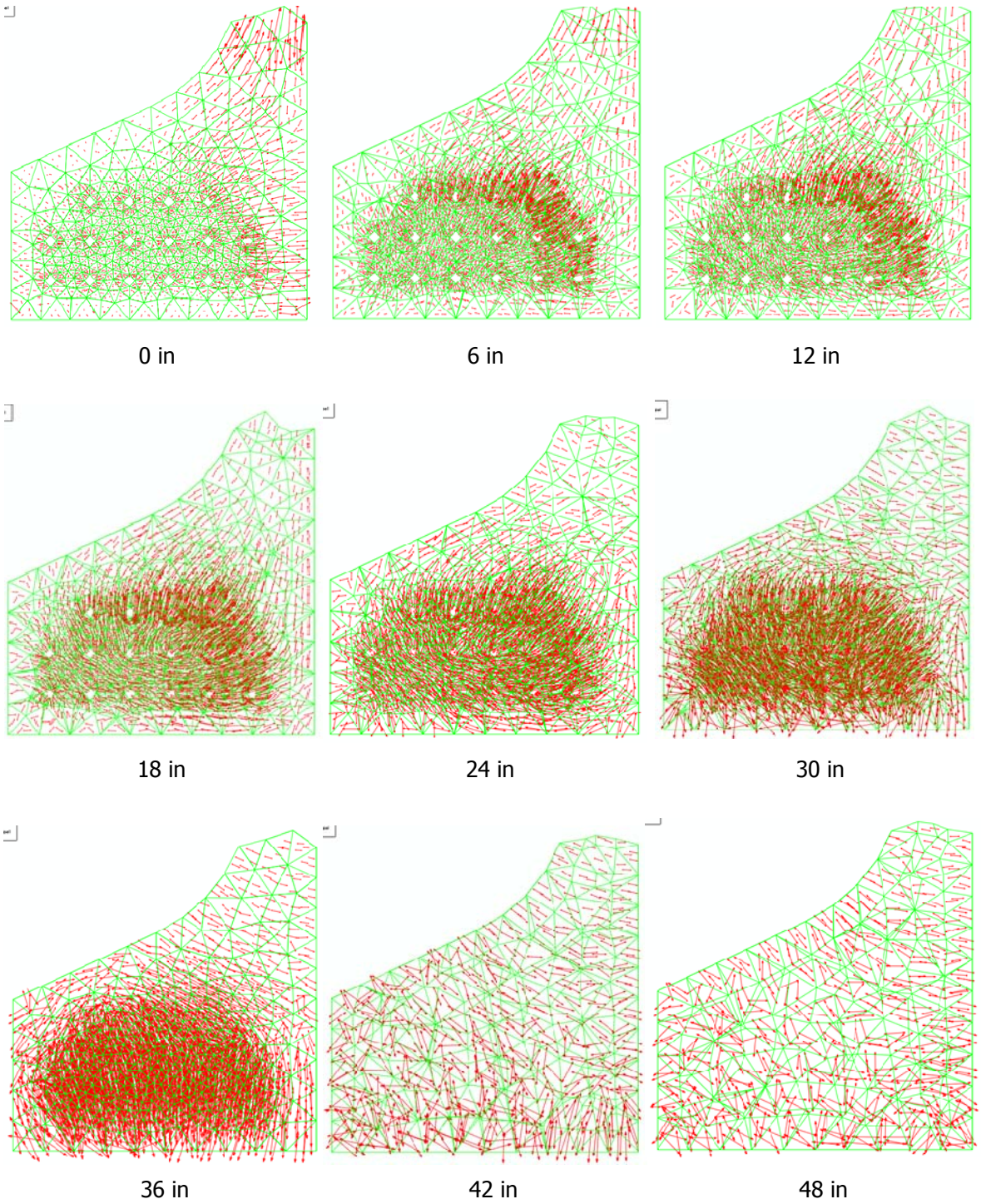

Figure 54 - Principal tensile strain directions on the cross section of the bottom flange at every 6 in from the girder end.

5.2. Resultant Forces in Reinforcement Bars

The reinforcement bars are modeled using linear elastic truss elements. After the nonlinear concrete elements reach their cracking strength force redistribution occurs. They soften and have reduced resistance capacity, transferring part of their previous stress to any adjacent rebar elements. If the reinforcing is capable of resisting the new force, with low strains, the crack size in the concrete will be controlled.

Determining the stresses/strains in the reinforcement bars was essential to evaluate the efficiency of the bars. The bars assisting in carrying the loads after cracking occurs can be identified, based on the resultant stress change that they undergo. The stresses in the reinforcement bars from a 54W girder end are shown in Figure 55 using colors to denote stress level. Dark blue represents very low stress and yellow to orange represents tension stress of 11-14 ksi. The results are taken from a model where only half of the girder cross section was included in the model considering symmetry.

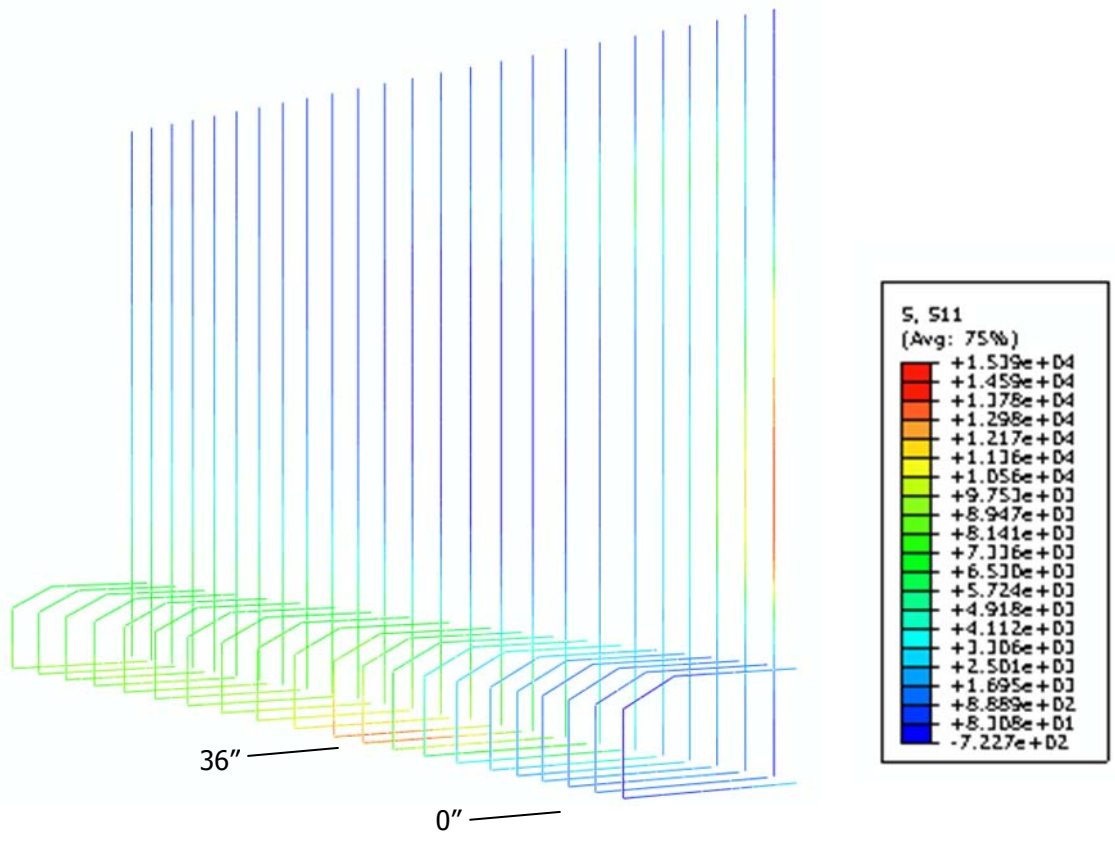

Figure 55 - Longitudinal stresses (psi) in the reinforcement bars.

The maximum rebar stress locations in the vertical web bars coincide with the location of the web cracks (see Figure 25). This result was expected as the participation of the reinforcement increases after cracking of concrete occurs. In this region, the reinforcement bars are parallel to the tension cracking strains in the concrete and therefore get engaged in load carrying after cracking. The vertical bars closest to the very end of the girder, crossing the web cracks, exhibit the largest stresses of up to 14ksi. The vertical bars further away from the girder end carry lower stresses in the web area.

On the contrary, the stresses in the bottom flange confinement stirrups are lower at the girder end and peak closer to the end of the transfer length. This is consistent with having the largest bursting effect near the end of the strand transfer length.

The peak stresses in reinforcement bars for this heavily prestressed girder do not exceed 15.5 ksi. The reinforcement bars remain well in the elastic domain and are only loaded to one fourth of their yield capacities.

5.3. Identifying the Causes of Cracking

Based on visual observations on numerous girders with cracking at precasting facilities and based on the finite element analysis findings on the direction and magnitude of strains and their change during prestressing, conclusions can be drawn regarding the sources of cracking. Each characteristic crack will be investigated separately.

5.3.1. Causes of the Inclined Cracks:

The analytically determined principal tensile strain directions shown in Figure 52 to 53 can be used to explain the visually apparent inclined cracks (shown in Figure 4) that develop at the girder end, start from near the top of the web, and extend downward as the distance from the end of the girder increases. The concrete tension strains near the top of the web shown in Figure 51 reach a value of 1900$\mu\varepsilon$, well above the cracking tension strain limit of the concrete. Cracking should definitely be expected in this region.

Due to the inclined cracks' proximity to the draped strands and their angle with the horizontal plane, these cracks are often associated with the use of draped strands. Finite element analysis without any draped strands (Figure 53) shows that the principal tension strain pattern and direction at the top of the web is still conducive to inclined crack development, even without the draped strands. This strain pattern is a result of the eccentricity of the straight strands and local internal bending. For very heavily prestressed girders, these strains can be higher than the theoretical cracking strain and cracking is expected.

Viewing the direction of the principal strains in Figure 53, the girder without draped strands is expected to have inclined cracks at an angle near to 45^{o} with the horizontal. In the girder with draped

strands the principal tension strains are close to perpendicular to the strands and an inclined crack that starts parallel to the draped strand would be expected.

Draped strands play a significant role in increasing the strains, and likelihood of cracking, in the region close to their center of gravity. For a girder with draped strands, a compression strut is formed in the upper web region around the draped strands after they transfer the stress to the concrete. Perpendicular to these principal compression strains, there are principal tensile strains often referred to as bursting strains. The direction of these added bursting tensile strains on either side, near the exterior of the web, is perpendicular to the axis of the draped strands. Without draped strands, principal tension strains already exist near the top of the web due to the bottom straight strands (Figure 53). The exterior strains near the top of the web, due to bursting, then nearly coincide with the direction of the principal tensile strains created by the straight strands. Therefore, the draped strands trigger an inclined crack formation sooner than would occur in a girder without draped strands. For certain girders, just removing the draped strands will reduce the upper web strains to a level below the concrete cracking limit.

The net cross sectional area of concrete resisting these tensile strains in the upper web is smaller when draped strands displace some concrete. For girders where the draped strands are in the web, obvious cracking is likely to occur along the draped strand alignment. Girders without draped strands will still exhibit inclined web cracking if a large highly stressed volume of straight strand is used in the bottom flange.

5.3.2. Causes of the Web Cracks:

These cracks are attributed to the eccentricity of the straight and draped strands in the direction of the girder depth. Figure 56 shows the eccentrically applied prestressing load along the depth, the free body diagram of the web and the consequent deflected shape of the web alone with potential cracking. The resultant moment, an axial load and a shear reaction carried by any horizontal section are also shown. The draped strands, if present, create a moment in the web in the direction opposite to the moment created by the straight strands. These two reaction moments, and the prestress reaction put the web under bending. The tension side of the web is at the girder end and therefore may experience cracking under heavy loads.

While the draped strands have a small vertical component applying compression to the web, it is not comparable to the tensile forces created by the eccentricity of the draped strands.

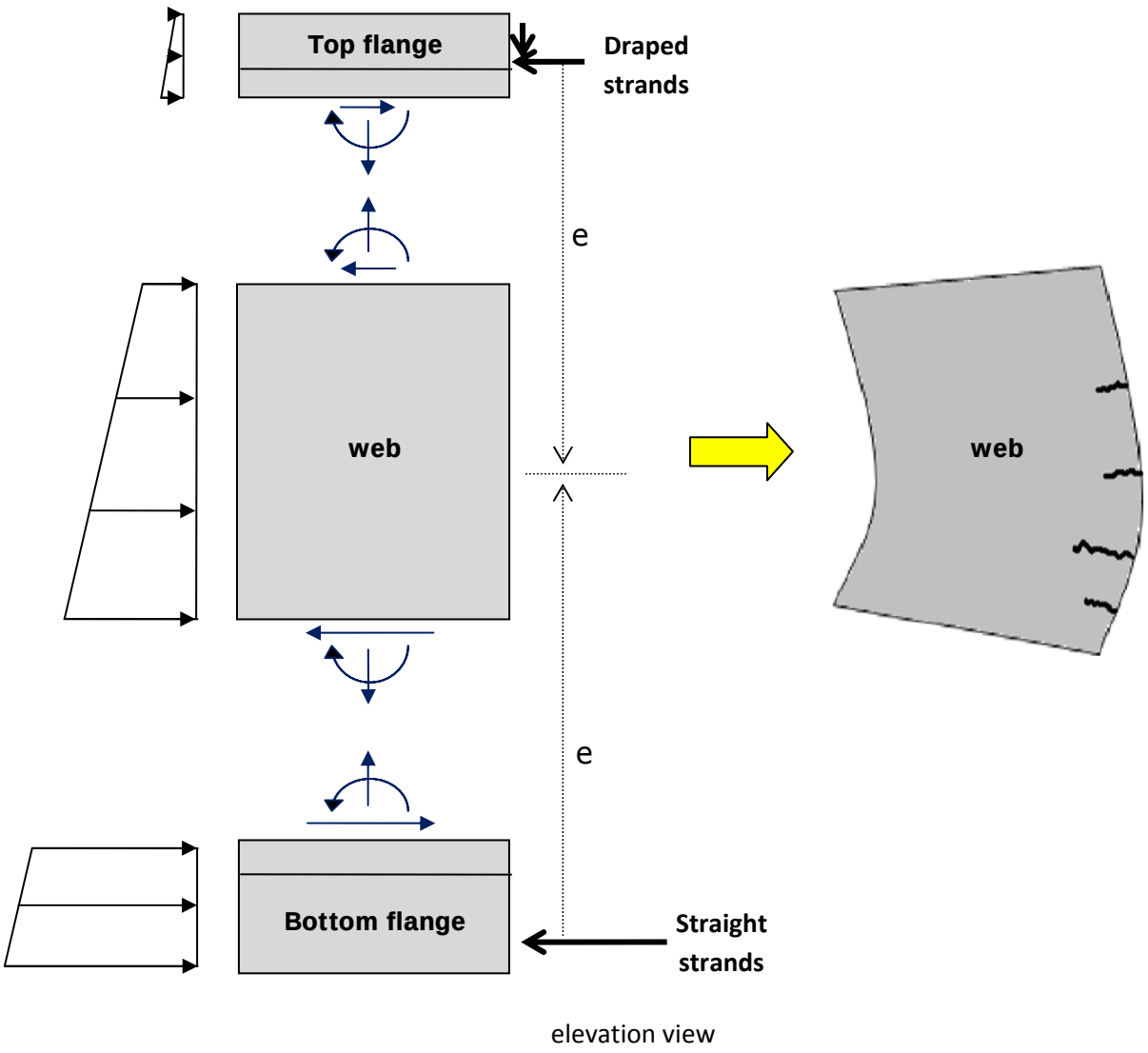

Figure 56 – Example free body diagram illustrating web cracking

5.3.3. Causes of the Y Cracks

These cracks form a separation line between the two sides of the bottom flange and the web. The vertical crack seems to be a result of the eccentricity of the strands in the bottom flange over the width of the girder. Conceptually similar to web cracking, strands on each side of the bottom flange create moments in opposite directions on vertical sections. The free body diagram representation of the forces on vertical sections along the bottom flange is shown in Figure 57.

The moments result on each side of the mid web section cause the bottom flange section to bend. The side of the mid web section close to the girder end goes under tension and may form a vertical

crack. The Y shape forms when this vertical crack meets the lower horizontal web cracks in a transition zone where the eccentric forces in the direction of the depth and the width overlap.

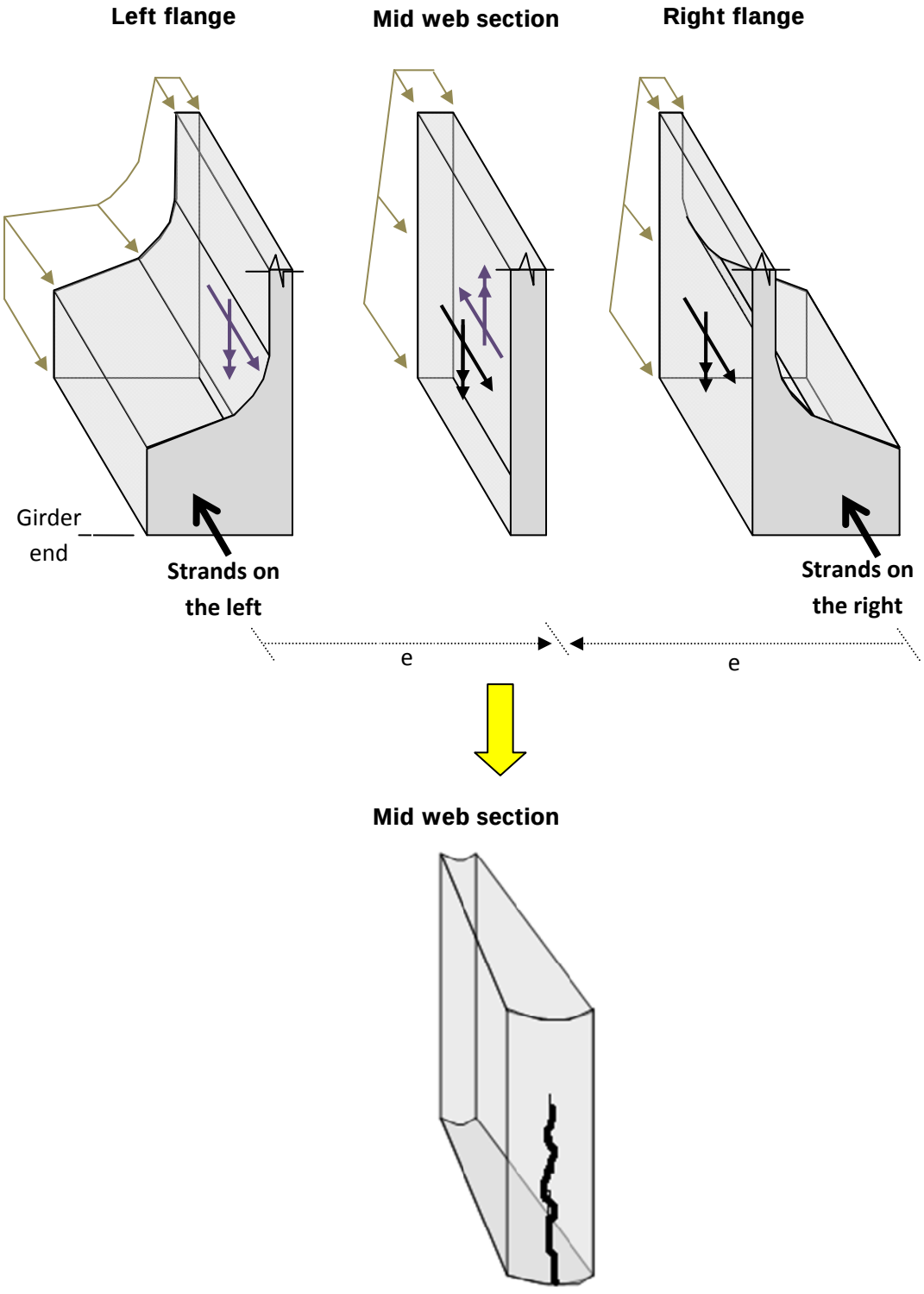

Figure 57 - Example free body diagram illustrating bottom flange Y cracking

Strands that are placed closer to the exterior face of the girder will create larger moments and can increase Y cracking strains. When the strands are unevenly distributed over the bottom flange, locations between strands can form paths the cracks can potentially form on. For girders with draped strands, the mid web section will lack the 8 straight strands and will likely form vertical cracking.

5.3.4. Causes of Excessive Bottom Flange Strains:

In addition to the three types of characteristics cracks explained above, the finite element models predict another region where plastic strains occur. This region is marked as Region IV in Figure 51 and Figure 52. However, no visible cracking representing these strains was detected during the field observations.

These strains in the bottom flange increase along the girder length, peak at the end of the transfer length, and stay above the theoretical cracking limits over the length of the girder. This result is contradictory to the field observations, as no cracking was detected away from the girder end in the bottom flange.

This concept relates to the radials strains created perpendicular to the compression strut created by the bottom flange strands. AASHTO, LRFD Design Specifications, Section 5.10.10.2 required stirrups around the strands to confine the bottom flange against these strains. Even though confinement stirrups were modeled in the finite element models, the strains were still above the theoretical cracking limits. The disagreement of this result with the field observation can be attributed to several factors.

The bottom flange of the real girders might be experiencing numerous micro cracks that are not visible during inspection. Figure 58 shows the directions of the plastic strains in the web at 36” and 42” from the girder end. It is possible that the plastic principal tensile strains in the bottom flange do not consistently follow the same direction over a distance long enough for the strains to form a crack in the field. The change in the direction of the strains becomes clearer after 36 in away from the girder end. It is hard to identify a pattern of strains in the bottom flange after this distance.

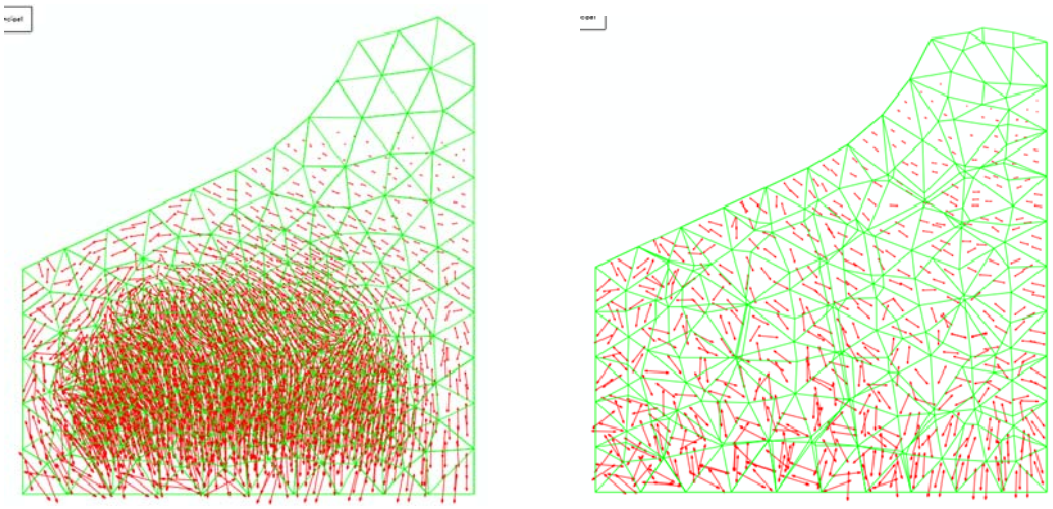

36″ 42″

Figure 58 – The directions of plastic principal tensile strains in the bottom flange at 36 (left) and 42 (right) inches away from the girder end

CHAPTER 6. EVALUATION of POTENTIAL SOLUTIONS

This section includes the study conducted to evaluate the effectiveness of potential solutions through modifications to the girder characteristics. Finite element modeling is a viable and economical alternative to testing for this purpose.

The Wisconsin 54W, 72W and 82W girders all exhibit the same combination of cracking, as witnessed at the precast plants in Wisconsin. The cracking in the girder webs appears to be more serious in the deep 82W girders. All of the girders exhibit the "Y" cracking in the bottom flanges. From visual observations, the degree of Y cracking appears to be related to the amount of prestressing applied to the flange, and not dependent on the girder type. Any of the girder sizes could be used as the basis for examining potential solutions, since similar stress situations exist in all.

The girder monitored at Spancrete as discussed in Chapter 4.2 was used as a control case for looking at solutions in this study unless otherwise noted. The girder with 32 straight and 8 draped strands, 129 ft long, belongs to the upper capacity range of 54Ws. This girder was instrumented during de-tensioning and exhibited visible cracking on site.

The potential design solutions to control cracking that were considered are listed below. Each potential solution was explored by making changes to the base model and comparing the results of the analyses to the current "control" condition.

1. The girder end zone reinforcement bar pattern.
2. Debonding and the level of debonding.
3. Combination of end zone reinforcement pattern and debonding.
4. The strand cutting order.
5. Lowering, lowering and spreading, or removing the draped strands.
6. Investigating any impact of coping the upper flange.

The most illustrative output to explain cracking was taken from the principal tensile strains or principal plastic tensile strains. Contour plots, principal tensile strain direction plots or quantitative strain plots are used to demonstrate the results in the following sections. The "Concrete Damage Plasticity" material model used in the analysis program Abaqus does not explicitly model cracks or report crack widths. Instead, the plastic strain developed in the material as it softens with cracking is reported. Approximate crack widths are estimated utilizing the principal tensile strain values as an additional means of comparing the effect of design changes.

6.1. The Girder End Zone Vertical Reinforcement Bar Pattern

The current WisDOT standards for the "W" type beam sections include special vertical stirrups in the end zone to resist bursting effects and control web cracking. A series of finite element models of 54W sections were created with varying girder end zone reinforcement bar patterns. These models were aimed to study the effect of end reinforcement area, size, and spacing on the effectiveness in controlling web cracks and tension strains.

The standard reinforcement details for 54W prestressed girder ends, as given by WisDOT Bureau of Structures {{96 Bureau of Structures 2011}}, are highlighted in Figure 59. A first set of five vertical #6 bars at 3in spacing is anticipated to be designed and placed closest to the girder end to carry the splitting forces causing web cracking. Vertical #4 bars at 4-1/4" spacing follow the first set of bars. Finally, the bottom flange is confined with overlapping "U" shaped #3 stirrup bars at the spacing of the vertical bars.

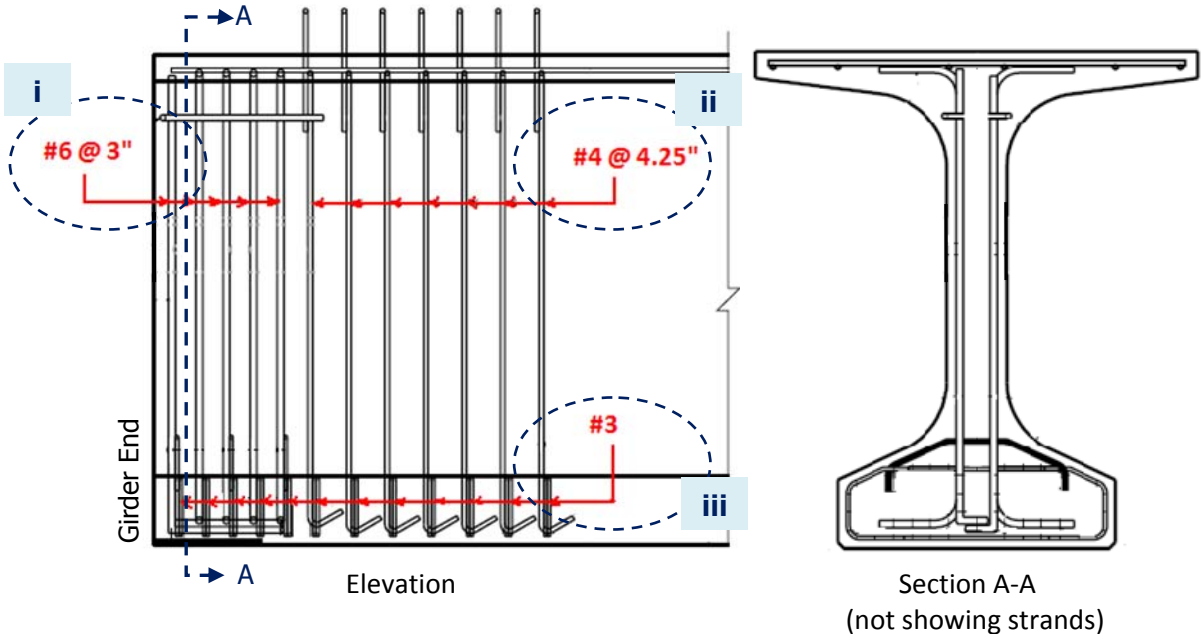

Figure 59 – The standard end zone reinforcement for 54W girders.

The compliance of this end reinforcement configuration for this section with the AASHTO LRFD Bridge Design Specifications {{60 American Association of State Highway and Transportation Officials 2008}} was found to be adequate as discussed previously in this report. Despite this fact, the web cracks remain visible at the girder ends.

Design variations were obtained by modifying the three groups of reinforcement at the girder end region: i. The first set of five vertical reinforcement bars from the girder end, ii. The second set of vertical reinforcement bars from the girder end, and iii. The bottom flange confinement reinforcement. Each group of reinforcement is marked on Figure 59.

i. <u>Modifying the first set of vertical bars from the girder end</u>:

The varied configurations of vertical web reinforcement implemented into finite element models are summarized in

Figure 60 and listed below.

- Standard Reinforcement (Five #6@3")
- Five #7 @3"
- Five #9 @3"
- Five #10 @3"
- Two #10 @3", three #6 @3"
- Five #6 @1 7/8"

.

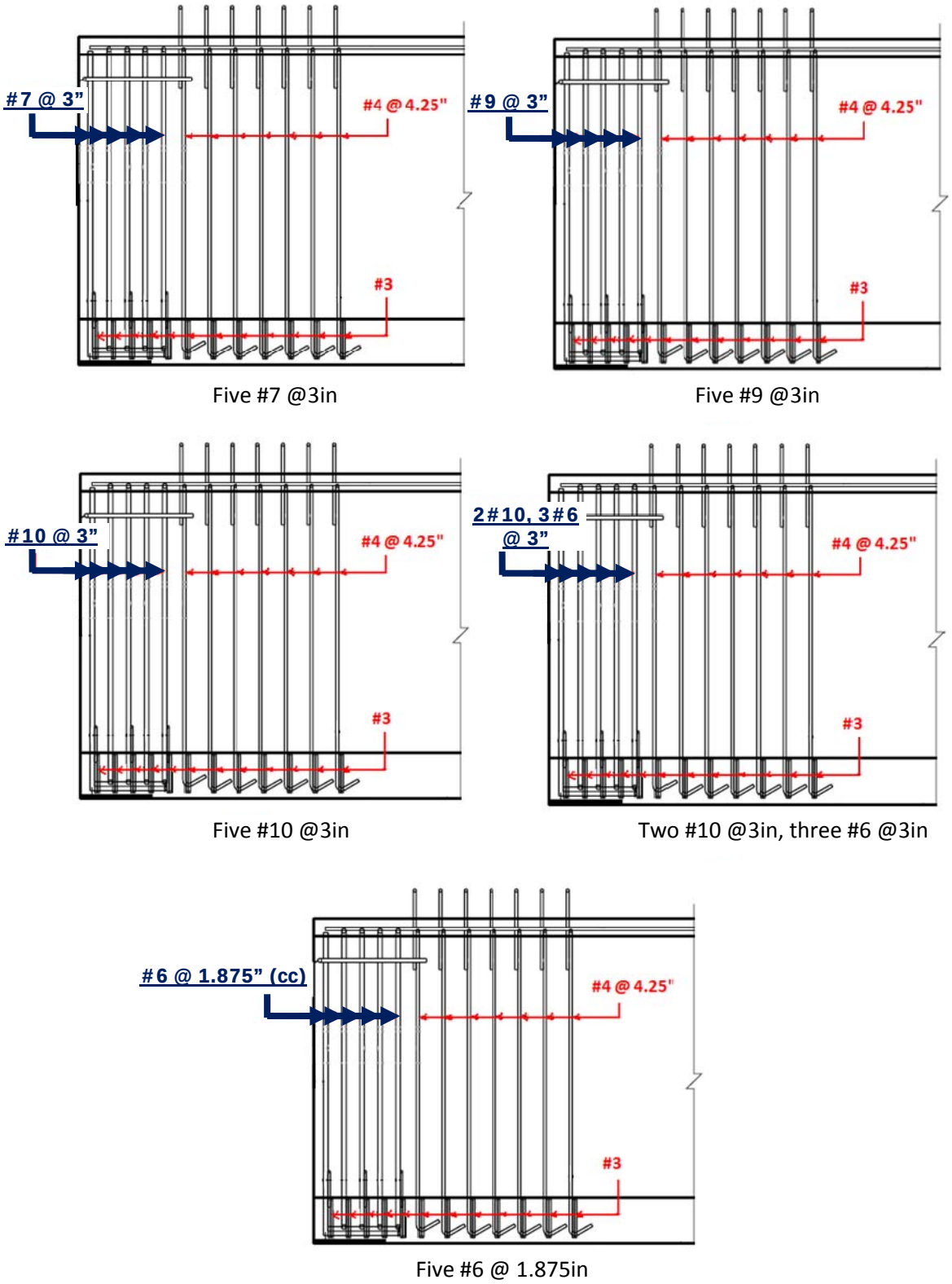

Figure 60 – Elevation views showing the modifications to the first set of standard vertical bars from the girder end.

The resultant principal tensile strains are compared for the web cracking and inclined cracking regions in Figure 61 and Figure 62 respectively along the lines marked on the upper right corner of each graph. These strains are recorded after the prestress release and do not include the potential amplification during girder lifting. A dashed line, denoting the expected maximum tolerable strain prior to cracking, is also shown for reference. (Using symmetry, only ½ of the girder was modeled – as evident in the upper right corner figures.)

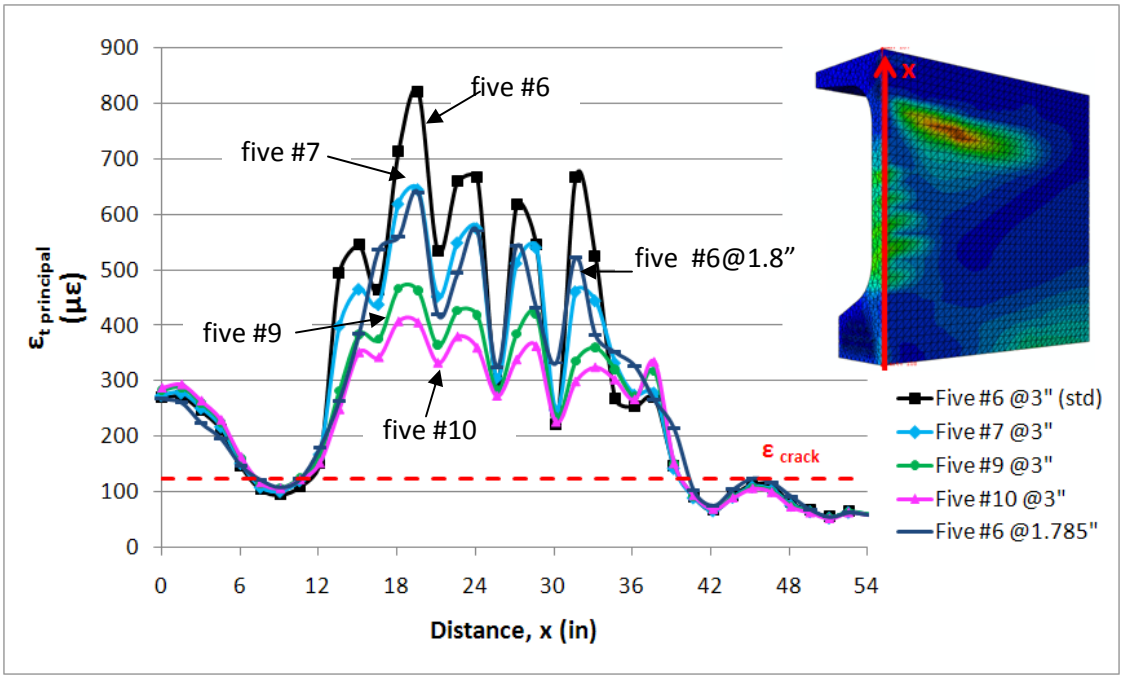

Figure 61 – Variation of principal tensile strains at the girder end along the depth of the girder for each reinforcement configuration.

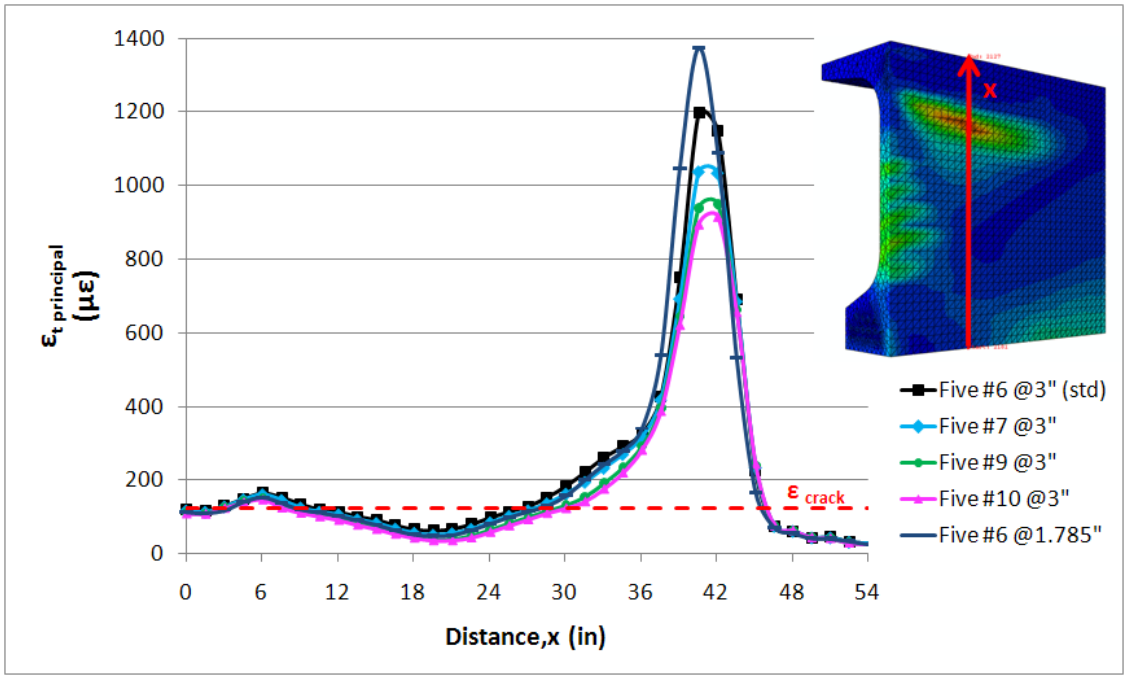

Figure 62 - Variation of principal tensile strains at 18in from the girder end along the depth of the girder for each reinforcement configuration.

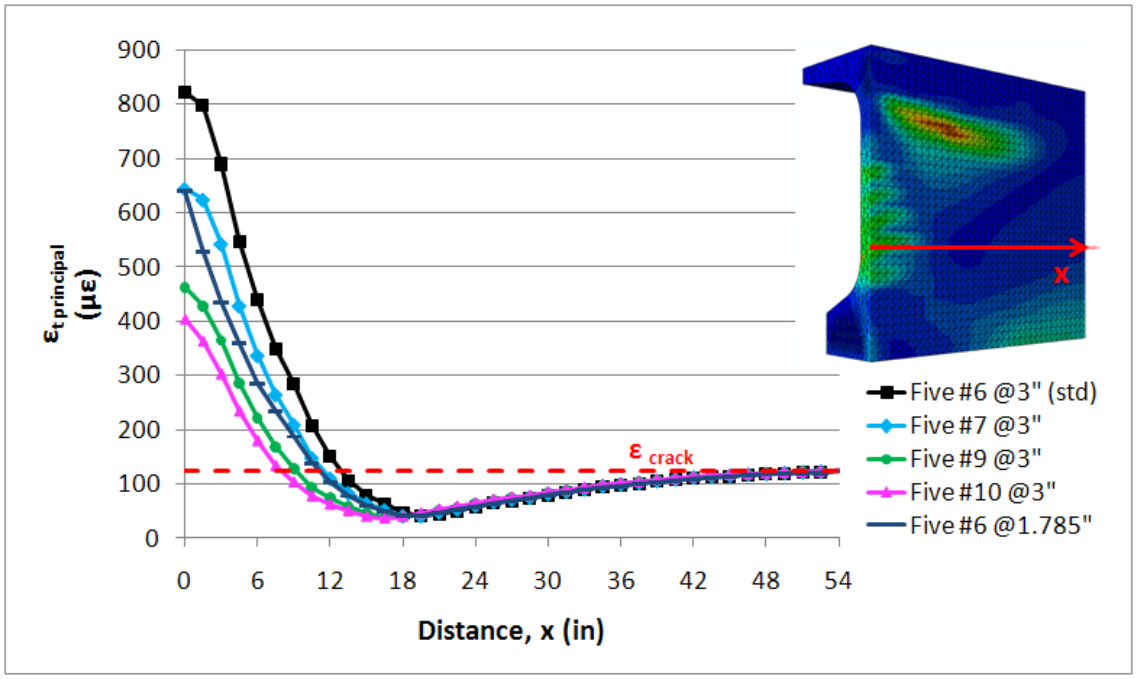

Figure 63 – The principal tensile strains along the largest web crack direction.

The behavior is also expressed in a contour plot form in Figure 101 in the Attachments section. The improvement of strains around each characteristic crack by changing the first set of reinforcement bars from the girder end is discussed below.

The strains causing the inclined cracks are plotted over the depth of the girder at a section 18 inches from the end in Figure 62. The strains causing the inclined cracking near the upper flange area were reduced by 15-25% by upsizing all five bars from #6 to #7-#10 bars. Reducing the spacing of the standard #6 bars increased the inclined cracking strains. The vertical reinforcement bars do not cross the inclined cracks perpendicularly. Therefore, the vertical bars have a limited impact in restraining the inclined cracks. The strains remain above the theoretical cracking limit.

The modification of vertical reinforcement bars was most effective in reduction of the strains in the web area at the very end of the girder, shown in Figure 61. Vertical reinforcement bars cross these cracks perpendicularly. The strain reduction compared to the standard #6 @3" bars was between 20%-50% for models with #7 and #10 bars. The model with #6 bars at 1.875 in spacing gave very similar results to using #7 bars at 3in spacing.

No significant difference was observed between the models in reducing strains in the bottom flange area where the Y cracks and excessive bottom flange tension strains are seen.

A special case in this study was the comparison of five #10 @3" bars with two #10 @3", and three #6 @3". This analysis was carried out to identify how effective each vertical rebar was in carrying web splitting forces.

Figure 64 and Figure 65 indicate that the two cases behave nearly identically and both are quite effective at reducing the tension strains in the web, but not below the cracking level. In Figure 6 the reduction of concrete strain near each bar is evident in the up and down pattern of the line for the #6 bar condition. The same pattern appears with the larger bars but to a lesser degree, showing that they are more effective at overall reduction of average strain.

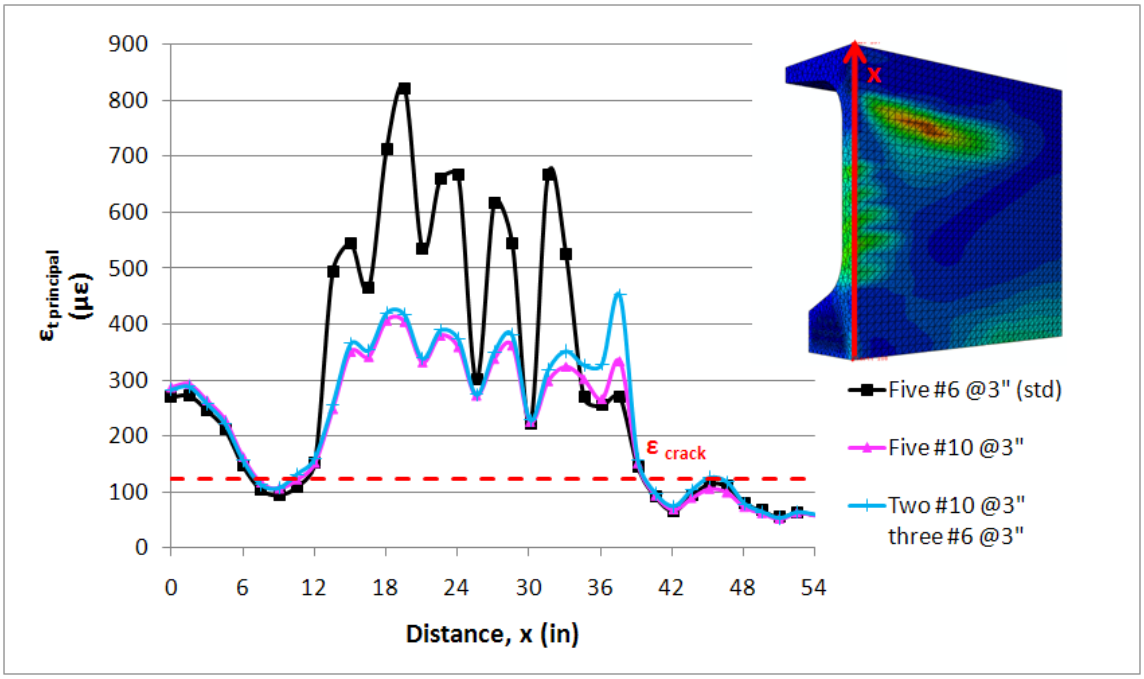

Figure 64 - Principal tensile strains along the depth as a result of using five #10 @3" bars versus three #10 @3", two #10 @3" at the girder end.

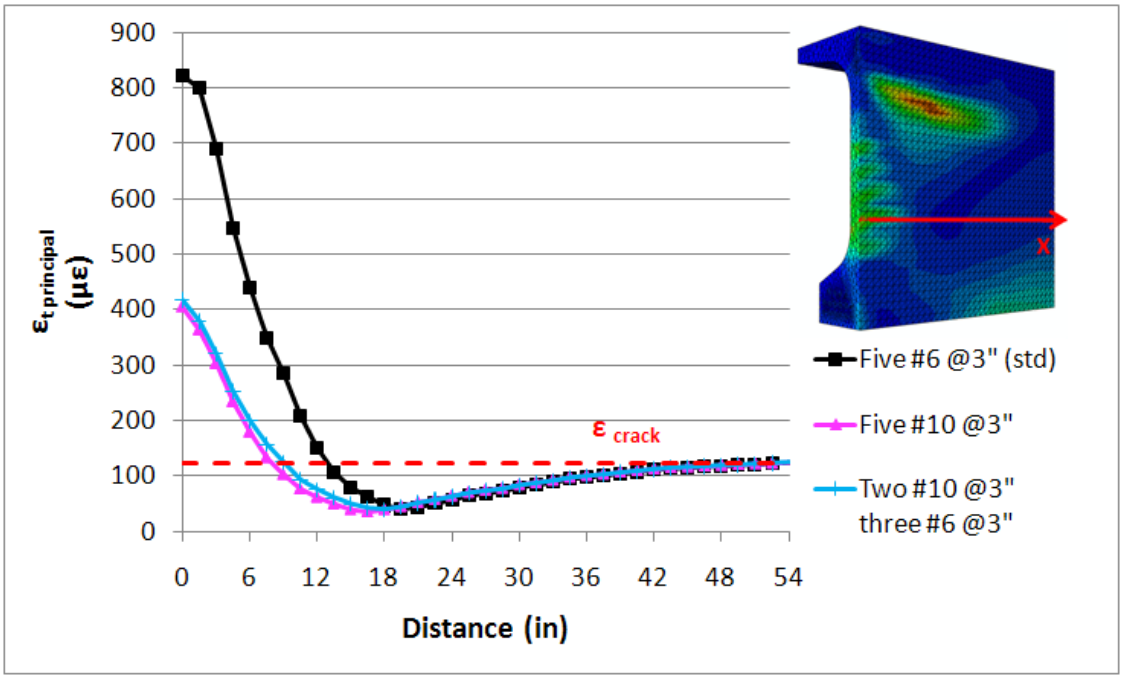

Figure 65 - Principal tensile strains along the largest web crack as a result of using five #10 @3" bars versus three #10 @3", two #10 @3" at the girder end.

These results indicate that the most effective bars in controlling the web cracking strains are the bars closest to the end face of the girder. Bars located after the first 2 bars (first 8 inches from the girder end) do not have a significant role in reducing the web end cracking strains.

The end zones of these types of girders are already congested with reinforcement bars and strands. The suggested larger size bars are harder to fit and harder to bend with the required radius. The analysis of the cases with five #10 @3" bars compared with two #10 @3", and three #6 @3" suggests that it is sufficient to only modify the first two bars to reduce the size of web cracks in the end region. This finding is in agreement with the findings of other researchers where the most effective bars were found to be the ones closest to the end. {{26 Tuan, C.Y. 2004}}

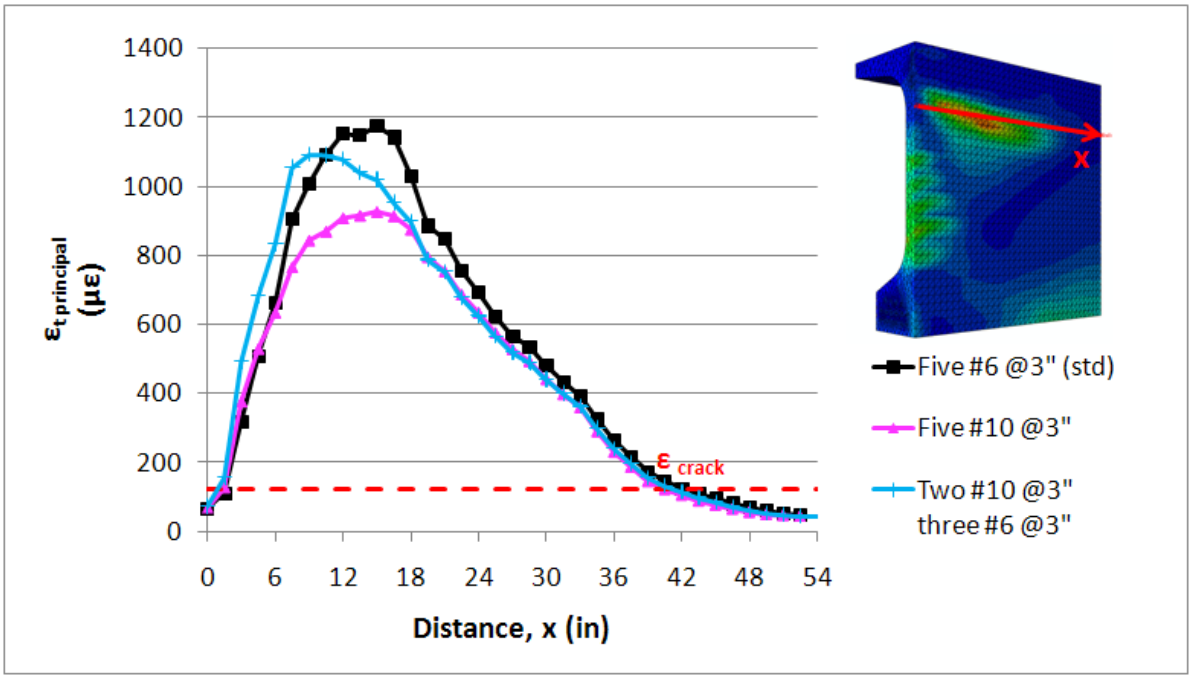

Figure 66 - Principal tensile strains crossing the inclined crack as a result of using five #10 @3" bars versus three #10 @3", two #10 @3" at the girder end.

On the other hand, having 2 #10 bars at the end shifts the initiation point of inclined cracking towards the girder end. 2#10 bars are not as efficient as 5#10 bars in restraining the inclined crack. This is illustrated in Figure 66.

In summary, increasing the vertical web reinforcing bar size at the end of the girder to larger bars can reduce the size of plastic tension strains, and therefore crack widths in horizontal web cracking and inclined web cracking. The increased reinforcing does not reduce the strain to levels below the concrete cracking strain. Increasing the vertical bar size provides added problems, due to the congestion of reinforcing at the girder end, and is likely to be an impractical solution.

ii. Modifying the second set of vertical bars from the girder end:

The selected cases of reinforcement configuration to measure the effect of the vertical web reinforcement bars further from the girder end are listed below. These bars cross the region of the web where inclined web cracking was observed.

- Standard Reinforcement (#4 @4 ¼")
- #5 @4 ¼" (50% more steel than standard case)

The modified reinforcement pattern is shown below in Figure 67. The first five vertical bars at the end of the girder are the standard reinforcement.

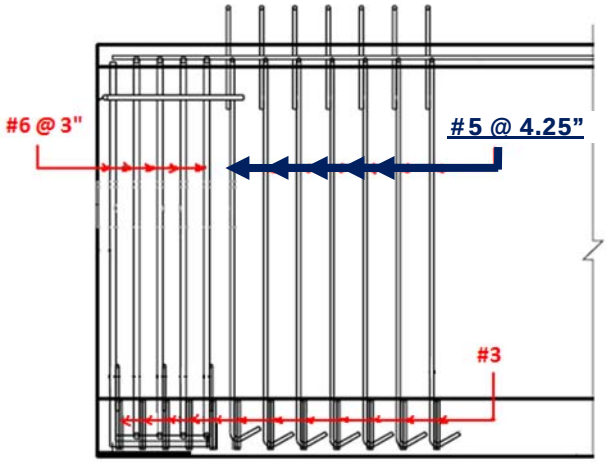

#5 @4 ¼"

Figure 67 - Reinforcement configuration where the size of the vertical reinforcement bars away from the girder end are varied from the standard pattern #4 to #5 bars.

Modifying the second set of reinforcement bars did not substantially change the concrete tension strains in any of the locations on the girder cross section. The resultant strain plots were almost identical for the two cases and are therefore omitted from this section. This finding is in agreement with the earlier prediction of the negligible impact of the reinforcement bars away from the girder end.

iii. Modifying the bottom flange confinement reinforcement:

Confinement stirrups are placed to control cracking in the bottom flange due to the tension strains created as a result of the spreading pattern of compression transferred to the flange by the strands and perpendicular to the principal compression strains along these strands.

The finite element models investigated for this case are:

- Standard detailing as in Figure 59 (#3 @3" and @4.25" stirrups)
- #5 @3" and @4.25" stirrups
- #3 @3" and @4.25" circular hoops (spiral)

First, the size of the bottom flange stirrups was increased. Second a girder with circular hoops instead of the bottom flange stirrups was modeled. The two cases are shown in Figure 68.

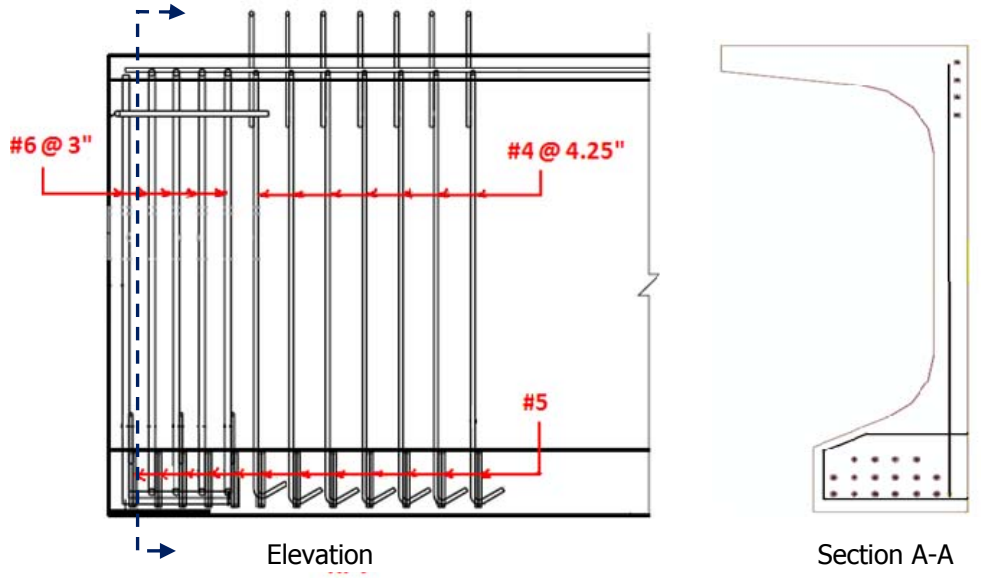

Elevation Section A-A

#5 @3" and @4.25" stirrups

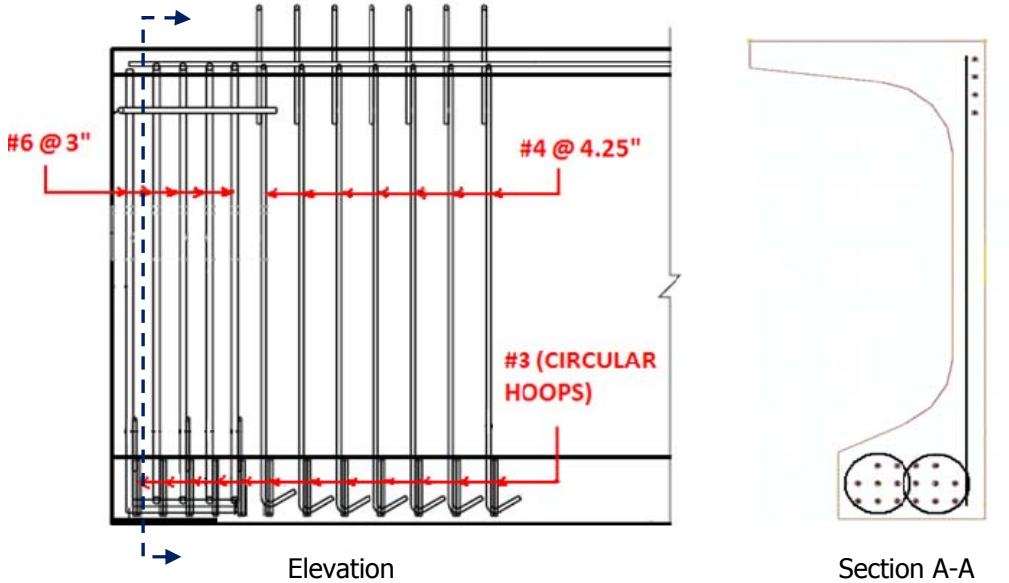

Elevation Section A-A

#3 @3" and @4.25" circular hoops

Figure 68 - Reinforcement configuration where the bottom flange confinement reinforcement bar size is varied from the standard pattern.

Increasing the size or varying the shape of the bottom flange confinement reinforcement did not lead to the expected reduction in concrete tension strains.

In summarizing the effects of changing the transverse reinforcing at the end of the girders, increasing the size of the first set of vertical reinforcement bars at the girder end was helpful in reducing the web tension strains the most (20-50%). Although not to the same extent, larger bars lead to smaller inclined tension strains in the web. The most effective bars were found to be the closest ones to the end, and upsizing the first two bars from the end is a possible step in reducing crack size. Increasing the size of the end bars, however, is not sufficient to reduce concrete tension strains below the cracking limit. Reinforcement bar modifications did not have significant effects on Y cracking strains or bottom flange tension strains in the concrete.

6.2. Debonding Stands at the Girder End:

Debonding some of the strands at the girder end will directly decrease the compression stresses transferred to concrete, and thus indirectly the tension stresses. Reduction of tension stresses might reduce web cracking, but the focus of debonding is particularly on reducing Y cracking in the bottom flange. It is anticipated that achieving the prestress transfer gradually by means of debonding could lead to limited cracking. The level of debonding necessary to eliminate or limit cracking is investigated in this section.

Debonding some strands at the girder end reduces or eliminates the need for the draped strands. If the draped strands could be eliminated, the setup and tensioning of strands in girders would be simplified.

AASHTO LRFD Bridge Design Specifications {{58 AASHTO, L. 2008}} 5.11.4.3 state that "The number of partially debonded strands should not exceed 25 percent of the total number of strands" and "The number of debonded strands in any horizontal row shall not exceed 40 percent of the strands in that row". It also requires that "Not more than 40 percent of the debonded strands, or four strands, whichever is greater, shall have the debonding terminated at any section." These requirements are partially based on preserving the contribution of the bonded strands to the shear capacity. The commentary notes that higher percentages of debonding have been used in some states with success and past experience can be considered when the shear resistance is carefully investigated at any section. Based on the commentary, some strand debonding cases that do not fully comply with the specifications were also studied.

The impact of debonding strands at the girder end as a potential solution was investigated through the following strand configurations. In each configuration the first part of the label "DB" refers to debonding and the following number represents the % of total strands that are debonded at the beam end.

- DB 0: All strands are bonded at the girder end. (Figure 69)
- DB 25-A and DB25-B: 25% of the total number of strands were debonded at the girder end. These strands were bonded at 15ft and 35ft from the girder end in groups of 4 and 6 strands, respectively. (Figure 70)
- DB 35-A and DB 35-B: 35% of the total number of strands were debonded at the girder end. These strands were bonded at 15ft and 35ft from the girder end in groups of 6 and 8 strands, respectively. (Figure 71)
- DB 50-A and DB 50-B: 50% of the total number of strands were debonded at the girder end. These strands were bonded at 15ft, 25ft and 35ft from the girder end in groups of 8, 8 and 4 strands, respectively. All draped strands were eliminated. (Figure 72)

These cases are also summarized in Table 4.

Model Name	**% of total strands debonded at the end**	**Number of Strands Bonded at (from the girder end)**			
		0 ft (straight + draped)	**15 ft**	**25 ft**	**35 ft**
DB 0	0 %	32 + 8	-	-	-
DB 25-A DB 25-B	25 %	28 + 2	4	-	6
DB 35-A DB 35-B	35 %	24 + 2	6	-	8
DB 50-A DB 50-B	50 %	20 + 0	8	8	4

Table 4 - Percentage of strands debonded at the girder end and number of strands bonded at 0 ft, 15 ft, 25 ft and 35 ft from the girder end.

Debonding is an alternate method to draping some strands at the girder end to ensure zero tension at the top fiber of the girder. The cases studied here checked the limits of tension and compression stresses at top and bottom fibers according to the ACI 318-05, Article 18.4 {{84 American Concrete Institute 2008}}. While 25% and 35% debonding still requires 2 draped strands, there was no need for draped strands with 50% of the strands debonded at the girder end.

For each level of debonding, cases A and B were created to investigate how debonding different sets of strands at the girder end could affect the tension stress and the resulting Y shaped cracking in the bottom flange.

Letter A represents a strand pattern where at the end of the girder, the strands left bonded to concrete were mostly the ones closer to the exterior sides of the bottom flange. Interior adjacent rows of strands were debonded.

Letter B represents strand patterns where at the end of the girder, mostly the interior strands were left bonded to concrete. The columns of strands left bonded to the concrete were also well distributed across the cross section. The differences between case A and case B models can be observed in Figure 69 through Figure 72.

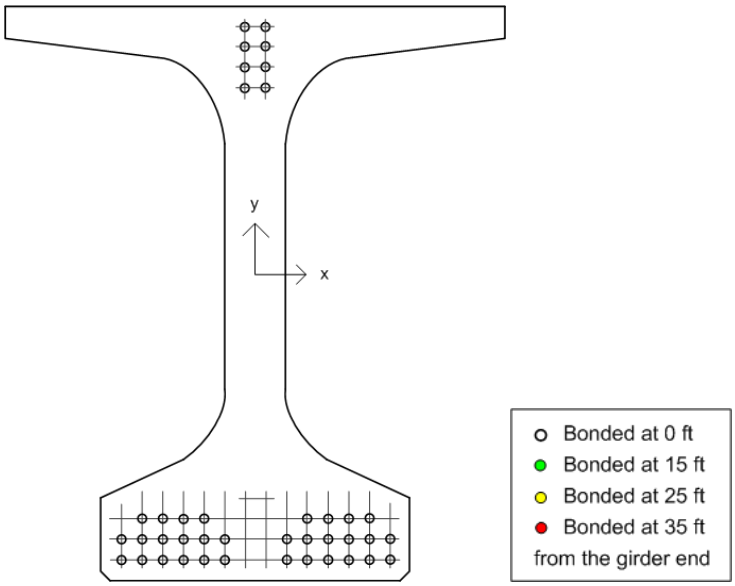

Figure 69 – Girder cross section from the end showing the strand pattern, used in case DB 0.

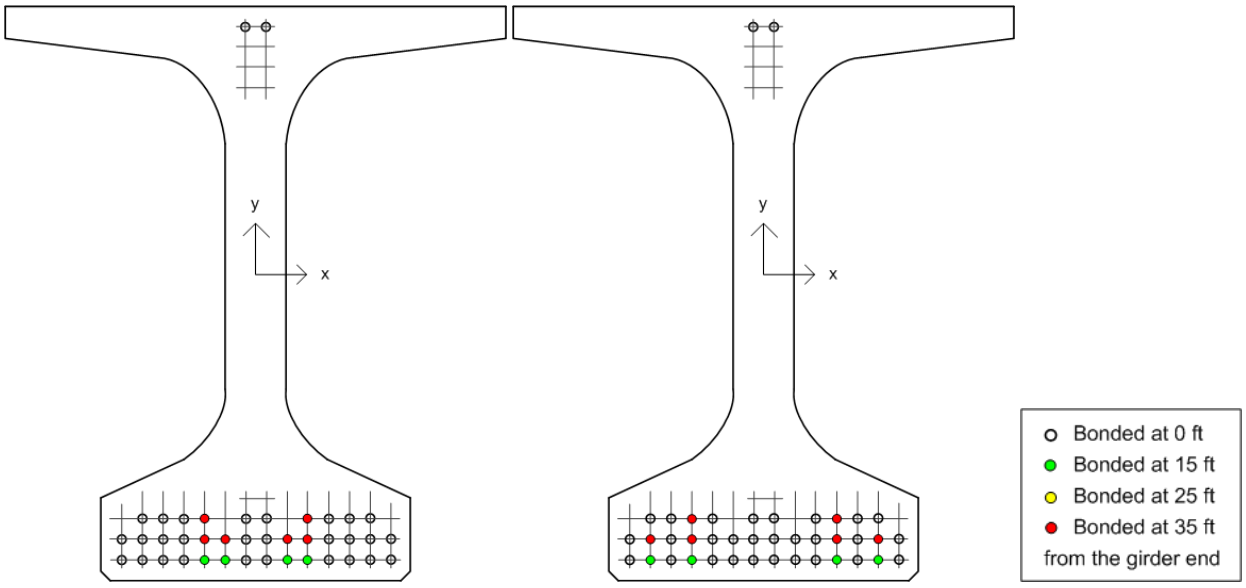

Figure 70 – Girder cross sections showing the strand patterns for DB25-A (on the left) and DB25-B (on the right).

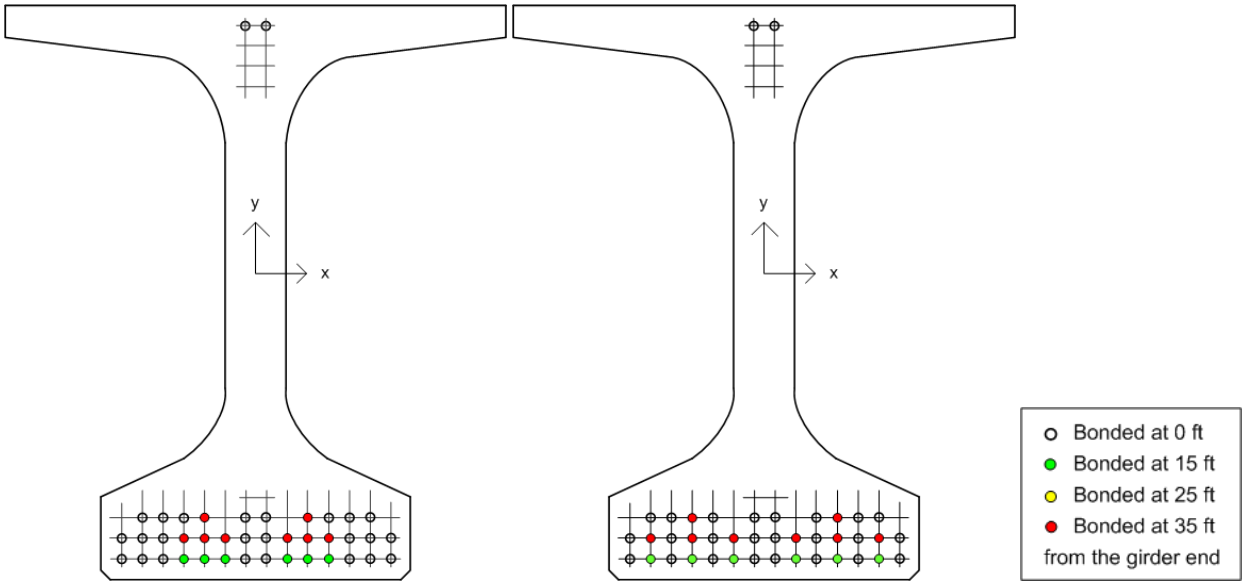

Figure 71 - Girder cross sections showing the strand patterns for DB35-A (on the left) and DB35-B (on the right).

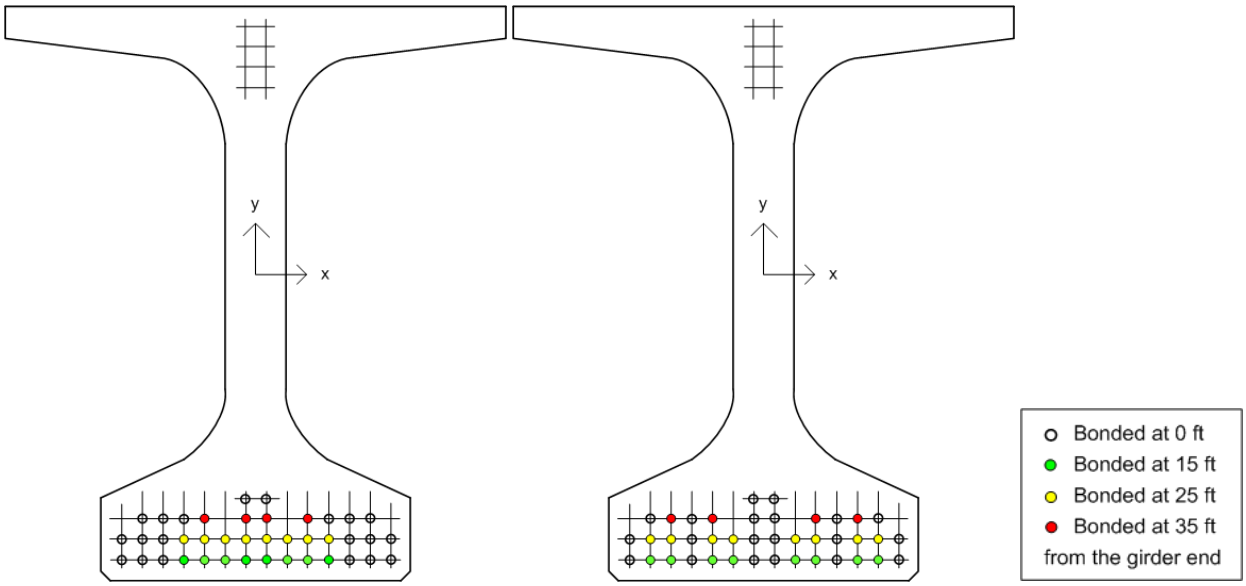

Figure 72 - Girder cross sections showing the strand patterns for DB50-A (on the left) and DB50-B (on the right).

The analysis results with the various strand patterns predict principle strains throughout the 3-dimensional girder cross sections. To compare the effects of the various strand patterns, just the principle tension strains on the exterior sides of the girders, along the end surface of the girders, and at cross sections where debonded strands become bonded will be shown here. "Contour plots" were selected as the easiest means of displaying those strain results. In the contour plots, regions of the girder surface with similar levels of strain are shaded in the same color.

Approximate predicted crack widths are marked on the principal strain contour plots in Figure 73 through Figure 76 for DB 0, DB 25-A, DB 35-A and DB 50-A. The contour plots of DB 25-B, DB 35-B, DB 50-B can be found in Figure 98 through Figure 100 in the attachments section. The contour plots show 54" long segments of a girder at the girder end and also at cross sections where strands are rebonded to the concrete. Cross sections showing which strands are being bonded at each section of a girder are shown on the bottom of each corresponding segment. These results are for girders right after the strands are cut, and do not include the crack opening during lifting or any creep, shrinkage and relaxation effects.

Figure 73 presents the results of an analysis of a standard design girder with 0% debonding. This model is used as a basis for comparison with the debonded girders to judge the effect of debonding on the reduction of tension strains and crack sizes. The model with no debonding predicts a inclined crack, multiple horizontal web cracks and a Y shaped bottom flange crack as marked. These three types of cracks are physically observed in similar girders at precast plants as well. The model also predicts high

strains in the bottom flange a transfer length away from the girder end. However, this region does not exhibit visibly detectable cracking in real girders.

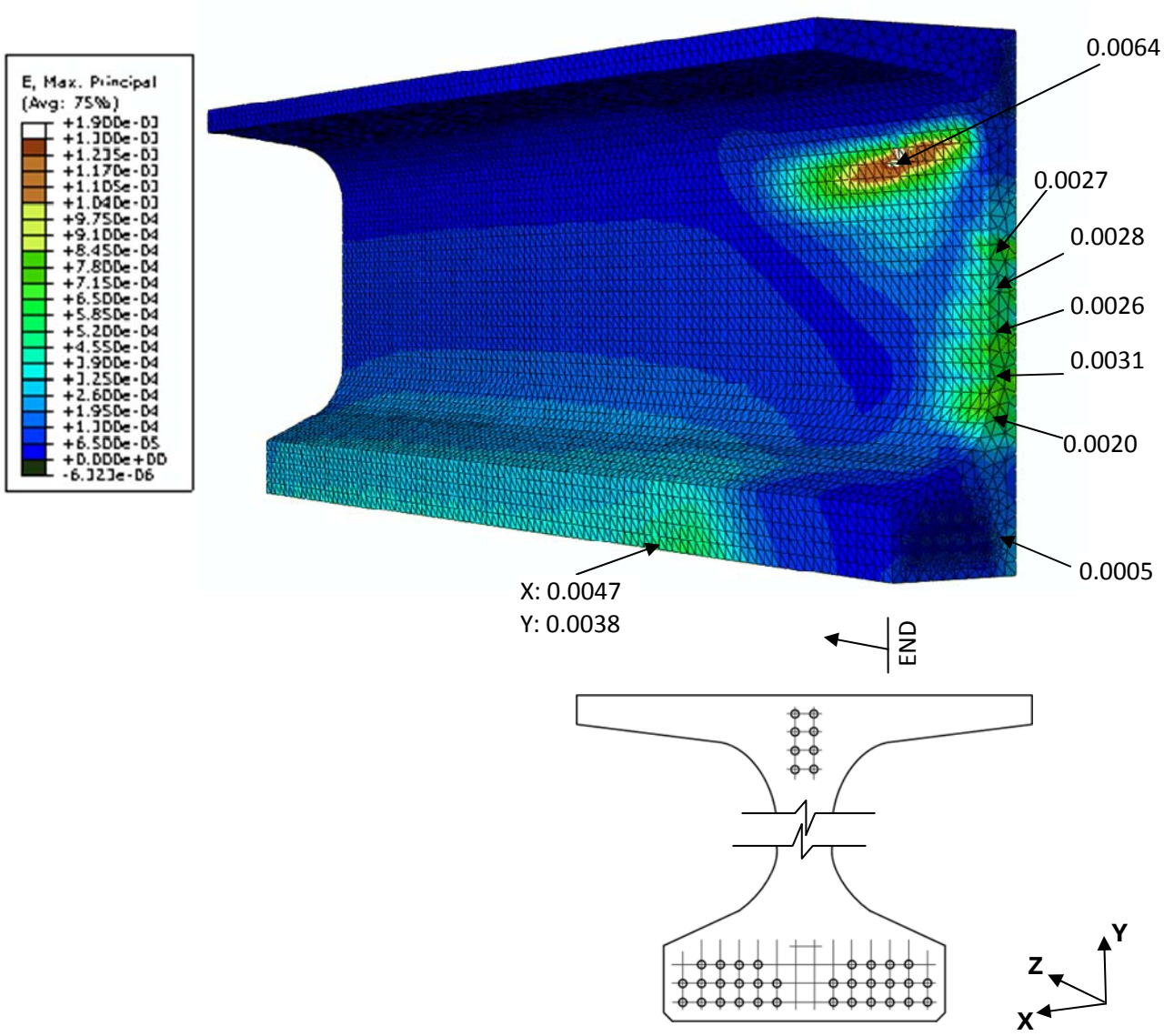

Figure 73 – Principal tensile strain contours and crack widths in inches for the girder end for DB 0.

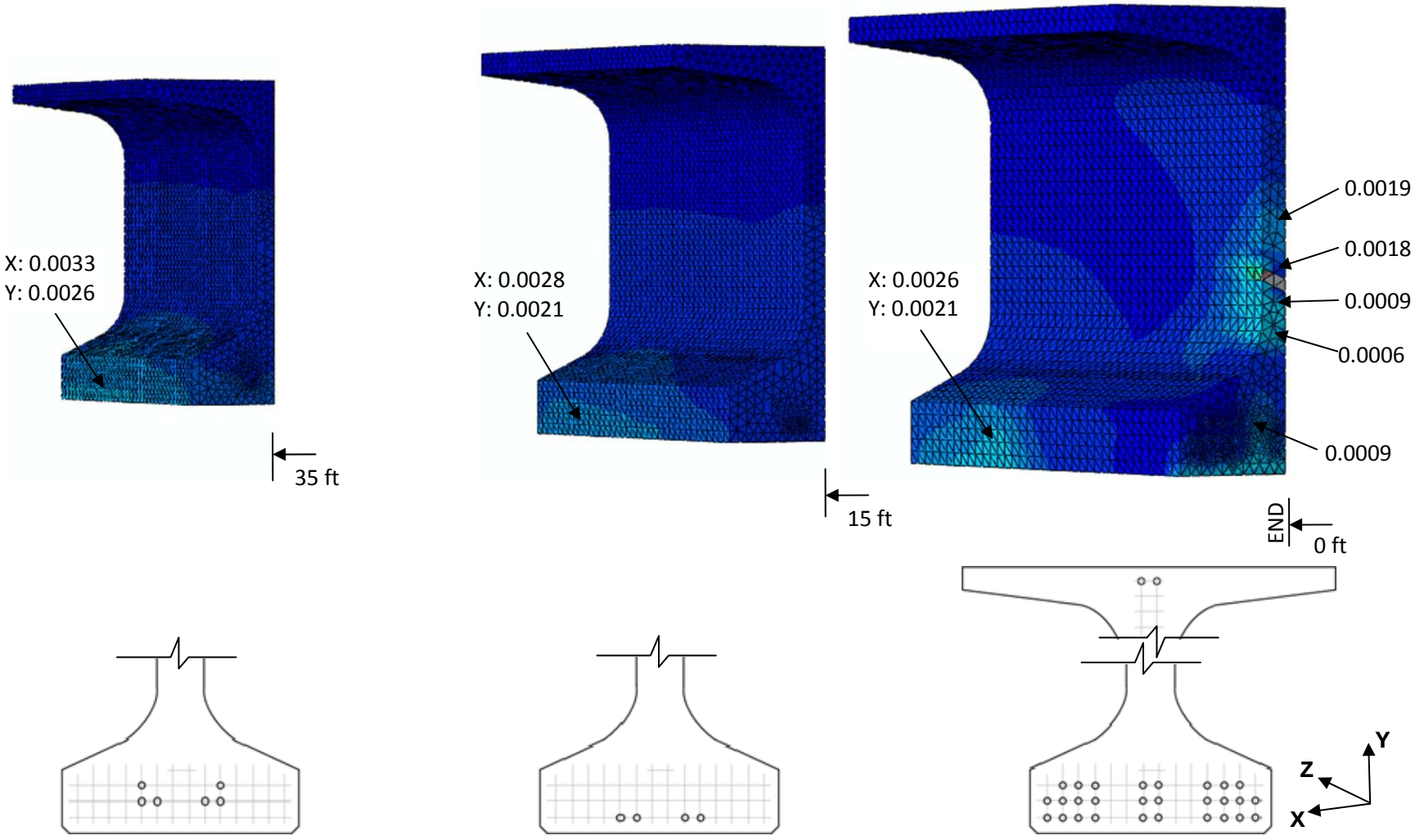

Figure 74 - Principal tensile strain contours and crack widths in inches for sections of girder where strands are bonded for DB 25-A.

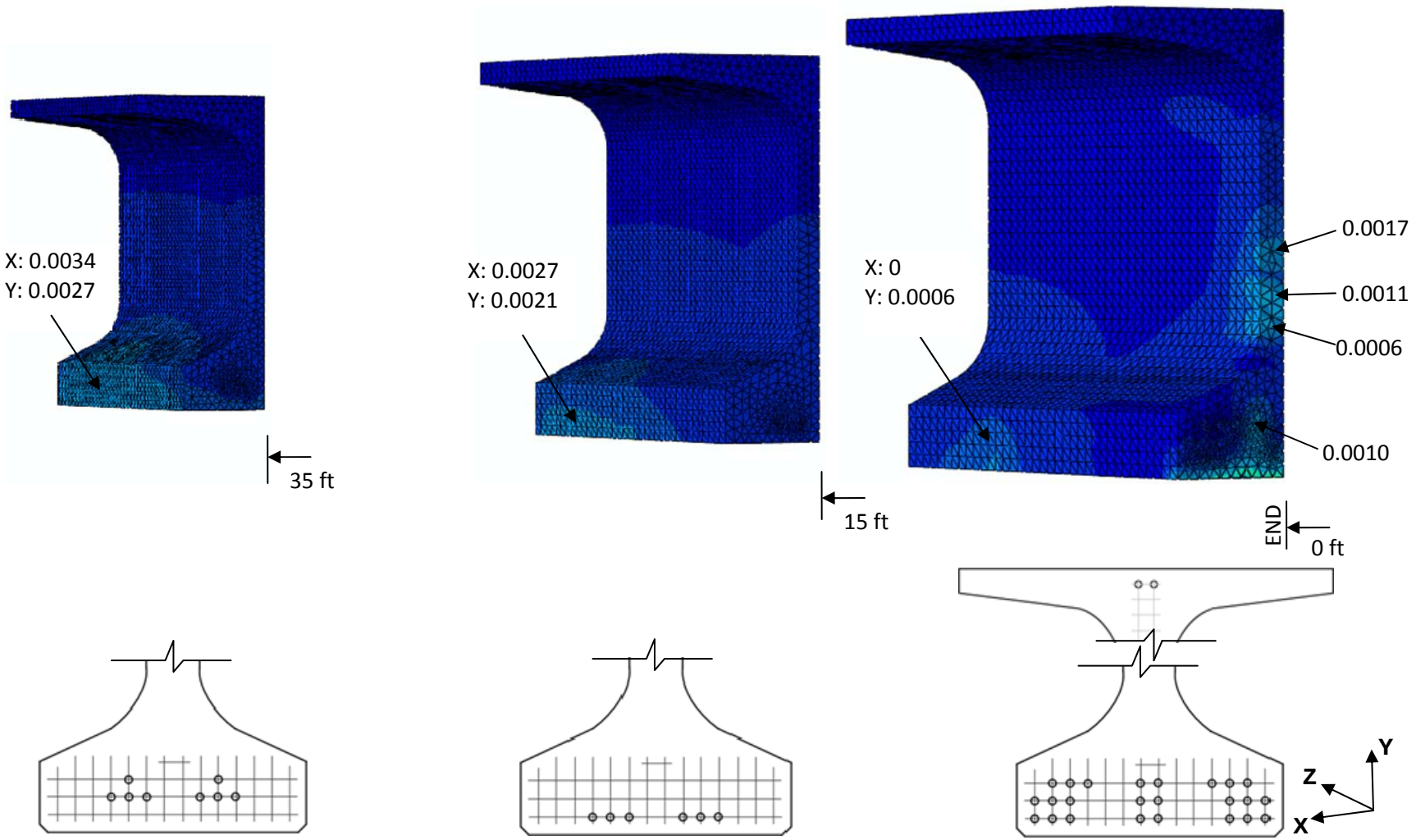

Figure 75 - Principal tensile strain contours and crack widths in inches for sections of girder where strands are bonded for DB 35-A.

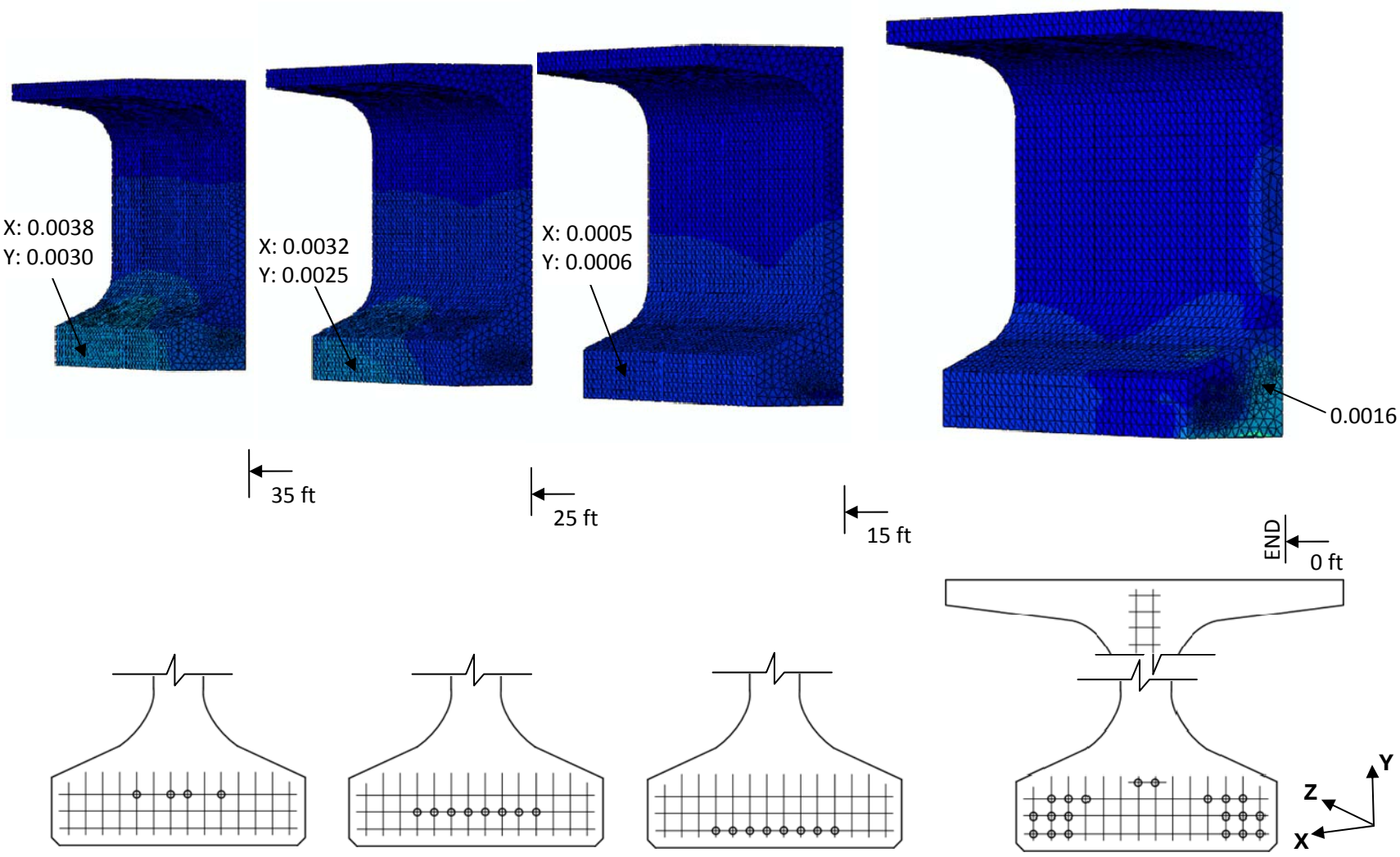

Figure 76 - Principal tensile strain contours and crack widths in inches for sections of girder where strands are bonded for DB 50-A.

Figure 73 to Figure 76 graphically exhibited strain conditions in the "A" type girder models. The impact of the debonding on different types of cracking can be summarized as follows.

The inclined web cracks: The bottom strands transfer stresses to the bottom flange concrete and result in the formation of inclined principal tensile strains in the upper region of the web. Any draped strands also create concrete bursting strains around those strands. When these two sets of strains combine, inclined web cracking is likely to occur. Debonding some strands in the end reduces both of these factors at the same time. The analysis results show that the inclined cracks can be eliminated completely by debonding as low as 25% of the strands at the girder end. While the girder in Figure 73 with no debonding exhibits the inclined crack, no plastic strains in the inclined crack region were observed for 25%, 35%, and 50% debonding cases as shown in Figure 74 through Figure 76.

No signs of inclined cracking were detected at the locations where some of the strands are bonded to concrete further away from the girder end at 15ft, 25ft and 35ft.

Web cracks: With increasing number of strands debonded at the girder end, the number of cracks and crack opening widths decrease consistently. This conclusion is drawn by comparing the results presented in Figure 73 to Figure 74, Figure 75 and Figure 76 for DB0, DB 25, DB 35, and DB 50 respectively. This result was expected since bonding fewer strands at the girder end would directly reduce the stresses transferred to the girder. The difference between the debonding case A or case B in terms of web cracks was practically negligible.

Sections of girder web further away from the end, where some strands are then bonded to concrete, were also crack free showing that the problem is not simply carried to another location.

Y cracks: Y cracks are caused by the eccentricity of the strands in the bottom flanges about the vertical center axis of the girder. Unlike the inclined and web cracks, Y cracks depend heavily on the way the strands are distributed in the bottom flange. If the strands to be debonded are not picked strategically, the results of finite element modeling showed that debonding some strands can increase the strains causing Y cracking. DB 25-A, DB35-A, DB50-A are models representing such undesirable cases where the approximate Y crack width was increased. These models, in common, remove the transfer of forces from the most interior strands at the girder end through debonding. The columns of strands debonded were also adjacent to each other. The remaining bonded strands are particularly compressing concrete near the tips of the flanges.

For the specific purpose of improving the Y cracking in the bottom flange, models denoted as DB 25-B, DB 35-B and DB 50-B were created. In these models, the interior strands at the girder end and the compression they transfer to the concrete remain. The debonded strands are distributed somewhat evenly across the girder width.

In all type "B" cases, the resultant principal tensile strains in the bottom flange area were below the theoretical cracking limit, meaning Y cracks can be eliminated using a proper strand pattern. The

significant difference in the principal tensile strains between girders with case A and case B strand distribution are shown in Figure 77.

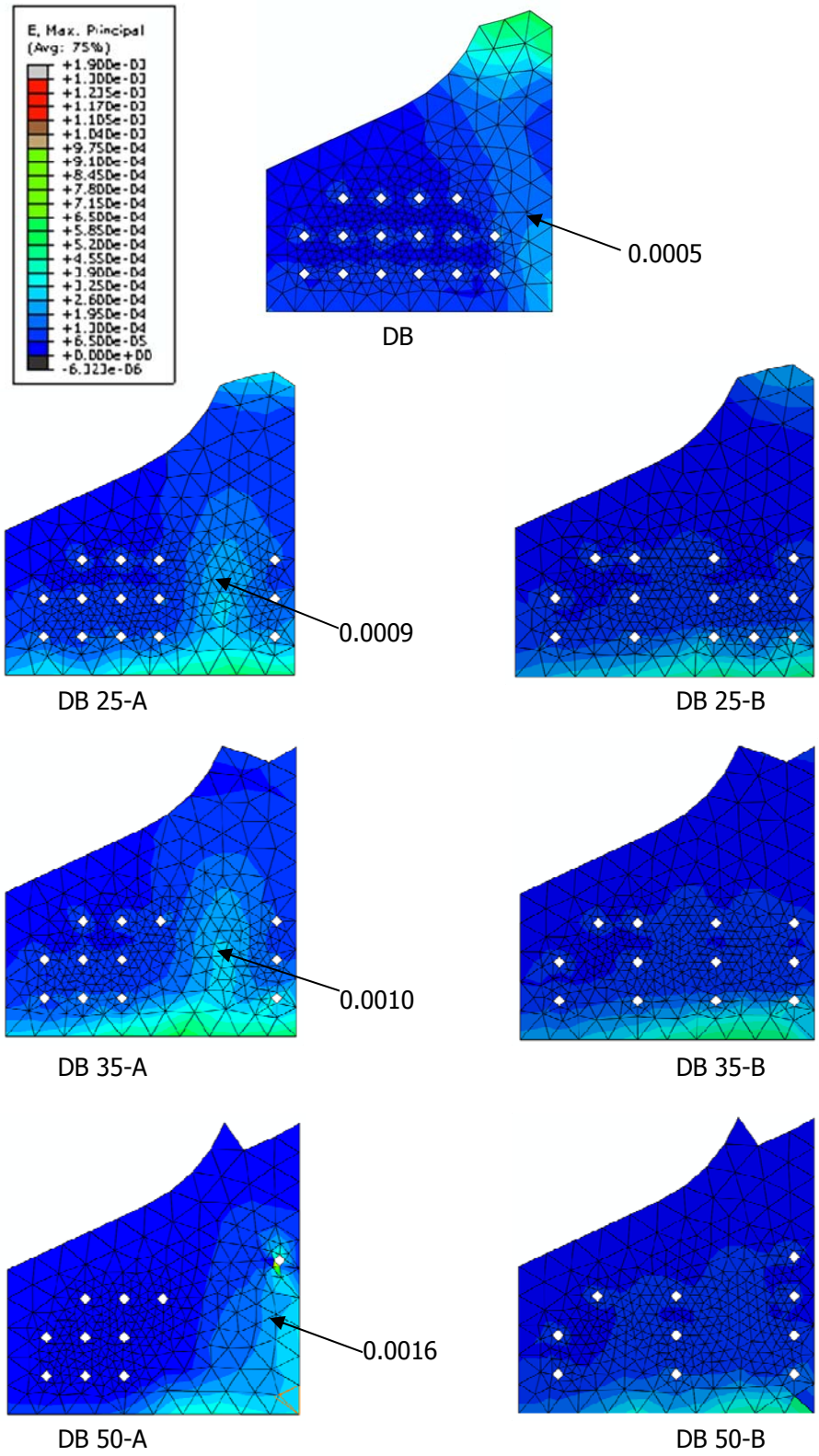

Figure 77 – Bottom flange principal tensile strain comparison of case A (left) and case B (right) models for various levels of debonding.

Bottom flanges at all bonding locations were checked for Y cracking for type "A" and "B" cases and found to have strains lower than the theoretical cracking tensile strain limit, indicating no cracking.

Excessive bottom flange bursting strains: Strains, in the bottom flange peaking at a location near the transfer length from the end, exceeding the theoretical tensile cracking strain are recorded in all models including DB 0. However, none of the more than 50 girders studied at precast plants exhibit visible cracking at the bursting region. This disagreement between the finite element models and reality either indicates a modeling error or because these high strains develop in various directions around the strands they just cause numerous micro-cracks that never join together to form visible cracks. In any case, debonding is observed to only decrease these strains. If these strains are not represented as cracks in the field in model DB0, they are very unlikely to cause visible cracking for other cases with debonding.

Overall the results of the debonding study indicate that carefully performed debonding can bring the concrete tension strains below the elastic cracking limit for the inclined and Y crack regions to a large extent with as low as 35% debonding. First, by removing the draped strands from the upper flange area, and second, by placing the draped strands in the bottom flange alone, debonding helps control the strains causing inclined cracks and Y cracks, respectively. The size and number of predicted web cracking was reduced for 25% and 35% debonding and minimized with 50% debonding.

The most critical cracks are thought to be the "Y" cracks in the bottom flange near the girder bearing region. These cracks could allow moisture to enter the strands and migrate along the strand length causing corrosion. Debonding is particularly successful at reducing or eliminating the Y cracks.

Given that the shear capacity is carefully checked with the lower prestress at the girder ends, debonding is an appealing solution to the girder end zone cracking problem. Preliminary calculations for the redesign of a 124ft span bridge with debonded 54W girders at 6ft spacing indicated that some additional stirrups would be needed for shear capacity, but could easily be accommodated in the girder.

6.3. Combining "Debonding" and "Modified End Zone Reinforcement"

By debonding as low as 25% of the strands at the girder end, it is possible to eliminate plastic tension strains and cracking in the inclined crack or Y crack regions for most cases, as discussed in Section 6.2. To eliminate web cracks, however, 50% of the total number of strands needed to be debonded.

Using more vertical reinforcing steel at the very end of the girder was the most effective method in decreasing the plastic web strains, but had a lesser effect on the inclined cracking and no effect on Y cracking. Replacing two of the #6 bars closest to the girder end with #10 bars leads to the most noticeable and practical improvement. Although the concrete tension strains were reduced by half, they remained above the cracking limit.

Since reinforcement bar modification and debonding work effectively for different types of cracks, combining the two potential solutions was evaluated.

This section investigates the combined impact of debonding and vertical reinforcement bar size modification at the girder end. Each model with different level of debonding was run with two #10 bars at the end, instead of #6 bars, as shown in Figure 78.

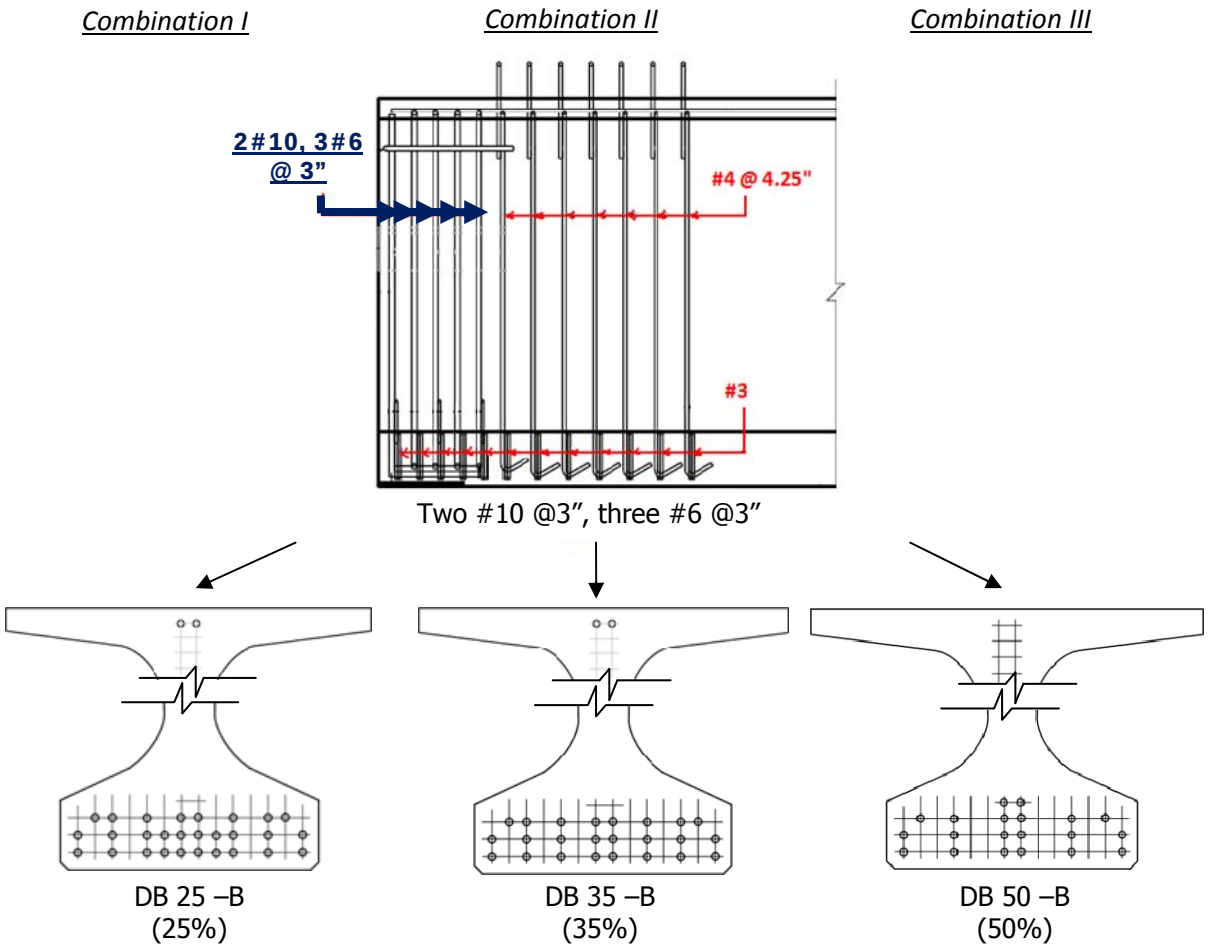

Figure 78 – Combinations of reinforcement bar modification and debonding.

The results of the models with the combined solution are compared to the girder with standard details in Figure 79. Numerical values of strains along the depth can also be seen in plots of Figure 80 and Figure 81 for web and inclined cracking locations as compared to the standard detailed girder.

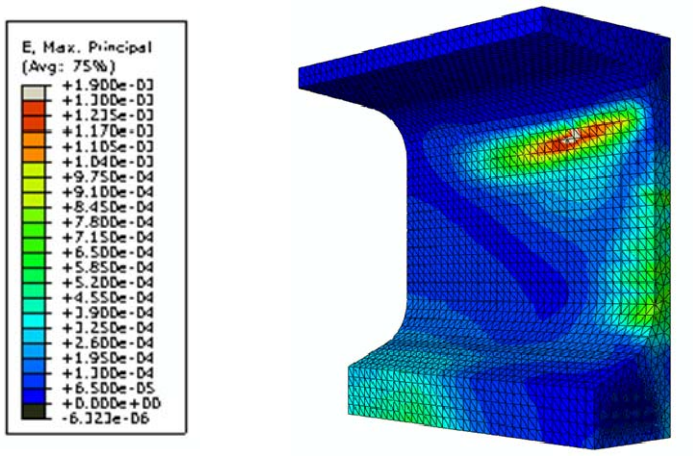

No debonding
Five #6 @3” (std)

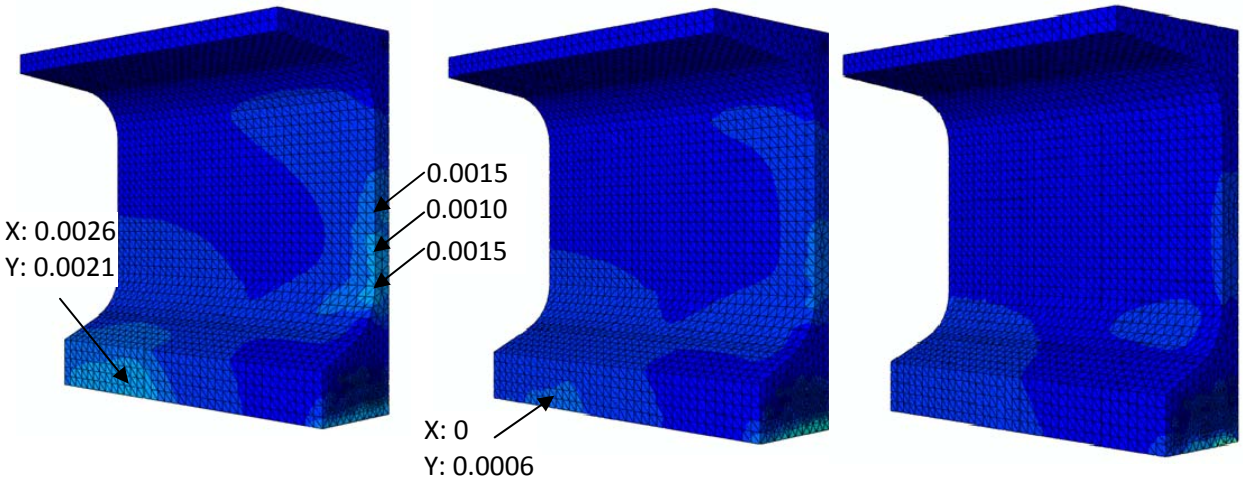

DB 25 - B
Two #10 @3”, three #6 @3”

DB 35 - B
Two #10 @3”, three #6 @3”

DB 50 - B
Two #10 @3”, three #6 @3”

Figure 79 – Principal concrete tension strain contour plots and crack widths for the combination cases as compared to the standard detailed girder.

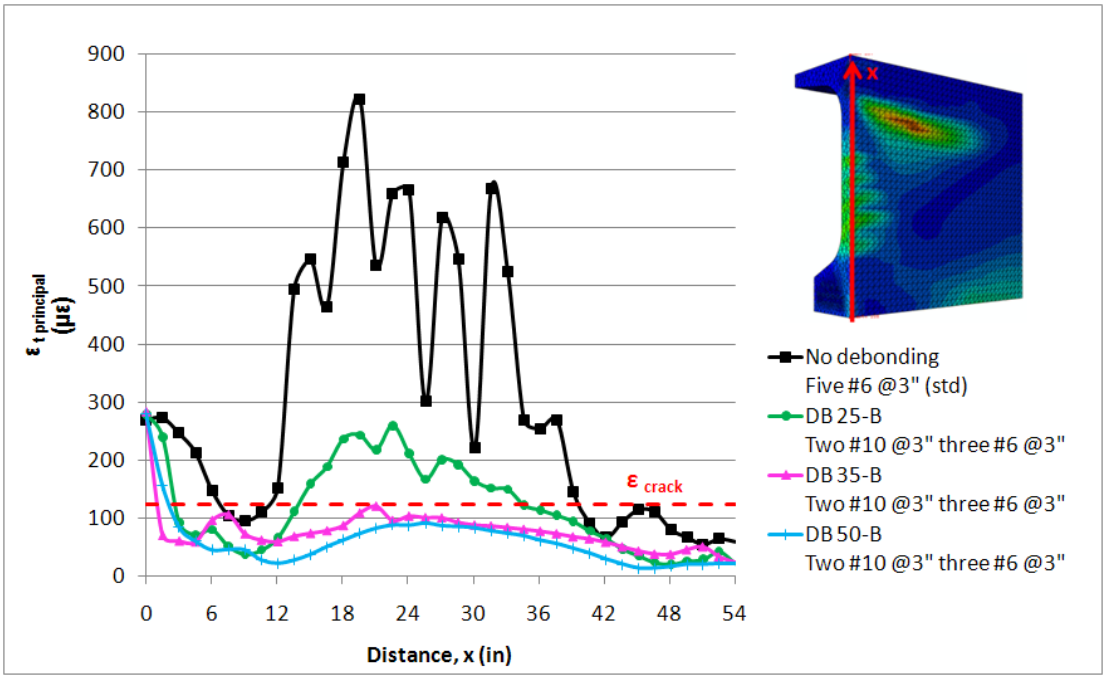

Figure 80 – Principal tensile strains at the girder end over the depth of the girder for combinations with rebar size modification and debonding.

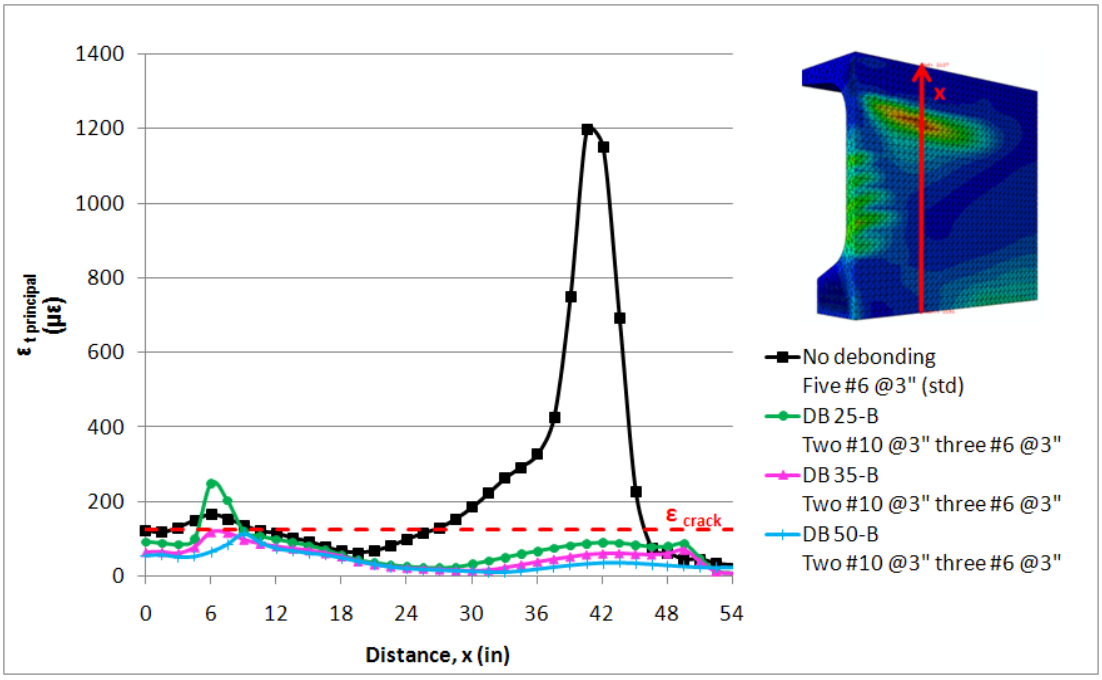

Figure 81 – Principal tensile strains at a section 18in from the girder end over the depth of the girder for combinations with rebar size modification and debonding.

To investigate the quantitative contribution of each case when superposed, the results of 35% debonding, the rebar modification and a combination of both are plotted against the standard girder case as shown in Figure 82 and Figure 83.

In summarizing the effect of combining debonding and reinforcement changes, the girder end cracking can effectively be eliminated with design changes while maintaining the overall bending capacity of the girders. Figure 80 shows that by combining a minimum of 35% debonding with two #10 bars at the girder end, web strains can be decreased below the cracking limit. Figure 81 indicates that plastic strains at the inclined cracking locations are below the theoretical cracking limit for all cases using debonded strands.

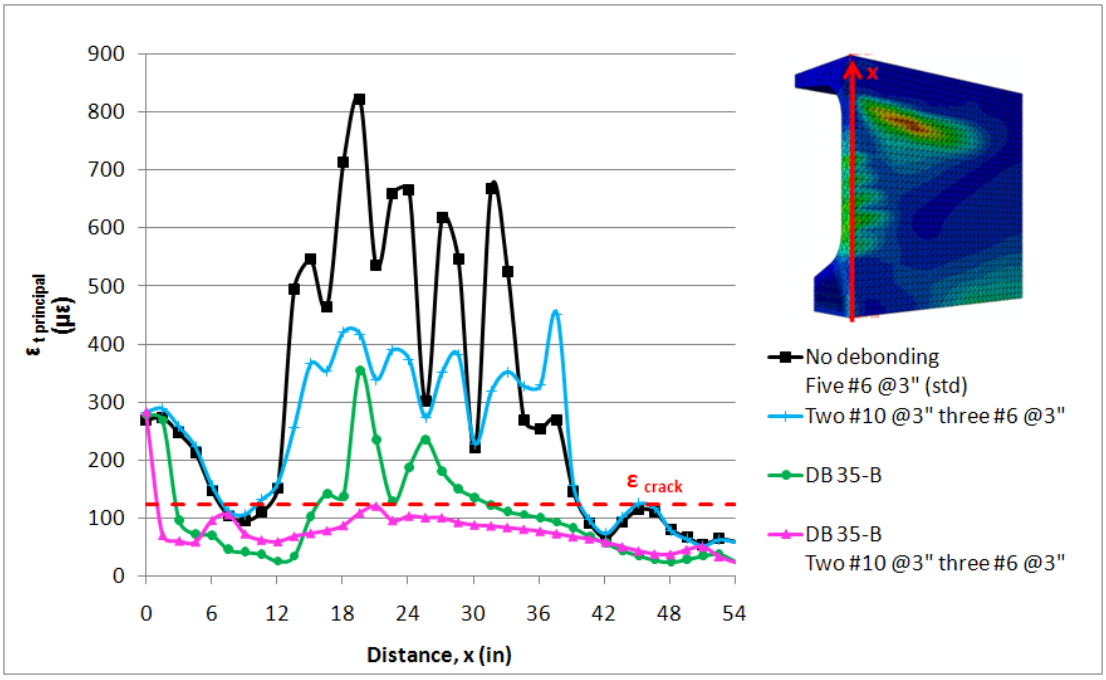

Figure 82 – The combined impact of debonding and vertical reinforcement bar modification in controlling the web cracks at the girder end.

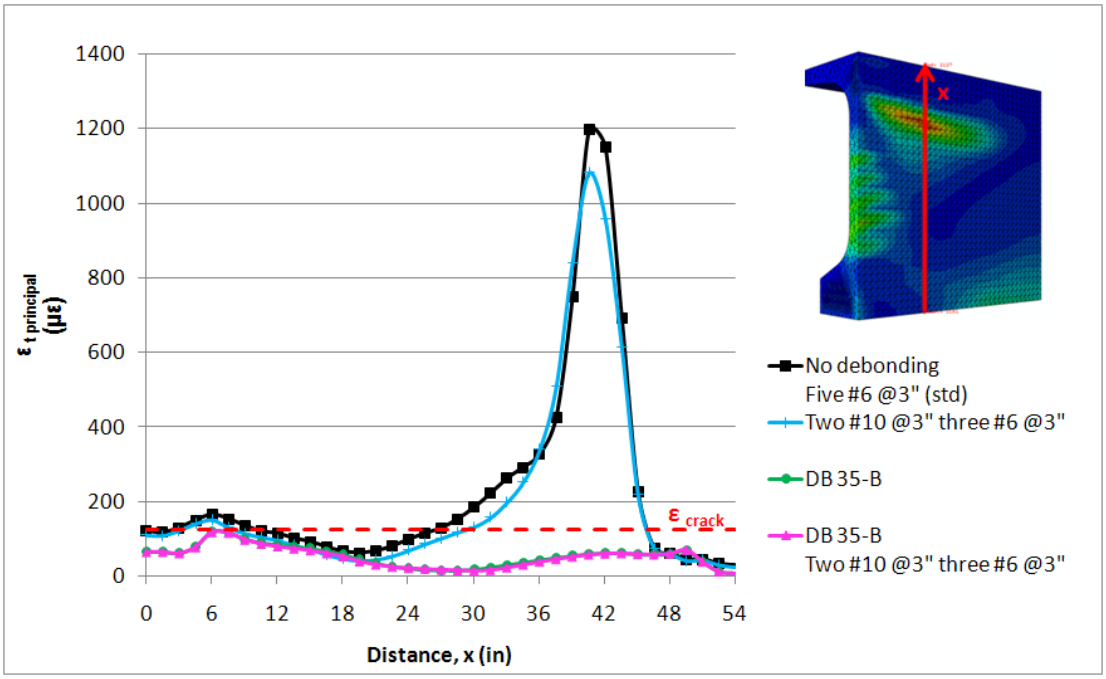

Figure 83 – The effect of reinforcement size increase and debonding alone compared to the combination of the two on the strains at a section 18 inches in from the end.

The combination of "35% debonding" and "two #10 @3", three #6 @3"" was implemented on a 82W girder. The results as compared to the a girder with no debonding and standard end reinforcement are shown in the Appendix Figure 102 and Figure 103. Similar results as discussed above were obtained with a 82W girder.

6.4. The order in which the Strands Are Cut

The order of strand cutting can also impact the development of cracks at the ends of the girders. If the bottom row of strands is detensioned first, their prestressing is applied to the girder with a larger eccentricity from the center of gravity and may cause tension cracking near the girder top. If the columns of strands near the sides of the bottom flange are released first, they create a transverse bending effect in the bottom flange that may cause a vertical crack through the middle of the flange. The results described in the previous sections (6.1 through 6.3) only showed the concrete strain conditions after all strands were cut. Models presented in the previous sections were based on a strand cutting order shown in Figure 84.

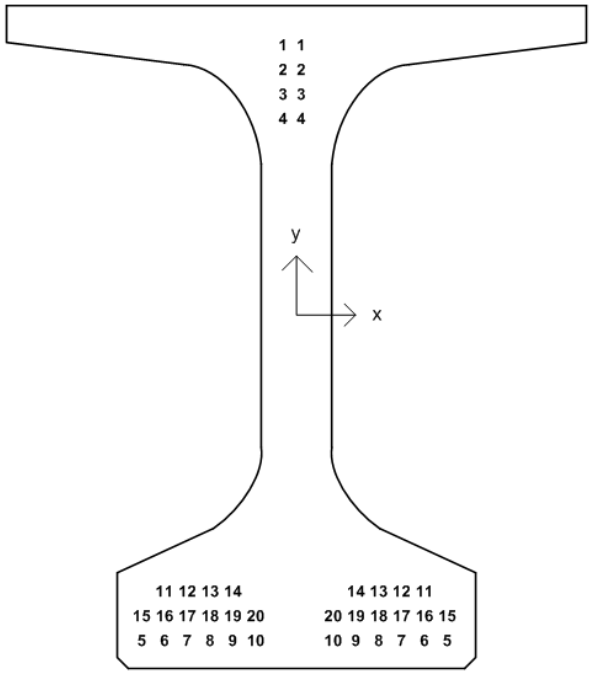

Figure 84 – Order of strand cutting provided the results presented in this report unless otherwise noted

The impact of the strand cutting order on the concrete strain levels at the girder end was also evaluated through finite element modeling. Finite element models with the following strand cutting orders were created and the results are compared to each other. The strand cutting order is also marked in Figure 85, where the strands are replaced by numbers each denoting the step in which each strand is cut. All models assume that the strands are cut symmetrically with respect to a vertical (Y) axis laying on the cross sectional plane. The restraint on the displacements of the girder end due to the uncut strands is not included in these analyses. Crack widths marked on the contour plots do not include the effects of strains induced by girder lifting. The cutting situations examined include:

1. All strands are cut at the same time (Figure 85 –Model 1).

2a. Strands with the largest vertical eccentricity were cut before the others. Draped strands were followed by the straight strands, cutting 2 strands with highest eccentricity at each step. (Figure 85 – Model 2a);

2b. Strands with smallest vertical eccentricity are cut first. Draped strands were followed by the straight strands, cutting 2 strands with low eccentricity at each step. (Figure 85 –Model 2b);

3a. Strands with the largest horizontal eccentricity (exterior strands) are cut first. Draped strands were followed by the straight strands, cutting 4 or 6 strands at each step. (Figure 85 – Model 3a);

3b. Strands with the smallest horizontal eccentricity (interior strands) are cut first. Draped strands were followed by the straight strands, 4 or 6 strands at each step. (Figure 85 – Model 3b).

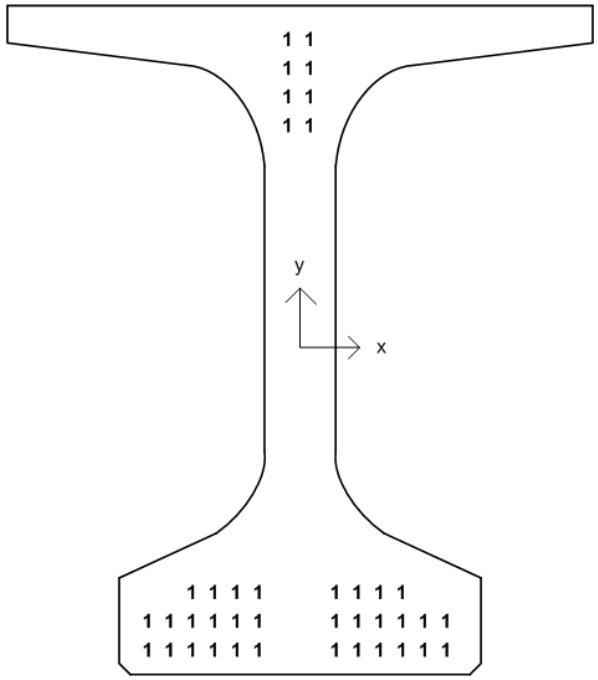

Model 1

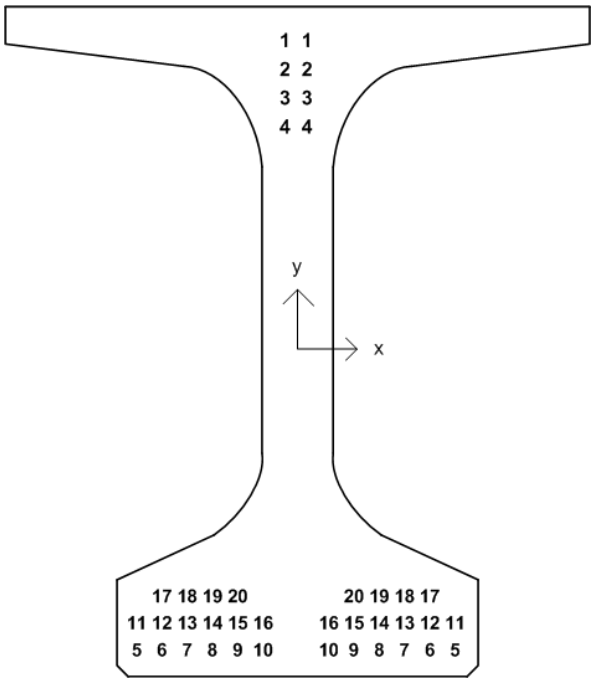

Model 2a

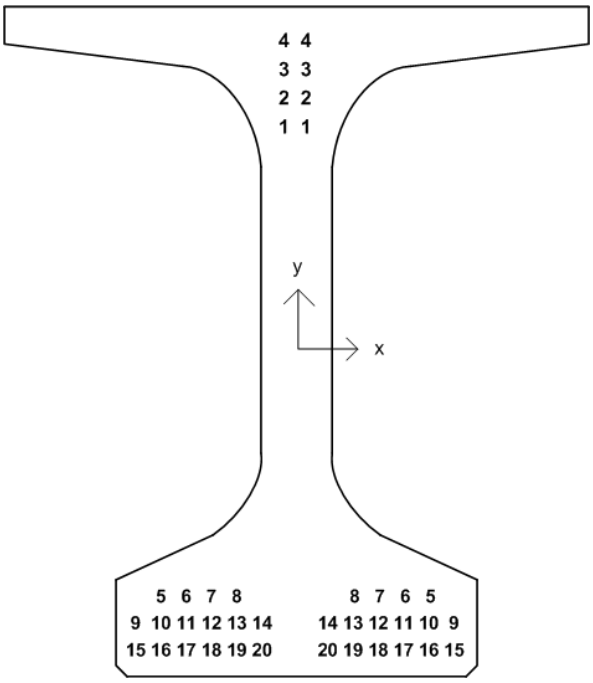

Model 2b

(Figure 85)

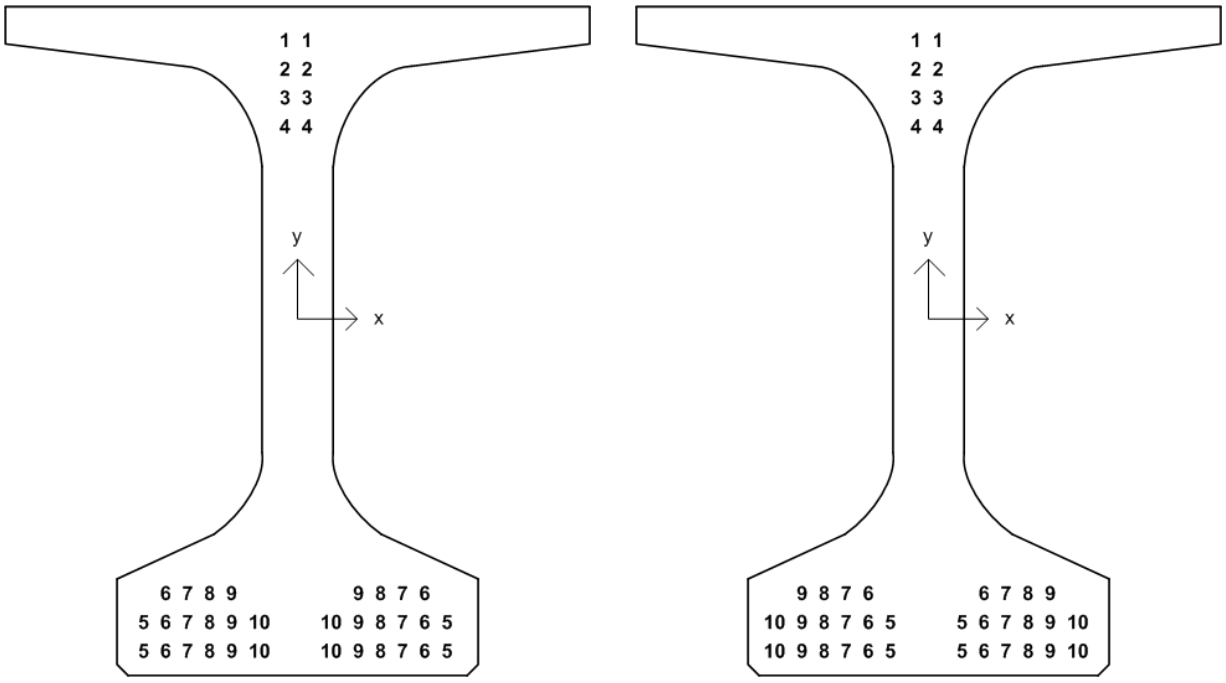

Model 3a Model 3b

Figure 85 – Various strand cutting patterns shown on the cross section of the girders taken at the girder end.

The strands in the bottom flange of the girder were cut row by row in the two versions of Model 2. For Model 2a and Model 2b, the resultant plastic principal tension strain directions and principal strain contours are shown in Figure 86 and Figure 87, respectively.

Starting with cutting strands having the smallest eccentricities about the x axis (2b) leads the cracks to form at later stages. For example, first signs of inclined upper flange plastic strains were seen at Step 7 for Model 2a while the same strains were detected at Step 9 for Model 2b. Similarly, the plastic strains responsible for the horizontal web cracking first occur at Step 9 for Model 2a and at Step 12 for Model 2b. Step numbers are marked on Figure 85 – Model 2a and 2b. Even though the delay in cracking occurs for the model where the strands with the smallest eccentricity are cut first, the final strains or the crack widths do not change considerably or consistently. The vertical eccentricity (about x-axis) of the strand cutting order does not seem to be critical. This could be due to the negligible magnitude of eccentricity difference of the strands compared to the girder depth.

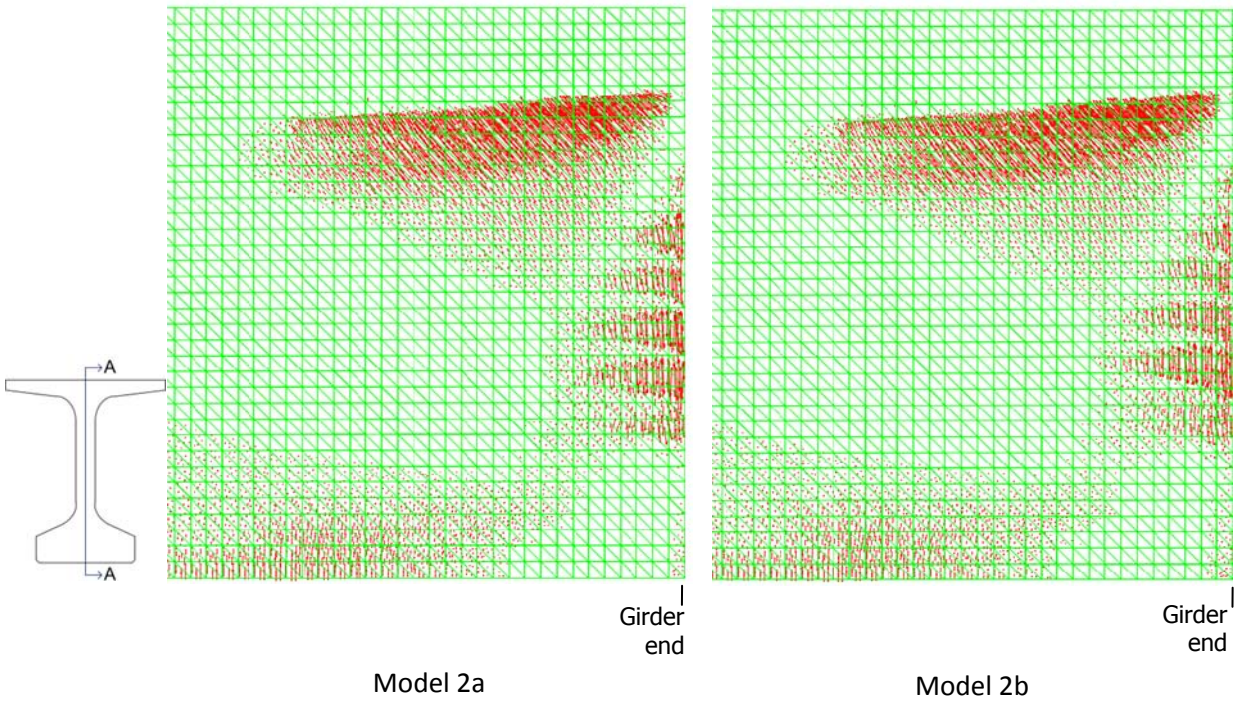

Figure 86 – Plastic principal tension strain directions for Model 2a (left) and Model 2b (right) shown along a transverse section of the web A-A of the girder.

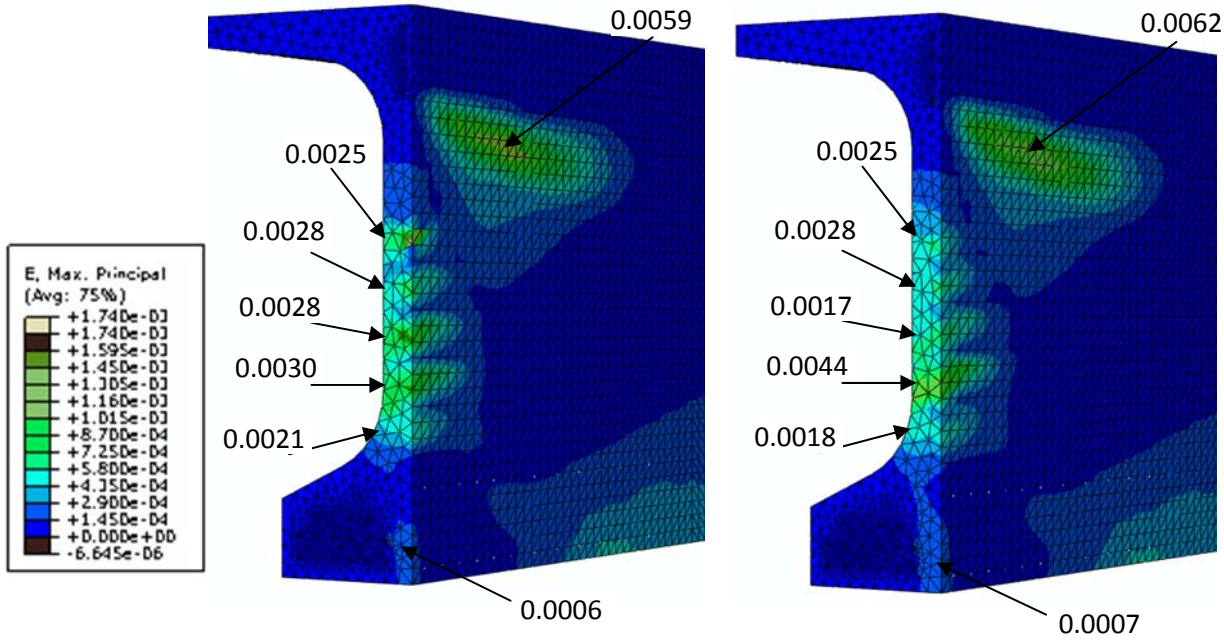

Figure 87 –Principal tensile strain contours for Model 2a (left) and Model 2b (right), with maximum expected crack widths marked in inches.

The effect of cutting strands closer to the sides of the girder first, versus interior strands, was hypothesized to affect the development of the Y cracks in the bottom flange. Due to the direction of the eccentricity of the strands with respect to the y axis, a vertical crack could propagate upward in the bottom flange eventually forming the Y cracks. The direction of the plastic strains in the bottom flange as presented in Figure 88 and Figure 89 for Models 3a and 3b indicate this Y crack.

Model 3b, where the most interior strands are cut first, exhibited plastic strains only at the beginning of step 10. Strands cut at step 10 are marked on Figure 85 – Model 3b. The magnitude of these strains did not increase considerably after or during this step. On the other hand in Model 3a, where the exterior strands were cut before the interior strands, plastic strains appeared earlier at step 5 as marked on Figure 85 – Model 3a. The magnitude of the plastic strains, which can be interpreted as the crack opening, kept increasing as the other strands were cut for Model 3a. Eventually, when all the strands were cut, the magnitude of the plastic strains in Model 3a was larger than the ones for Model 3b.

Figure 88 and Figure 89 compare the magnitudes of the principal strains for Model 3a and 3b. By comparing the results of Model 3a with 3b, it can be concluded that cutting the interior strands first and going towards the exterior strands would delay cracking, and could limit the crack size. Therefore, it is recommended that the strand cutting should start from the interior strands and move outward if possible.

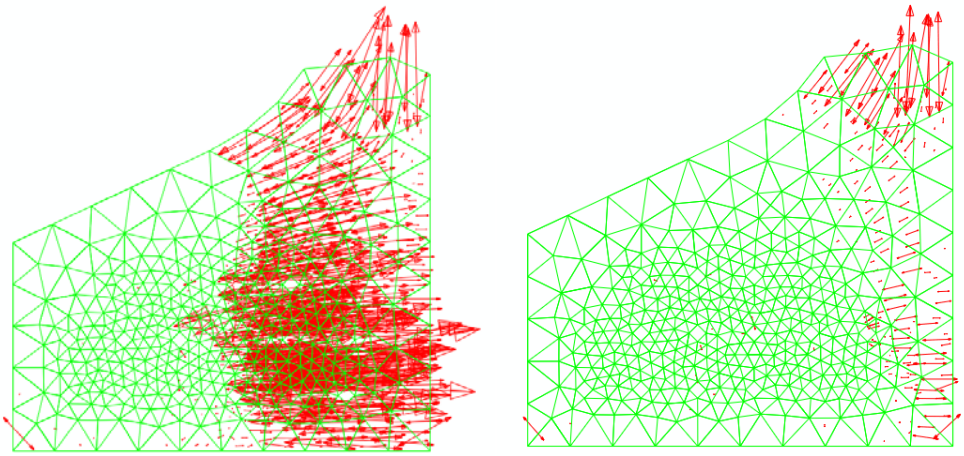

Figure 88 - Principal plastic tension strain direction (arrows) and magnitude (length of red lines) for Model 3a on the left, and Model 3b on the right at a cross section taken at the very end of the girder.

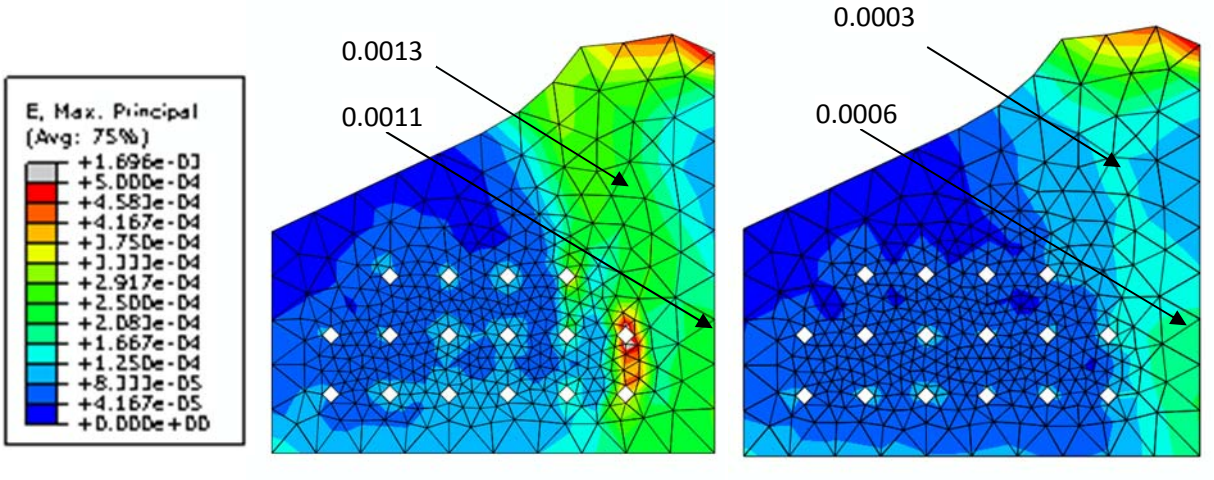

Figure 89 – Principal strain contour plots for Model 3a on the left, and Model 3b on the right at a cross section taken at the very end of the girder.

The strain results shown in Figure 86 through Figure 89 can be compared with the strain results shown in Figure 90 and Figure 91 for Model 1 where all strands are detensioned simultaneously. Simultaneous detensioning is possible if a single large hydraulic jack is used during girder fabrication.

Clearly the pattern or order of strand cutting will have an effect on crack formation if strands are detensioned in a step by step manner. This effect is important and represents the non-linear inelastic action that occurs in the girder and the FEM analysis when plastic tension strains form with cracking. An analysis of the strain conditions in the girders must include a step by step representation of the strand releasing order.

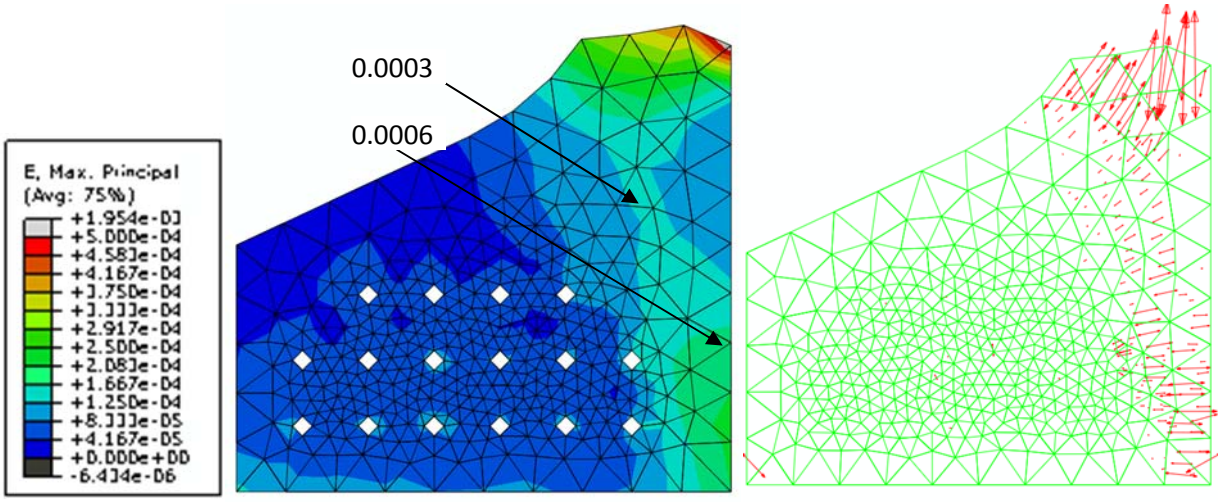

Figure 90 – Strain contour (left) with crack widths marked in inches and plastic strain directions (right) for Model 1 at a cross section taken at the very end of the girder.

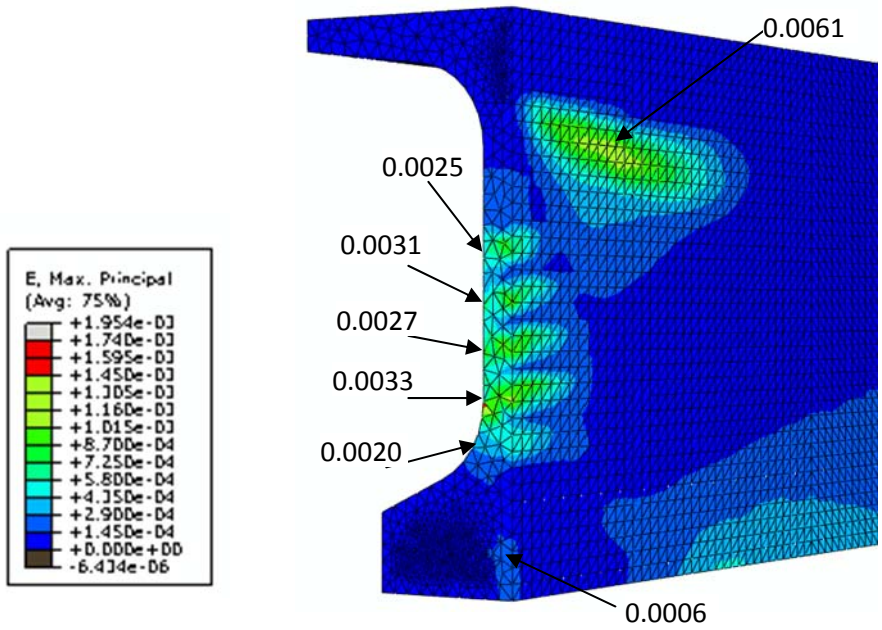

Figure 91 - Strain contour with crack widths marked in inches for Model 1.

The findings presented in this section relative to strand cutting patterns are in agreement with the earlier findings from the debonding cases regarding the distribution of debonded strands in the bottom flange. The presence of the compression force closer to the Y axis, due to the cut interior strands, has a constraining role on the bottom flange strains. In absence of this compression force closer to the Y axis along the girder length, Y cracks are more likely to occur.

6.5. Modifications with the Draped Strands

6.5.1. Removing the Draped Strands:

Straight strands alone create strains leading to principal tensile strains in the upper portions of the girder webs perpendicular to the inclined cracking observed. Draped strands apply compression along their axis and consequently create principal tensile strains perpendicular to their axis. They are expected to contribute to inclined cracking in the upper web and flange area by amplifying strains. To isolate the contribution of the draped strands in inclined cracking, finite element models with the two strand patterns shown in Figure 92 were created.

The model without draped strands does not meet the requirement for top fiber tension limit and is only used to study difference the absence of the draped strands makes.

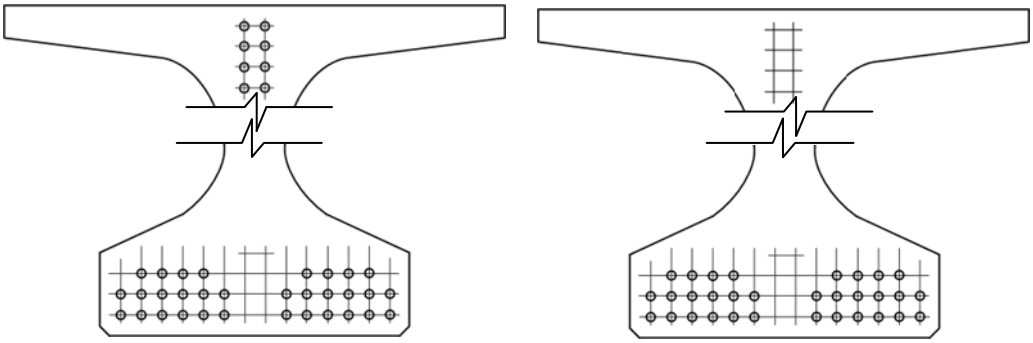

With draped strands Without draped strands

Figure 92 - Strand patterns at the girder end with and without draped strands.

In the absence of the draped strands, the strains in the upper flange, in the area where the draped strands would be located were considerably lower as shown in Figure 93. These strains are expected to cause the inclined upper flange cracks.

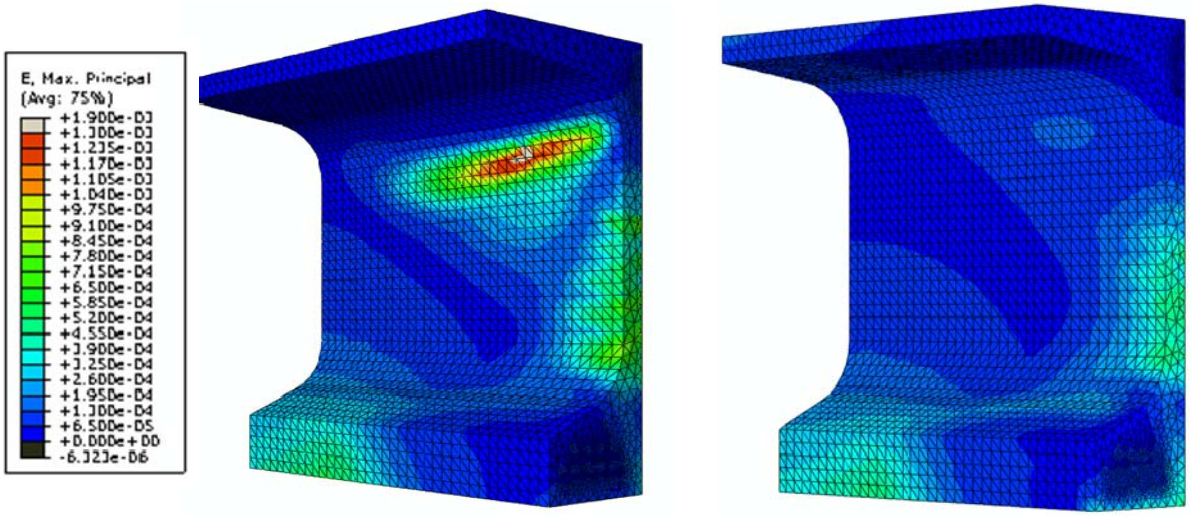

With draped strands Without draped strands

Figure 93 – Principal tensile strains in concrete with (left) and without (right) the draped strands

The reduction of the inclined cracking strains is also presented quantitatively in Figure 94 at a line along the depth, at 18in from the girder end.

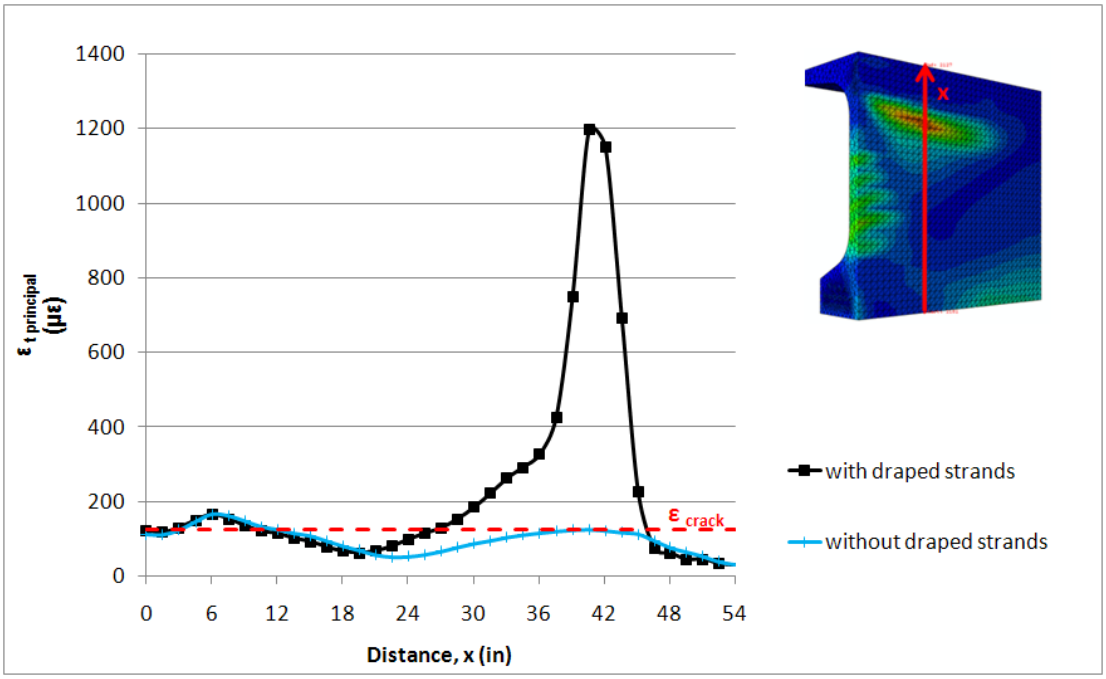

Figure 94 – Principal tensile strains for models with and without draped strands along a vertical section at 18in from the girder end.

In addition to the inclined strains, due to their eccentricity along the depth, draped strands create a moment in the opposite direction of the bottom flange strands along the web. Therefore, removing the draped strands from the model also decreased the web strains causing web cracking as can be seen in Figure 93.

6.5.2. Lowering the Draped Strands

Precast concrete manufacturers reported observing less severe cracking in girders where the center line of the draped strands was lower in height. This trend might also result from the fact that the girders where the draped strands need not be high are also girders with fewer strands.

Two identical models with different draped strand heights, but same total number of strands, were created to investigate the validity of this observation. The results of the two models are shown in Figure 95, where the locations of the draped strands are marked on the elevation views. Each girder had 26 straight and 8 draped strands.

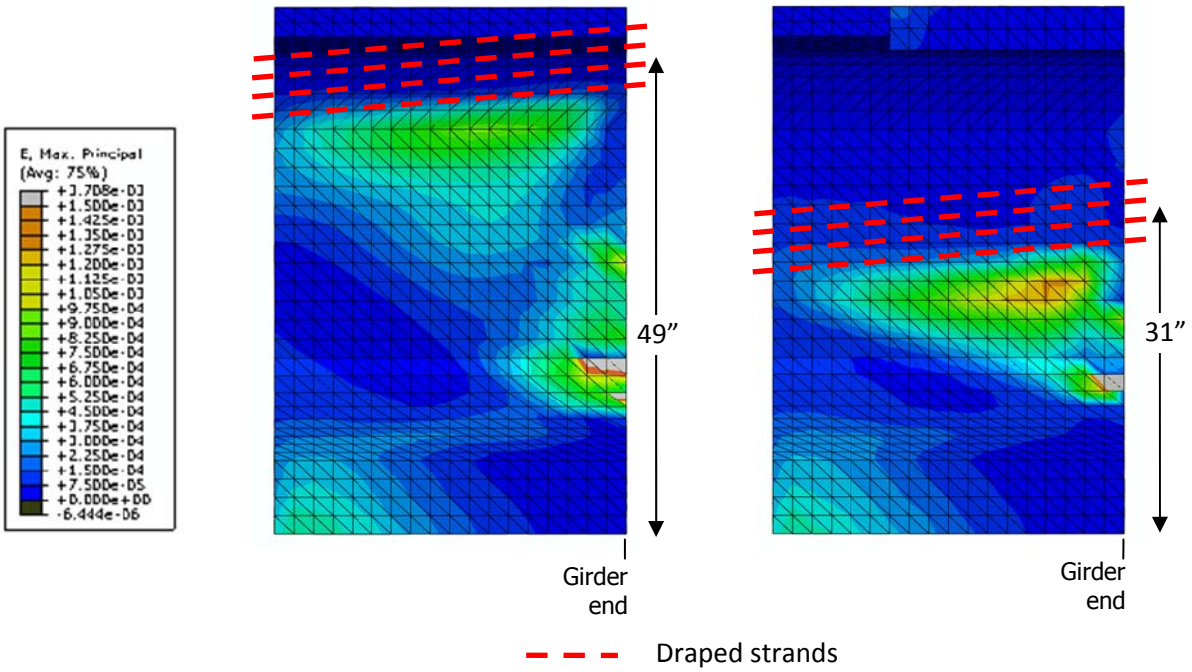

Figure 95 - Principal tensile stress contour plots on the elevation view of the two cases with high (left) and low (right) draped strands. (resultant eccentricities are listed)

Lowering the draped strands to the web of the girder lowers the location of the potential inclined crack but actually increases the intensity of the tension strains in the concrete. The web of the girder has a smaller concrete area than the upper flange, and therefore a more concentrated compression strut develops in the web with higher inclined strains if the draped strands are located in the web. As a result, the model with higher draped strands had smaller inclined cracking strains as shown in Figure 96.

On the other hand, lower draped strands have smaller eccentricities along the depth and therefore cause smaller horizontal web cracking strains. The area where the horizontal web cracks occur is constrained between the draped strands and the bottom flange strains and therefore is smaller with lower draped strands.

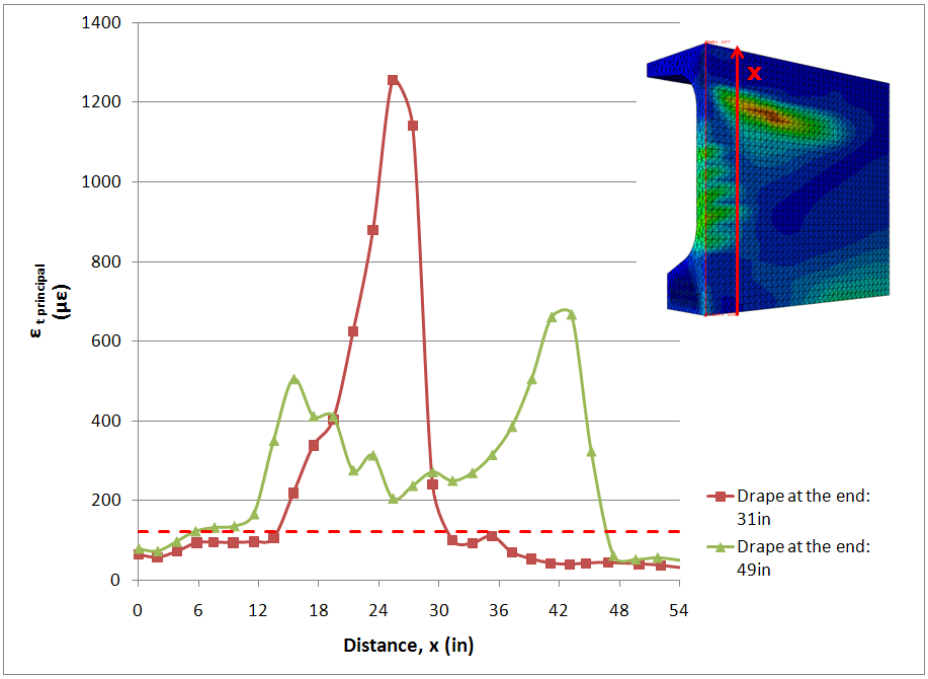

Figure 96 - Principal tensile strains over the depth at a section 8in from the girder end for different draped strand locations.

It should be noted when the draped strands are located low in the web, the number of straight strands that can be used is usually limited as constrained by flexural tension stresses in the top flange. Draped strands work to cancel the tensile stresses at the top fiber and are the most efficient when located with the largest eccentricity (closer to the top). Moving the draped strands down as in this example, would normally be accompanied by reducing the number of straight strand – making the girder much less efficient.

6.5.3. Spreading out the Draped Strands

Draped strands are typically spaced with a 2in center to center spacing in Wisconsin. This causes the concrete compression stresses transferred by the draped strands to be rather concentrated. An alternative is to spread the draped strands along the girder web allowing the stress to transfer over a larger area. A model with 2in draped strand spacing was compared to a model with 8in draped strand spacing to investigate the potential reduction in the strains. The center lines of the draped strands were the same height, 31in from the bottom of the girder for both models. The total number of strands was held constant.

The resultant contour plots of principal concrete tensile strains are shown for both models in the elevation view in Figure 97.

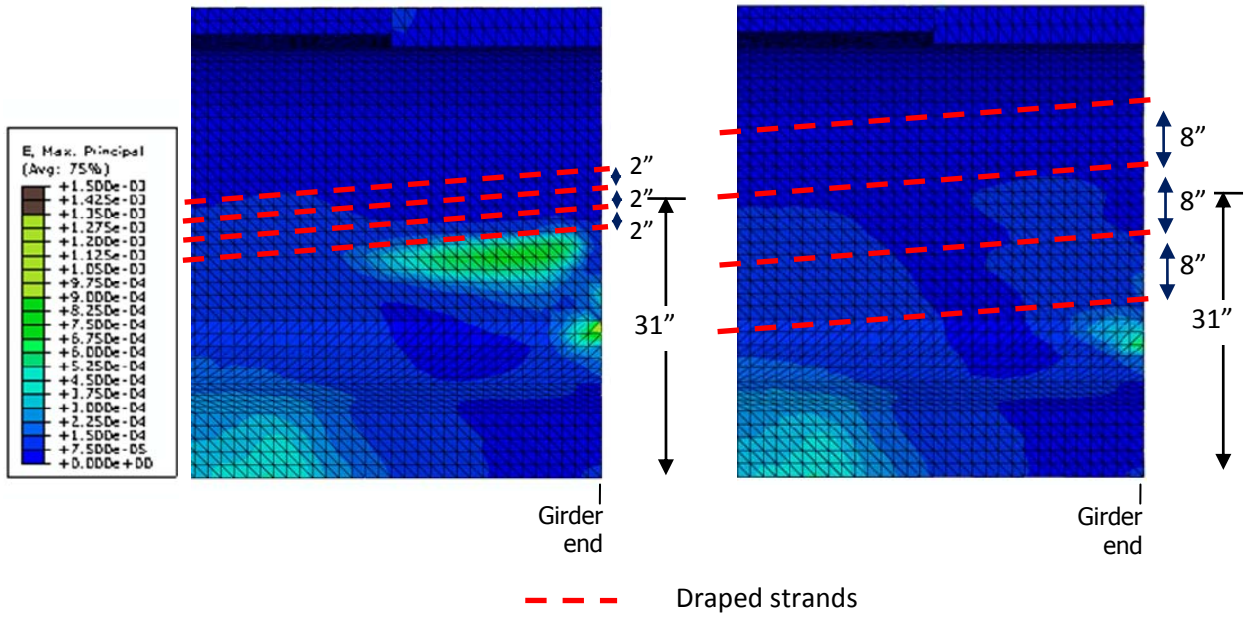

Figure 97 - Principal concrete tensile stress contour plots in an elevation view for the two cases with concentrated (left) and spread out (right) draped strands.

Fanning out the draped strands is shown in Figure 97 to be effective in eliminating the plastic strains in the inclined cracking area, and has negligible impact on the web or Y cracks. This solution, however, may be purely academic since the fanned strand pattern requires that the maximum resultant eccentricity of the strands be reduced from a location 5in from the girder top to a location 14in from the girder top. This loss of eccentricity would require a reduction of bottom flange straight strands and a reduction of girder load capacity.

6.6. Coping the Upper Flanges for Girders with Skew

The upper flanges of the wide flange girders are occasionally coped for bridges with skew. The impact of the absence of the upper flanges on girder end cracks was investigated through two identical models with and without coped flanges.

A comparison of the results of the two models indicated that no significant change in the strain pattern or likely cracking at the girder ends occurs by coping the upper flanges of the girders.

CHAPTER 7. SUMMARY and CONCLUSIONS

This main objective of this research project was proposing solutions that could control cracking which occur during or after the prestress release in the end zones of deep wide flanged prestressed girders. In harsh climates like Wisconsin, these cracks may provide a path for deicing salts to reach the reinforcement bars or the strands. Corrosion of the rebars or the strands may lead to durability problems or structural capacity losses.

The deepest Wisconsin standard wide flange girders, 54W, 72W and 82W, experience the most severe cracking. The number of cracks and the crack widths are larger for deeper girders with heavier prestressing. A bridge project case where the 82W girders were rejected due to quality problems related to cracking was reported.

All deep wide flange girders exhibit similar types of cracking. These characteristic cracks are categorized as inclined cracks, horizontal web cracks, and bottom flange junction Y cracks. Y cracks were determined to be the high priority for this study due to their proximity to the bottom flange strands. If the water seeping through Y cracks reach to strands, it may result in structural capacity losses.

The main method of investigation was finite element analysis utilizing the commercially available finite element software, Abaqus/CAE. Finite element analysis was preferred because the full stress and strain field can be obtained on the entire body. Repetitions, modifications, parametric studies are cost efficient compared with experimental studies.

Attempting to reduce the prestressed girder end cracking requires understanding of the stress and strain distribution. Small cracks occur relatively early during the detensioning process causing the strains to be redistributed. Linear analyses are not capable of simulating this behavior after cracking occurs. Series of nonlinear analyses including the strain softening behavior of concrete and the transfer of strains to rebars after cracking were performed.

The finite element analyses results were verified using data gathered through tests. Strains in two girders manufactured by Spancrete, Inc. and County Materials Corp. were monitored during and after prestress release. In addition, the literature was searched for available data to be used for comparison. The results of the comprehensive testing conducted at University of Texas, Austin (O'Callaghan 2008) was used to evaluate the accuracy of the models. While, desired correlation between the finite element models and the Spancrete test could not be achieved, County Materials and the girder tested at the University of Texas, Austin provided satisfactory validation of the models.

The reasons behind each characteristic crack type were investigated based on the results of the nonlinear finite element analysis. The inclined cracking was attributed to the combination of the strains created by the bottom flange strands and the strains created by the draped strands. For certain girders, the plastic strains in the inclined cracking area can be eliminated by removing the draped strands.

The web cracks stem from the eccentricities of the bottom flange and the draped strands in the vertical direction. Similarly, the eccentricity of the bottom flange strands in the direction of the girder width plays a significant role in the formation of the Y cracks. The Y cracks are also related to the distribution of the strands in the bottom flange.

Excessive strains were detected along the bottom flange, peaking at the end of the transfer length in the finite element models. The girders investigated in the filed do not exhibit visible cracking in this location. The girders might be experiencing multiple micro cracks in the bottom flange instead of several large visible cracks.

A study was conducted to evaluate the impact of any modifications to the end zone reinforcement; debonding some strands at the girder end; debonding with a change in the end zone reinforcement; modifications to the strand cutting order; removing, lowering or spreading the draped strands; coping the top flange of the girders. The improvement achieved by implementing these methods in the finite element models on each type of cracking lead to the following conclusions.

On the reinforcement bar size:

i. Using larger size vertical bars at the girder end was found to limit the strains in the web area. Modifying the first two pair of bar size to #10 from #6 could decrease the web strains by 50%. The strains, however, remain above the theoretical cracking limit after the modification. The improvement in the inclined strains is not as significant since the vertical rebars do not cross the inclined cracks perpendicularly.

ii. The most effective vertical bars are the bars closest to the girder end. Modifying the bars after the first two pairs of bars do not improve cracking further. If possible, increasing the size of only the first two pairs of bars is a possible way of controlling the horizontal web cracks. Considering the congested end zone, this might not be a practical modification.

iii. Modifying the second set of rebars further away from the end had no effect on the strains at the girder end.

iv. Modifying the bottom flange stirrup size, does not seem to improve Y cracking. No recommendations on modifications of the size of the stirrups can be proposed.

On debonding strands at the girder end:

v. Debonding strands at the girder end directly lowers the stresses transferred to the concrete at the end and controls cracking of each type.

vi. Debonding some bottom flange strands at the end removes the need for the draped strands. In the absence of draped strands, strains causing inclined cracking are considerably lower. Debonding some strands in the bottom flange at the girder end has the potential to completely eliminate the inclined cracking problem.

vii. The number of horizontal web cracks and the size of these cracks can be reduced significantly by debonding. For shallower 54W girders 50% debonding can eliminate web cracks, while 25-35% debonding can reduce the web strains approximately by 50-70%.

viii. Perhaps the most important finding of this project was that, methodically selected debonding can significantly reduce or eliminate the hazardous Y cracking strains. The strand layout in the bottom flange plays an important role in Y crack formation. Debonded strands at the end should be as close to the exterior face as possible. This will reduce the resultant eccentricity of the strands along the width of the bottom flange. The debonded strand pattern should not create locations of concentrated compression, i.e. should be uniformly distributed along the width of the bottom flange. It is recommended that, when possible, columns of debonded strands should not be adjacent to each other. A girder with the strand layout describes is very unlikely to develop Y cracking. Strands to be debonded at the girder end should be carefully selected since debonding without following these guidelines could also increase the size of the Y crack.

On the reinforcement bar size and debonding strands at the girder end:

ix. When a girder is analyzed with debonded strands at the girder end and with increased size vertical reinforcement bars, the result is a superposed reduction in strains.

x. Increasing the size of the first two pair of bars from the end was very effective in reducing the web strains. On the other hand, methodically debonding 35% of the strands, virtually eliminated inclined strains, and Y strains and reduced the web strains on 54W girders. An efficient alternative recommended is to change the first two pairs of bars at the girder end to #10 bars while debonding 35% of the strands at the girder end.

On the strand cutting order:

xi. Changing the strand cutting order does not impact the inclined or web cracking strains. These cracks are related to the eccentricity of the strands along the girder depth. The difference in the eccentricity of the strands in the vertical direction is small compared to the depth of the girder. Therefore, changing the strand cutting order in the vertical direction does not impact cracking considerably.

xii. The eccentricities of different row of strands in the bottom flange in the direction of the width of the girder are comparable to the girder width. A strand cutting order where the strands with the smallest eccentricity along the width were cut first reduces the strains for Y cracking and should be preferred where possible.

On the draped strands:

xiii. A girder without draped strands is unlikely to develop plastic inclined strains. The inclined cracking could be eliminated for certain girders by removing the draped strands.

xiv. Lowering the draped strands, will carry the inclined strains from the top flange to the web area. These stresses will be resisted by a smaller concrete area in the web and will result in higher strains. This may create a larger inclined crack. On the other hand, the horizontal web cracks will be restrained to a smaller zone between the lowered draped strands and the bottom flange strands. The number and size of the web cracks are predicted to be smaller. It should be noted that lower draped strands are not as efficient in limiting the top fiber tensile stresses as higher draped strands. For heavily prestressed girders, lower draped strands may not be an option.

xv. Spreading the draped strands will spread the stresses and engage a larger concrete area to resist the loads. Therefore, the inclined strains remains controlled. As the center line is lowered, this method also has a limited use.

Other:

xvi. Coping the top flange, does not change the cracking related strains anywhere in the girder.

Table 5 rates the impact of each method on each type of crack researched in this study. "HIGH" rating indicates that the method has the potential to eliminate cracking. "MODERATE" rating is used for methods which reduced strains for particular types of cracking significantly, but was not sufficient on its own to eliminate plastic strains. "MILD" is used for solutions which have a mild improvement on the crack type. Finally, the rating "NONE" is assigned for methods which did not cause any significant improvement on the cracking problem.

SOLUTION		INCLINED CRACKING	WEB CRACKING	Y CRACKS
End Zone Reinforcement	First vertical set from the end	MILD	MODERATE	NONE
	Second vertical set from the end	NONE	NONE	NONE
	Bottom flange stirrups	NONE	NONE	NONE
Debonding		HIGH	MODERATE	HIGH
End Zone Reinforcement & Debonding		HIGH	HIGH	HIGH
Strand Cutting Order		NONE	NONE	MODERATE
Draped Strands	Removed	HIGH	NONE	NONE
	Lowered	NONE	MODERATE	NONE
	Lowered & Spread	HIGH	MODERATE	NONE
Coping the top flange		NONE	NONE	NONE

HIGH = can eliminate cracking
MODERATE = can reduce strains significantly
MILD = can reduce strains
NONE = has negligible impact

Table 5 – The impact of methods of improvements studied on each type of cracking.

According to Table 5, inclined cracking can be controlled via removing, or spreading the draped strands the most. Debonding some bottom flange strands also result in the removal of the draped strands and help minimize the inclined cracking. The vertical bars at the end are only mildly effective in the inclined cracking zone.

Debonding and changing strand cutting order methods can both modify the resultant eccentricity of the bottom flange strands in the direction of the girder width. Carefully selected provides the best solution for the Y cracks, and can eliminate them completely for certain girders. Changing the strand cutting order can also limit Y crack sizes.

Web cracking strains were found to be limited using larger reinforcement bars at the girder ends. If some of the strands are debonded in the bottom flange in addition to the larger end reinforcement bars, web cracking can be eliminated for W52 girders with 35% debonding.

APPENDIX

This section includes supplementary materials referred in this report.

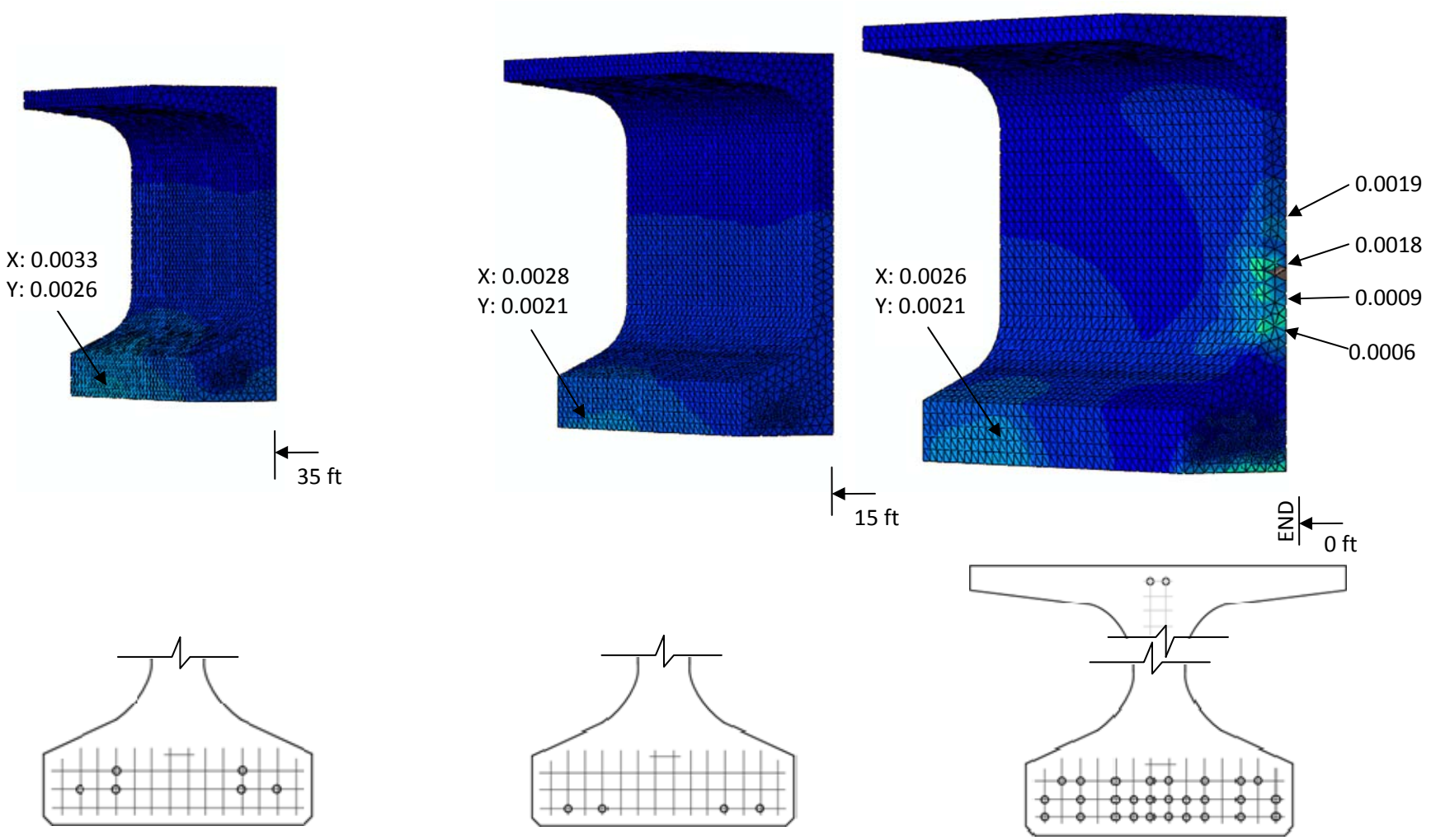

Figure 98 - Principal tensile strain contours and crack widths in inches for sections of girder where strands are bonded for DB 25-B

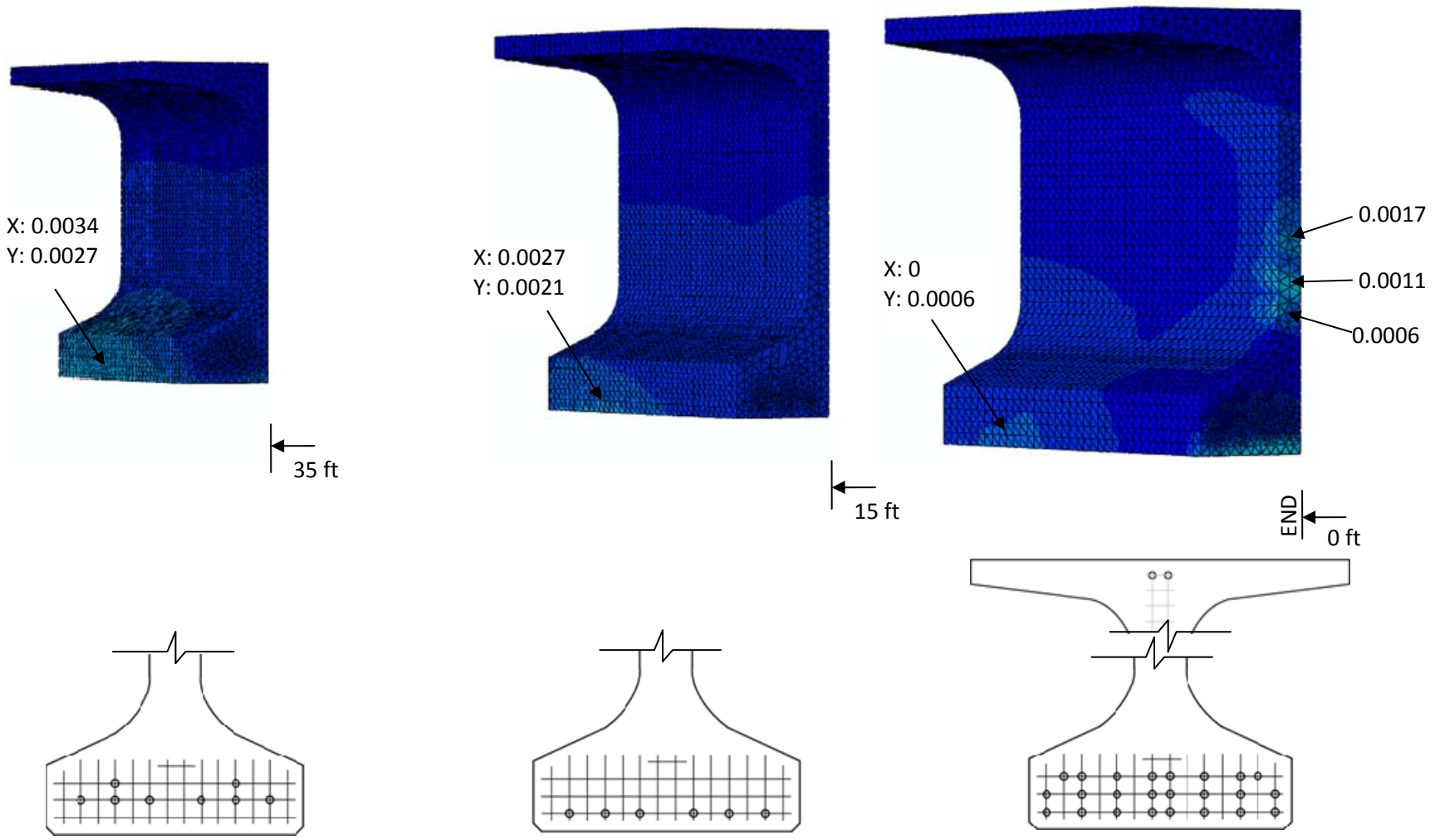

Figure 99 - Principal tensile strain contours and crack widths in inches for sections of girder where strands are bonded for DB 35-B

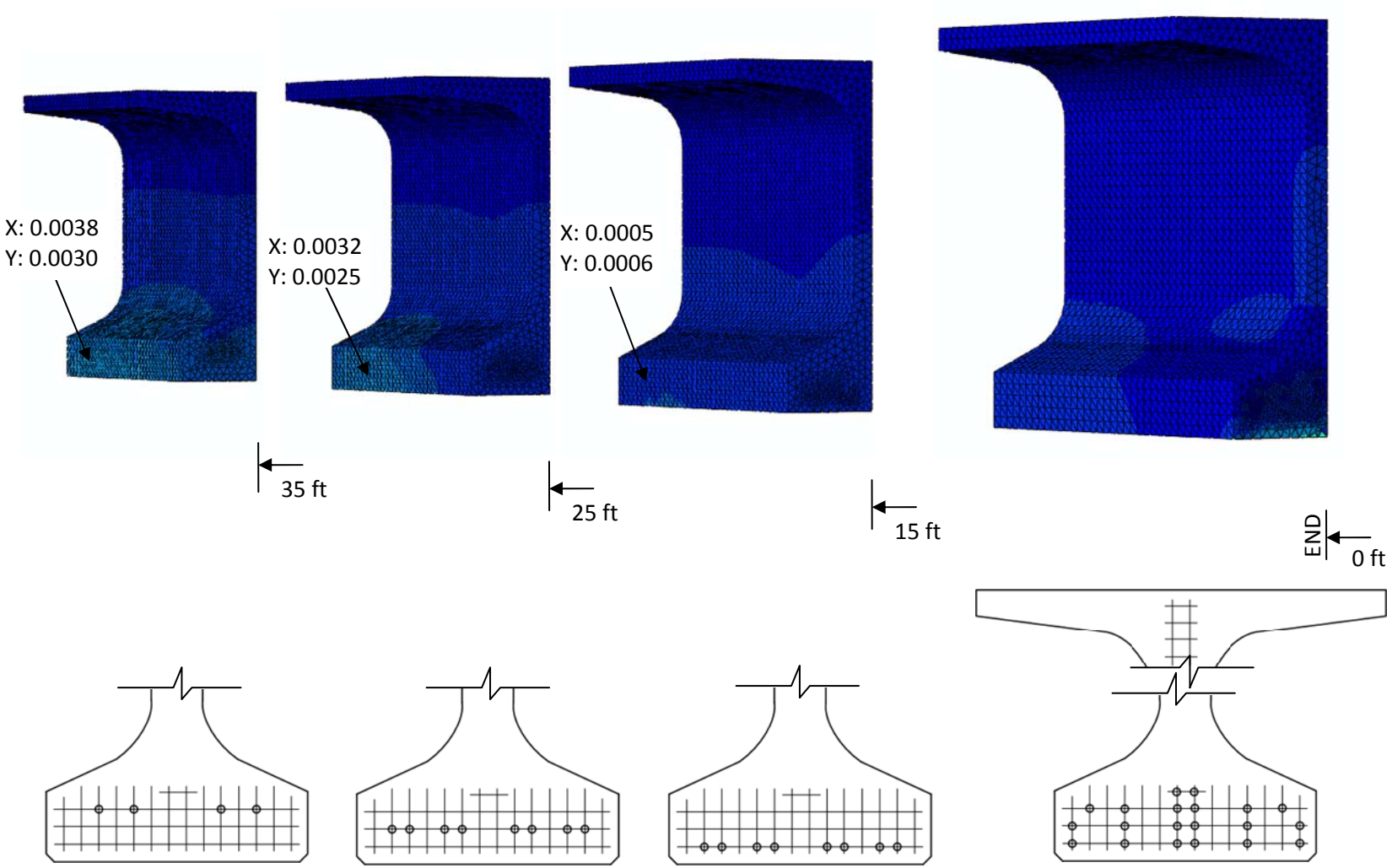

Figure 100 - Principal tensile strain contours and crack widths in inches for sections of girder where strands are bonded for DB 50-B

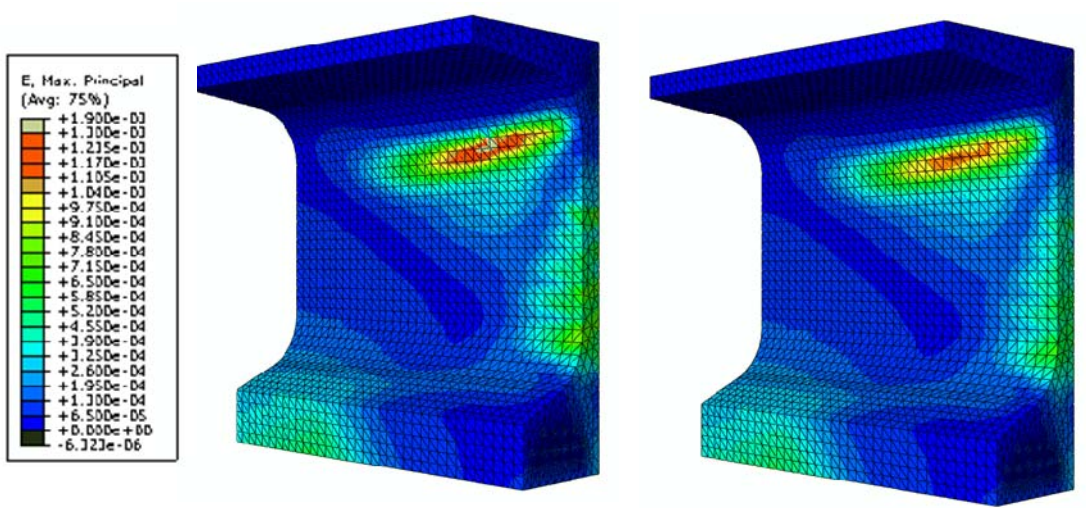

Five #6 @3in (std)

Five #7 @3in

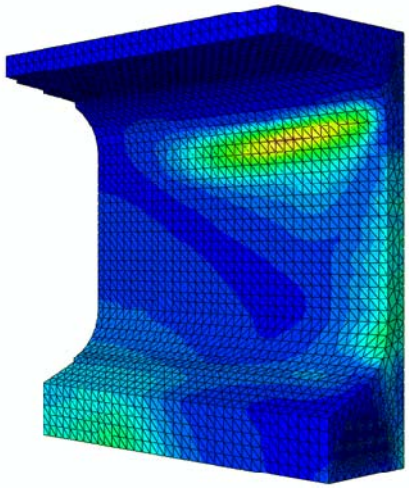

Five #9 @3in

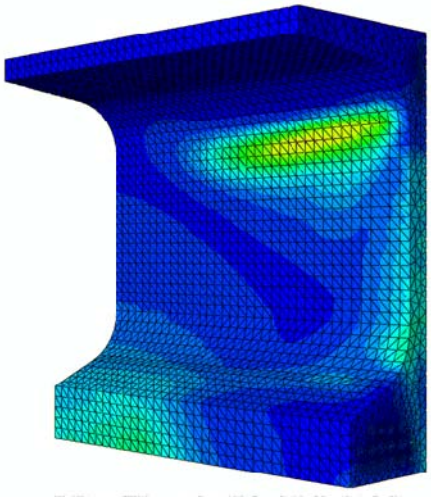

Five #10 @3in

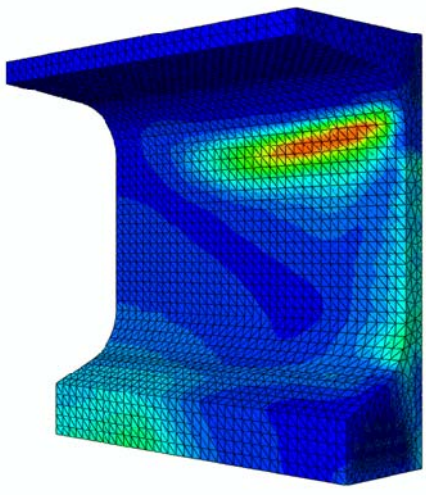

Three #10 @3in, two #6 @3in

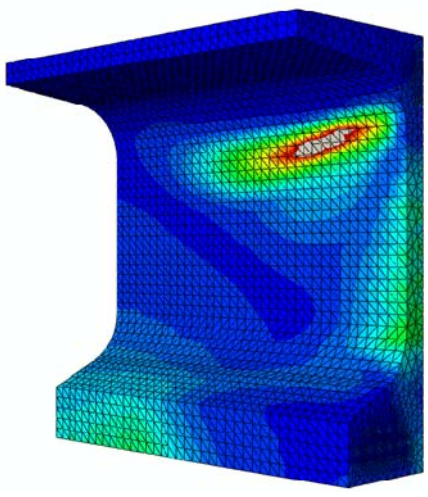

Five #6 @1.875in

Figure 101 - Principal tensile strain contour plots for varying reinforcement bar patterns at the very end

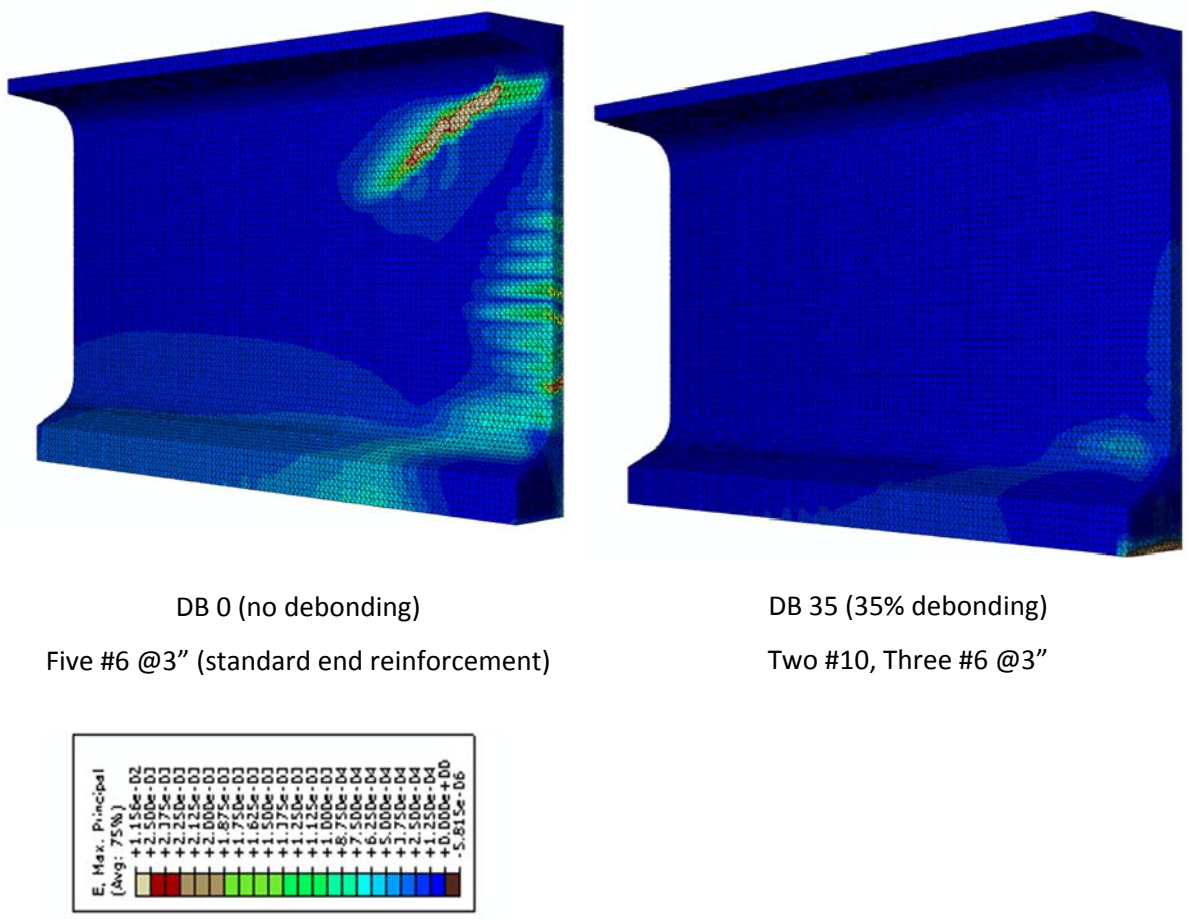

DB 0 (no debonding)

Five #6 @3” (standard end reinforcement)

DB 35 (35% debonding)

Two #10, Three #6 @3”

Figure 102 – Principal tensile strains on a 82W girder with no debonding and five #6 @3” bars (left) and 35% debonding and two #10, three #6 @3” bars (right)

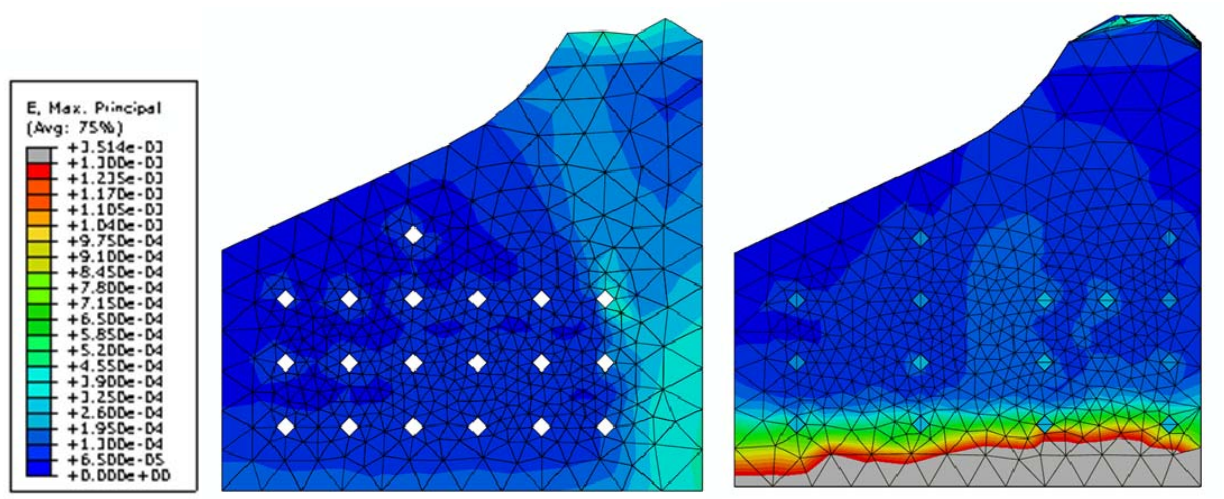

DB 0 (no debonding)

Five #6 @3" (standard end reinforcement)

DB 35 (35% debonding)

Two #10, Three #6 @3"

Figure 103 - Principal tensile strains on a 82W girder bottom flange at the girder end with no debonding and five #6 @3" bars (left) and 35% debonding and two #10, three #6 @3" bars (right)

REFERENCES:

1. American Association of State Highway and Transportation Officials, 2010, *AASHTO LRFD Bridge Design Specifications, Customary US Units, 5th Ed.* Washington, DC: , 2010.

2. GERGELY, P.; and Sozen, M. A., 1967, Design of Anchorage-Zone Reinforcement in Prestressed Concrete Beams*. PCI Journal*, 1967, vol. 12, no. 2. pp. 63-75.

3. CRISPINO, E. D.; Cousins, T. E.and Roberts-Wollman, C. L., 2009, *Anchorage Zone Design for Pretensioned Precast Bulb-T Bridge Girders in Virginia.* , 2009.

4. CASTRODALE, R. W.; Lui, A.and White, C. D., 2002, *Simplified Analysis of Web Splitting in Pretensioned Concrete Girders.* , 2002.

5. BREEN, J. E., et al., 1994, *Anchorage Zone Reinforcement for Post-Tensioned Concrete Girders.* National Cooperative Highway Research Program. , 1994. ISBN 0077-5614/0-309-05354-4.

6. MARSHALL, W. T.; and Mattock, A. H., 1962, Control of Horizontal Cracking in the Ends of Pretensioned Prestressed Concrete Girders*. PCI Journal*, 1962, vol. 7, no. 5. pp. 56-74.

7. TUAN, C. Y., et al., 2004, End Zone Reinforcement for Pretensioned Concrete Girders*. PCI Journal*, 2004, vol. 49, no. 3. pp. 68-82.

8. DUNKMAN, D. A., 2010, et al. *Bursting and Spalling in Pretensioned Concrete Beams.* Washington, D.C. ed. , May 29-June 2, 2010, 2010.

9. MIRZA, J., M. Tawfik, 1978, "End Cracking in Prestressed Members During Detensioning", PCI Journal, V23, N2, Mar 1978

10. STEINBERG, E., J. Beier, S. Sargand, 2001, "Effects of Sudden Prestress Force Transfer in Pretensioned Concrete Beams", *PCI Journal*, V46, N1, Jan 2001

11. KANNEL, J.; French, C.and Stolarski, H., 1997, Release Methodology of Strands to Reduce End Cracking in Pretensioned Concrete Girders*. PCI Journal*, 1997, vol. 42, no. 1. pp. 42.

12. MYERS, J. J., et al., 2001, *Precast I-Girder Cracking: Causes and Design Details.* , 2001.

13. DASSAULT Systèmes Simulia Corporation, 2009, ABACUS Software, Abaqus Analysis User's Manual

14. BUCKNER, C.D., 1995, A Review of Strand Development Length for Pretensioned Concrete Members, *PCI Journal,* 1995, V40, N2

15. TABATABAI, H., Dickson, T.J., The History of the Prestressing Strand Development Length Equation, *ACI Journal*, 1954, V50, N5

16. O'CALLAGHAN, M. R., Bayrak, O., 2008, *Tensile Stresses in the End Regions of Pretensioned I-Beams at Release*, University of Texas technical Report IAC-88-5DD1A003-1,

Wisconsin Highway Research Program
University of Wisconsin-Madison
1415 Engineering Drive
Madison, WI 53706
608/262-3835
www.whrp.org